Divergence-Convergence ratios govern functional circuitry in the Early Visual Pathway

Phd Thesis

Arturo José Valiño Pérez

Programa de doctorado en Neurociencias
Instituto de Neurociencias
Universidad Miguel Hernández-CSIC

Thesis Director:
Luis Miguel Martínez Otero

Ca-director
Jorge Brotons Mas

Cover page inspired in drawings from Santiago Ramon y Cajal´s Histology of the Nervous System of Man and Vertebrates (1911).

Divergence-Convergence ratios govern functional circuitry in the Early Visual Pathway

Doctoral Thesis presented by

Arturo José Valiño Pérez

- 2021 -

Thesis Director:

Luis Miguel Martínez Otero

Co-director:

Jorge Brotons Mas

PhD Program in Neuroscience

Instituto de Neurociencias – UMH-CSIC

Sant Joan d'Alacant, 15 of February 2021

To whom it may concern,

The doctoral thesis entitled "Divergence-Convergence ratios govern functional circuitry in the Early Visual Pathway" has been developed by myself, Arturo José Valiño Pérez. This thesis is presented in a conventional format. It is based on experimental studies undertaken at the Neuroscience Institute of Alicante during the PhD program in neuroscience of the Miguel Hernández University.

Yours sincerely

Arturo José Valiño Pérez

Sant Joan d'Alacant, 15 of February 2021

To whom it may concern,

The doctoral thesis entitled "Divergence-Convergence ratios govern functional circuitry in the Early Visual Pathway" has been developed by myself, Arturo José Valiño Pérez. This thesis includes the following chapter, of which I am the second author and three congress communications of which I am first author. I declare that these publications have not been used and will not be used in any other thesis in agreement with my thesis director Luis Miguel Martínez Otero and co-director *Jorge Brotons Mas*:

- Molano-Mazón M. et al. (2017) The Brain's Camera. Optimal Algorithms for Wiring the Eye to the Brain Shape How We See. In: Ibáñez J., González-Vargas J., Azorín J., Akay M., Pons J. (eds) Converging Clinical and Engineering Research on Neurorehabilitation II. Biosystems & Biorobotics, vol 15. Springer, Cham. https://doi.org/10.1007/978-3-319-46669-9_15

- A.J. Valiño, M. Molano, J. Brotons, V. Borrell, S. Sala, L. Martínez. A developmental threshold relating retinal and V1 areas predicts the structure of V1 Orientation Preference Maps. SENC (Sociedad Española de Neurociencia), Palacio de Santiago, Santiago de Compostela, 4/9/2019 – 6/9/2019. SENC-2019_Preliminary-Programme.pdf

- A.J. Valiño, J. Brotons, F.T. Sommer, J.A. Hirsch, S. Sala L. Martínez. Thalamic influence on the statistical wiring of visual cortical receptive fields and maps. SFN (Society for Neuroscience), Walter E. Washington Convention Center (Washington D.C), 11/11/2017 - 15/11/2017. Thalamic influence on the statistical wiring of visual cortical receptive fields and maps (abstractsonline.com)

- A.J. Valiño, J. Brotons, S. Sala, L. Martínez. Statistical Wiring of visual cortical receptive fields and maps. SENC, Alicante, 27/09/2017 – 30/09/2017. SENC2017_ebook.pdf (mcusercontent.com)

Yours sincerely,

Arturo José Valiño Pérez Dr. Luis Miguel Martínez Otero Dr. Jorge Brotons Mas

Sant Joan d'Alacant, 15 of February 2021

D. Luis Miguel Martínez Otero, Científico titular de investigación del Consejo Superior de Investigaciones Científicas y D. Jorge Brotons Mas, profesor investigador de la Universidad Cardenal Herrera e investigador colaborador en el Instituto de Neurociencias de Alicante.

Autorizan la presentación de la Tesis Doctoral titulada "Divergence-Convergence ratios govern functional circuitry in the Early Visual Pathway" realizada por D. Arturo José Valiño Pérez, bajo nuestra inmediata dirección y supervisión como director y codirector, respectivamente, de su Tesis Doctoral en el Instituto de Neurociencias (UMH-CSIC) y que presenta para la obtención del grado de Doctor por la Universidad Miguel Hernández.

Y para que conste, a los efectos oportunos, firmamos el presente certificado.

El director	*El codirector*
Dr. Luis Miguel Martínez Otero	*Dr. Jorge Brotons Mas*

Sant Joan d'Alacant, 15 of February 2021

Dña. Elvira de la Peña García, Coordinadora del programa de Doctorado en Neurociencias del Instituto de Neurociencias de Alicante, centro mixto de la Universidad Miguel Hernández (UMH) y de la Agencia Estatal Consejo Superior de Investigaciones Científicas (CSIC),

CERTIFICO:

Que la Tesis Doctoral titulada "Divergence-Convergence ratios govern functional circuitry in the Early Visual Pathway" has sido realizada por D. *Arturo José Valiño Pérez*, bajo la dirección de D. Luis Miguel Martínez Otero como director, y doy mi conformidad para que sea presentada a la Comisión de Doctorado de la Universidad Miguel Hernández.

Y para que conste, a los efectos oportunos, firmo el presente certificado.

Dra. Elvira de la Peña García

E-mail : elvirap@umh.es
www.in.umh.es
Tel: +34 965 919533
Fax: +34 965 919549
Av Ramón y Cajal s/n
CAMPUS DE SANT JOAN
03550 SANT JOAN D'ALACANT– ESPAÑA

Agradecimientos / Acknowledgements.

A Luis Miguel Martínez Otero por darme esta oportunidad y por hacerme reflexionar con sus interesantes conversaciones.

A mis compañeros de laboratorio Pablo, Rafa, Amanda y Marcos por estar ahí echando una mano siempre que ha hecho falta.

A mis compañeros del laboratorio 221, y en especial a Ana por soportar mis continuas preguntas burocráticas.

A Josemi, Aída, Ana, Mike, Lucía, Jordi, Salma, y Roberto por hacerme la vida más agradable.

A mi codirector Jorge por los buenos momentos.

A los Sergios, por su amistad incondicional.

A Salva, por todo lo que me ha enseñado, por su compresión, paciencia e inestimable ayuda.

A mis padres y a mis hermanos por apoyarme siempre pase lo que pase.

A mi querida abuela y a sus amigos San Judas Tadeo, San Expedito y al politeísmo en general.

Para Yago y para todos mis amigos de Coruña por este año especialmente difícil.

A Laura por darme todo su apoyo en los momentos difíciles y al Titi por ser lo mejor que me ha pasado nunca.

Index

Abstract

One of the main goals of visual neuroscience is to understand how the early visual pathway (EVP) works, that is, what are the operations that it performs and why. For this, structure, function and behavior must be related. However, relating structure to function in a coherent way is not so easy. Even though connectomics is a growing and promising field, in many cases, it can give an excess of information that we do not know yet how to interpret or relate to cortical function. To have a complete map of the synapsis of a cortical structure does not necessary mean that it is possible to understand how the weights are distributed across the circuit and therefore how the functional architecture is built.

In this work I will show how a comparative neurobiology approach (Pettigrew 2004) is really useful to build models of cortical function. It enables to identify the basic parameters that may constrain the development of cortical circuits, which gives the basis to generate hypothesis of the operations the visual system is performing, and to proof them using computational models.

In the first place, I present an extension of our previous statistical wiring model (Martinez et al 2014) that, using a single coverage optimization principle, maximizes the transfer of visual information from the retina to the primary visual cortex (V1), and accounts for the functional and topological differences found at the level of V1 across the mammalian phylogenetic tree. In particular, the model reproduces the experimentally derived differences in cortical magnification factor, which we express in terms of relative retina-to-V1 cortical area; it describes the existence of a continuum of different divergence-convergence ratios (DCr) between the retina and V1 through the lateral geniculate nucleus of the thalamus (LGN); and finds a developmental threshold, based on the extent of the emergent local correlations, that explains the transition between the decorrelated V1 salt-and-pepper cortical structures typical of rodents, and the topologically organized cortical orientation-preference maps (OPMs) characteristic of carnivores and primates. The model correctly predicts the cortical structure of all mammalian

species that have been experimentally explored, and makes clear testable predictions about how the cortical topology of other transition species, those that are right at the threshold of continuous distribution, should be.

In the second place, since retinotopy is the most present and relevant functional constraint across mammalian species. A mathematical model of the development of correctly oriented topographic maps in visual cortex is presented that takes into account the synchronization between the two retinas mediated by retino-retinal (R-R) connections, to explain the role of molecular and activity dependent mechanisms in the establishment of retinotopic maps across phylogeny. Demonstrating that the presence or absence of R-R connections across different species is completely related to their different DCr values through phylogeny.

In third place, we present a set of experimental results where V1 of a strain of mutant mice (Brn3b-Zic2) that have a larger proportion of ipsilateral fibres, was characterized using optical imaging of intrinsic signals. This manipulation alters the input that reaches V1 and, therefore, increases the DCr of the ipsilateral fibres through the EVP. As a result, Brn3b-Zic2 mice develop Ocular Dominance (OD) columns that resemble those presented in Ocular Dominance maps (ODM) of carnivores and primates, which emphasizes the role that the DCr plays in the development of V1 functional structure.

Resumen

Uno de los objetivos de la neurociencia visual es comprender cómo funciona la vía visual temprana, es decir, cuáles son las operaciones que está realizando y por qué. Para ello, es fundamental relacionar estructura, función y comportamiento. Sin embargo, relacionar la estructura con la función de manera coherente no es tan fácil. Aunque la conectómica es un campo en crecimiento y prometedor, en muchos casos puede dar un exceso de información que aún no sabemos interpretar o relacionar con la función cortical. Tener un mapa completo de la sinapsis de una estructura cortical no significa necesariamente que sea posible comprender cómo se distribuyen los pesos a lo largo del circuito y, por tanto, cómo se construye la arquitectura funcional.

En este trabajó demostraré como un enfoque de neurobiología comparada (Pettigrew 2004) es realmente útil para construir modelos de función cortical. Por un lado, esta aproximación permite identificar los parámetros básicos que pueden estar constriñendo el desarrollo de los circuitos corticales. Por otro lado, una vez identificados, estos mismos parámetros sirven como cimientos para generar hipótesis sobre las principales operaciones que realiza el sistema visual temprano y su comprobación mediante modelos computacionales.

En primer lugar, presento una extensión de nuestro modelo de cableado estadístico anterior (Martinez et al 2014) el cual, partiendo de un único principio de optimización de cobertura, maximiza la transferencia de información visual desde la retina a la corteza visual primaria (V1) y explica las diferencias funcionales y topológicas encontradas al nivel de V1 en el árbol filogenético de mamíferos. En particular, el modelo reproduce las diferencias derivadas experimentalmente en el punto de magnificación cortical, que expresamos en términos de área cortical relativa de retina a V1; describe la existencia de un continuo de diferentes ratios de divergencia-convergencia (RDC) entre la retina y V1 través del núcleo geniculado lateral del tálamo; y encuentra un umbral de desarrollo, basado en el alcance de las correlaciones locales emergentes, que explica la transición entre las estructuras

corticales decorrelacionadas de sal y pimienta en V1 típicas de los roedores, y los mapas de orientación organizados topológicamente, característicos de los carnívoros y primates. El modelo predice correctamente la estructura cortical de todas las especies de mamíferos que se han explorado experimentalmente y hace predicciones claras y comprobables sobre cómo debería ser la topología cortical de otras especies en transición, es decir, aquellas que están justo en el umbral de la distribución continua.

En segundo lugar, dado que la retinotopía es la constricción funcional más preservada y relevante en mamíferos, se muestra un modelo matemático del desarrollo de mapas topográficos correctamente orientados en V1, que tiene en cuenta la sincronización entre las dos retinas mediada por conexiones retino-retinianas (R-R), para explicar el papel de los mecanismos moleculares y dependientes de actividad en el establecimiento de mapas retinotópicos a través de la filogenia. Concluyendo, finalmente, que la presencia o ausencia de conexiones R-R entre diferentes especies, está completamente relacionada con las diferentes RDC a lo largo del árbol filogenético.

En tercer lugar, presentamos un conjunto de resultados experimentales donde V1 de una cepa de ratones mutantes (Brn3b-Zic2) que tienen una mayor proporción de fibras ipsilaterales, se caracterizó mediante imágenes ópticas de señales intrínsecas. Esta manipulación altera la entrada que llega a V1 y, por tanto, aumenta la RDC de las fibras ipsilaterales a través de la vía visual temprana. Como resultado, los ratones Brn3b-Zic2 desarrollan columnas de dominancia ocular similares a las presentes en mapas de dominancia ocular de carnívoros y primates, lo que enfatiza el papel que juega la RDC en el desarrollo de la estructura funcional de V1.

Technical summary

Neurons in V1 of mammals respond only to a restricted set of stimulus orientations (Heimel et al 2005, Hubel & Wiesel 1962, Kaas 2012a, Kaschube et al 2010, Ringach et al 2016, Van Hooser 2007). However, the functional aspects of the circuit are different between carnivores, rodents and primates. In carnivores and primates, V1 cells with similar orientation preferences tend to cluster together in an orderly fashion giving rise to the renowned cortical orientation-preference maps (OPMs) (Blasdel 1992a, Blasdel 1992b, Bonhoeffer & Grinvald 1991, Kaschube 2014, Kaschube et al 2010, Ohki et al 2006, Van Hooser 2007). On the other hand, in rodents and lagomorphs these clusters of cells are more decorrelated and smaller, giving rise to a "salt and pepper" configuration in V1 (Jimenez et al 2018, Liang et al 2018, Ohki et al 2005, Ohki & Reid 2007, Van Hooser 2007).

Since OPMs of carnivores and primates have a highly conserved functional structure through evolution it has been proposed that these mammals share common developmental rules based on cortical self-organization (Kaschube et al 2010). In contrast, rodents and lagomorphs, more closely related to primates than to carnivores (Kaschube et al 2010, Springer et al 2004, Weigand et al 2017b), lack this type of cortical organization. On the one hand, this can suggest a completely different set of developmental mechanisms. On the other hand, it could imply similar developmental and optimization principles under different biological constraints, which in turn generates a distinct type of columnar disposition of neurons in V1.

There is an intense debate concerning the homogeneity or heterogeneity of the cortex across mammalian species. This is quite paradoxical since, if the cortical structure is so different (DeFelipe et al., 2002; Herculano-Houzel, Collins, Wong, Kaas, & Lent, 2008) how can completely identical OPMs develop in primates and carnivores? In contrast, if the V1 structure is so similar, (Carlo & Stevens, 2013; DeFelipe et al., 2002; Rockel, Hiorns, & Powell, 1980) how can the functional architecture be so different between primates and rodents and so similar in primates and carnivores?

This suggests that there might be underlying functional and anatomical constraints shared among these species that may explain these similarities and differences. At this point, comparative functional and anatomical data is crucial to identify the biological constraints that are governing the structure and the function of the circuit. Which, in turn, enable to build a computational model to test the importance of these parameters in cortical function.

The mechanisms involved in the functional topology of V1 are much debated. On the one hand, feedforward models propose that the functional topology of V1 comes from the convergence and integration of inputs from the lateral geniculate nucleus of the thalamus (dLGN) (Hubel & Wiesel 1962, Kremkow & Alonso 2018, Martinez et al 2014, Paik & Ringach 2011, Ringach 2004, Ringach 2007, Soodak 1987). On the other hand, intracortical models suggest the interconnectivity of V1 neurons as the organization mechanism involved in the formation of this functional maps (Kaschube et al 2010, Martinez & Alonso 2003, Swindale 1996). The experimental and modelling data that validate or refute each theory is controversial (Alonso & Martinez 1998, Alonso et al 2001, Jin et al 2011, Kaschube et al 2010, Schottdorf et al 2015).

However, there is a clear preserved homology across all mammals and that is the retinotopic map over which the rest of functional maps of V1 emerge. Because the retinotopic map is clearly inherited from the input, we chose a linear feedforward model (Martinez et al 2014, Paik & Ringach 2011, Ringach 2004, Ringach 2007, Schottdorf et al 2015, Soodak 1987) to investigate up to what point the developmental and functional mechanisms related with the retinothalamic input are involved in the formation of the mammalian early visual pathway. Then we identified the parameters that we though can be constraining the cortical function across phylogeny, which we summarized as the divergence-convergence ratio (DCr) across layers. This ratio relates the relative size of the different layers in EVP and the connections between them. Since the thalamacortical convergence reported for carnivores and rodents is high, of around 20-80 connections per neuron (Alonso et al 2001, Lien & Scanziani 2018), we explored how this different anatomical and functional constraints modify the functional topology of V1 to understand the main

computations V1 is performing. The model can account for many features of the different cortical organizations of V1 across evolution. As a result, a simple wiring principle is able to generate many important characteristics of V1 neurons and we can confirm that the retinothalamic input drives the development of V1 functional structure.

In summary, our model indicates that the divergence - convergence mechanisms related to cortical expansion are tuned in mammalian species to recover as much information as possible and, as a consequence of the biological constraints mediated by the uneven V1 overexpansion respect to that of the retina across phylogeny (Table 1), OPMs or salt and pepper configurations are formed.

Since topographic retinal maps are a common feature of all mammals and are clearly constraining the functional topology of V1 when related to the different DCrs across species, the mechanisms by which retinotopy is formed and maintained throughout development are extremely important. Furthermore, retinotopic maps need to be congruent across both hemispheres in V1, that is, to generate a continuous representation of the visual field in V1 in both hemispheres. Taking this into account, I developed a model to understand the basic mechanisms involved in the correct formation of retinotopic maps.

The mechanisms implied in generating retinotopic maps can be summarized in two large groups: genetic or molecular mechanisms (Herrera et al 2019, Huberman et al 2008, Swindale 1996) and activity-dependent mechanisms. It is assumed that the initial topography is due to molecular mechanisms while the refinement of the map is mediated by activity-dependent mechanisms (Ackman et al 2012, Crair et al 1997, Huberman et al 2006). Until recently there was no evidence of what guided these activity-dependent mechanisms acting before eye opening. Crair, however (Ackman et al 2012), has shown that retinal waves generated spontaneously in the retina are transmitted to the postsynaptic layers (superior colliculus, dLGN and V1) synchronously in both hemispheres governing their spontaneous activity.

Additionally, retino-retinal (R-R) projections have been seen in many species at the beginning of development (Murcia-Belmonte et al 2019). These fibers seem a good candidate for the synchronization of the activity of both retinas since there are no other functional connections between hemispheres at the level of the dLGN or superior colliculus (SC). With this model, what we are trying to understand is the role played by the synchronous activity of both retinas mediated by R-R connections in the correct formation of continuous and congruent retinotopic maps in both hemispheres. To do this, the problem has been addressed using a Kohonen self-organization model (SOM), where we explore how the synchronization of the activity and the specificity of the molecular mechanisms modulate the formation of these maps.

Our model indicates that the role of the R-R connections is to synchronize the spontaneous activity across both hemispheres to generate retinotopic maps correctly oriented on both hemispheres in species with high DCrs. However, species with low DCrs, that is, with a small postsynaptic target compared to the presynaptic area, can develop congruent maps without synchronous activity dependent mechanisms. So the appearance of R-R connections across phylogeny is related to an increase in the DCr through phylogeny. Thus, species with a similar size for their presynaptic and postsynaptic target (low DCr) can rely only on molecular guidance cues and do not have R-R connections. However, as the postsynaptic targets increase (high DCr) across phylogeny, species develop R-R connections to synchronize their spontaneous activity as a complement to the molecular guidance mechanisms enabling the development of correctly oriented retinotopic maps in both hemispheres.

Finally, I will present experimental data, supporting these modelling results. We used optical imaging of intrinsic signals (Grinvald et al 1999) to show that a strain of mutant Brn3b-Zic2 mice that artificially overexpress Zic2 (Herrera 2018, Herrera et al 2003, Herrera et al 2019) and hence have a larger proportion of ipsilateral fibers, do indeed develop ODMs such as those present in carnivores and primates (Van Hooser 2007, Weigand et al 2017a). This result is fully consistent with our model's predictions and contrasts sharply with the single binocular region

that characterizes WT mice (Cang et al 2005a, Sato & Stryker 2008). Our results further support the idea that ODMs, as well as OPMs, are nothing but a consequence of the different DCr found across phylogeny, which reflect the different overexpansion of V1 found across mammals, as the visual system design maximizes visual space coverage and acuity through convergence of retinal and thalamic inputs, while preserving their retinotopy.

Abbreviations

- **EVP**: Early visual pathway.
- **dLGN**: Dorsolateral geniculate nucleus.
- **V1**: Primary Visual Cortex.
- **RGC**: Retinal ganglion cell.
- **SC**: Superior colliculus.
- **SGS**: Stratum griseum superficiale.
- **R-R**: Retino-retinal.
- **DCr**: Divergence-convergence ratio.
- **SOM**: Self-organizing model.
- **Cmag**: Cortical magnification factor.
- **OBias**: Orientation Bias.
- **RF**: Receptive field.
- **OPM**: Orientation preference map.

Introduction

The survival of a living organism depends on its ability to extract and integrate the most relevant signals from the world fast and efficiently adapting to changes in the environment. If we have learned anything as human beings, is that nature is harsh and unforgiving, only the best adapted survive. Therefore, and thanks to millions of years of evolution, the arms race focused on exploiting our environment better than our neighbor, what in many cases is to end him before he ends us, has promoted the evolution of sensory systems of various kinds: from the quorum sensing of bacteria, the myocytes of sponges, the appearance of neurons in the coelenterates, to the nervous system of a squid (from which we have learned so much), to the ability to perceive our own existence, in other words, consciousness, something which makes us think we are special, but sorry, we are not.

In any case, for many living beings, having the ability to detect visible light is essential for the development of their functions. Again, we can have simple organisms with cells with photo pigments that respond to light, which generates positive or negative tropisms. To the appearance of an organ that came to stay, the eye and the visual system, which for many species has become the most important sense for their survival.

The early visual pathway (EVP) is formed by the retina, the dorsolateral geniculate nucleus (dLGN) and the primary visual cortex (V1). The information from different parts of the visual world is extracted by separate channels of retinal ganglion cells (RGCs) that transmit this information in parallel through the dLGN to finally reach V1 where everything starts to merge. From this stage, the visual information travels to two different separate pathways in the brain. The “what” pathway related to object recognition in the temporal part of the brain and the “where” pathway to recognize the position of an object in visual space.

In this work I will explore computational models that explain the main operations V1 is performing and the basic mechanisms that guide the correct development of the characteristic functional properties of V1. To understand and

extract the most important parameters of these models, it has been completely necessary to adopt a comparative biology approach to identify the common and different components of EVP processing in mammals, and unravel the functional and anatomical constraints governing the functional architecture and operations performed in V1.

In the following pages I will describe the EVP using a comparative approach mostly based on mammals, focusing mainly in differences between carnivores, primates and rodents.

The eye

It should be noted that the great complexity of the eye was and will continue to be for some, irrefutable proof of an intelligent design (Paley 2009). Even Darwin found it difficult to assume the slight gradations of natural selection as the underlying mechanism constructing the eye. Hudges in 1977 (Hughes 1977) begins his book with this quote from Darwin;

to suppose that the eye with all its inimitable contrivances ... could have been formed by natural selection, seems, I freely confess, absurd in the highest degree.

But,

when I think of the fine known gradations, my reason tells me I ought to conquer the cold shudder.

The basic parts of the eye are reflected in the following diagram (Figure 1.1). Light passes through the lens whose shape is changed by the ciliary muscles to accommodate the image projected onto the retina, which in turn sends the information through the optic nerve to the brain.

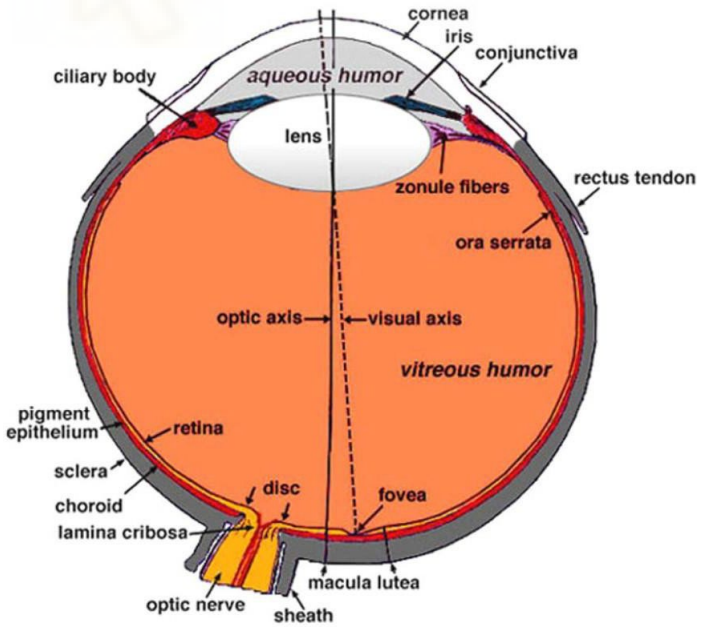

Figure 1.1. **Sagittal section of a human eye**, adapted from (Helga Kolb & Ralph 2007).

As a rule of thumb, eye size increases with body size and larger eyes promote a better visual acuity, although there are other factors that may affect eye size across different species (Figure 1.2). Thus, in small species eye size increases more rapidly with body weight than in larger species, and there are overall differences in size across different vertebrate classes (Howland et al 2004, Hughes 1977),

It can also be established that the greater the axial axis of the eye, the larger the retinal image, which in turn implies an increase in visual acuity, understood as the ability of an animal to resolve static spatial details (Caves et al 2018, Veilleux & Kirk 2014). As the focal length increases, the size of the image projected to the retina becomes larger which increases the area, and therefore, the number of neurons in the retina devoted to process the visual signal. Therefore, visual acuity, measured in cycles per degreee (cpd), that is, the number of black and white bands that an organism can discriminate within a single degree of visual angle, increases with eye size (Figure 1.3).

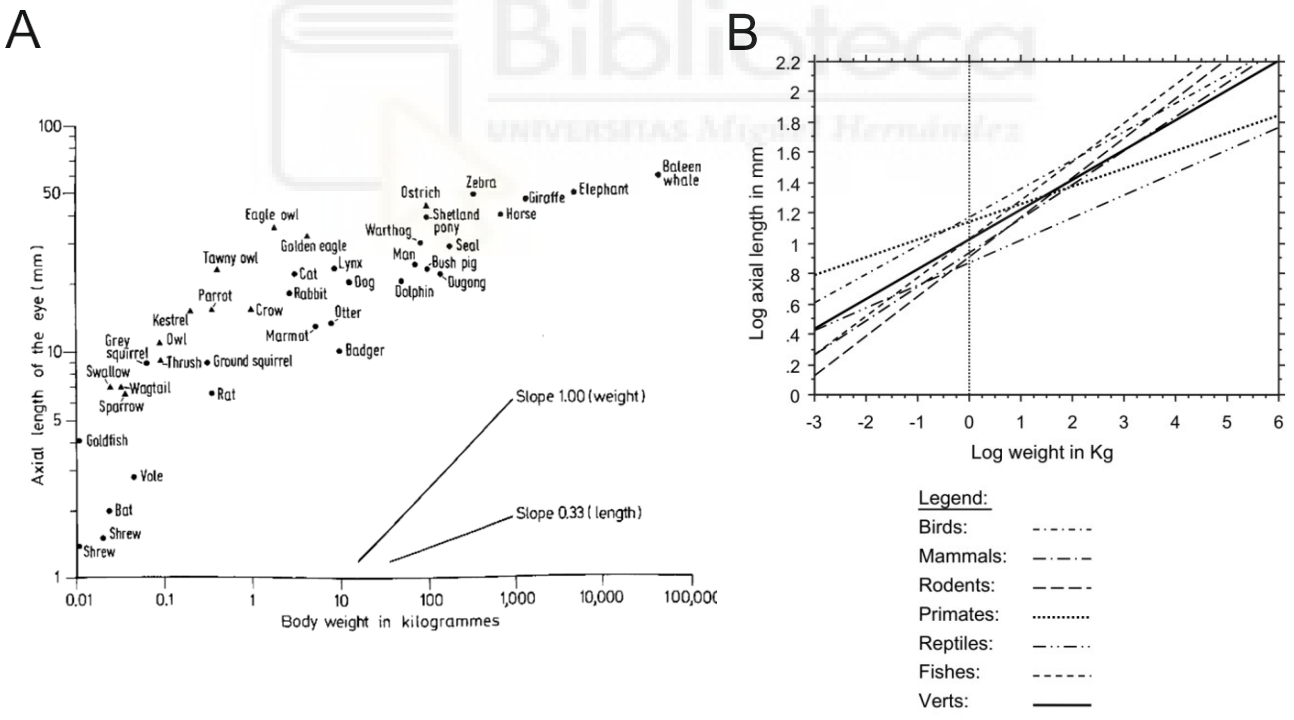

Figure 1.2. **Eye size grows with body weight**. **A**. Log of axial eye (mm) against body weight (Kg) for different species, adapted from (Hughes 1977). **B**. Log of axial eye (mm) against log body weight (Kg) for different vertebrates, adapted from (Howland et al 2004).

The eye is a very complex organ and it is possible to relate many anatomical specializations to the biological needs determined by the ecological niche of each specie. Animals that are fast and require a high visual acuity have larger eyes, as it can be observed, birds have overall larger eyes compared to other species (Figure 1.2) (Ross & Kirk 2007, Veilleux & Kirk 2014). Another example is the cheetah, the fastest carnivore has also large eyes in relation to its body weight. Within this order of ideas, nocturnal animals tend to have larger eyes and even anatomical specializations such as the tapetum lucidum to reflect light internally and absorb as many photons as possible (Dyer et al 2009, Hughes 1977). A clear example of eye size adaptation is found in the transition from day to night life in monkeys from the new world of the Aotus genus. Coming from a diurnal ancestor, they lack tapetum lucidum, but have developed larger eyes and retinal areas compared to their closest suborder relatives (Dyer et al 2009).

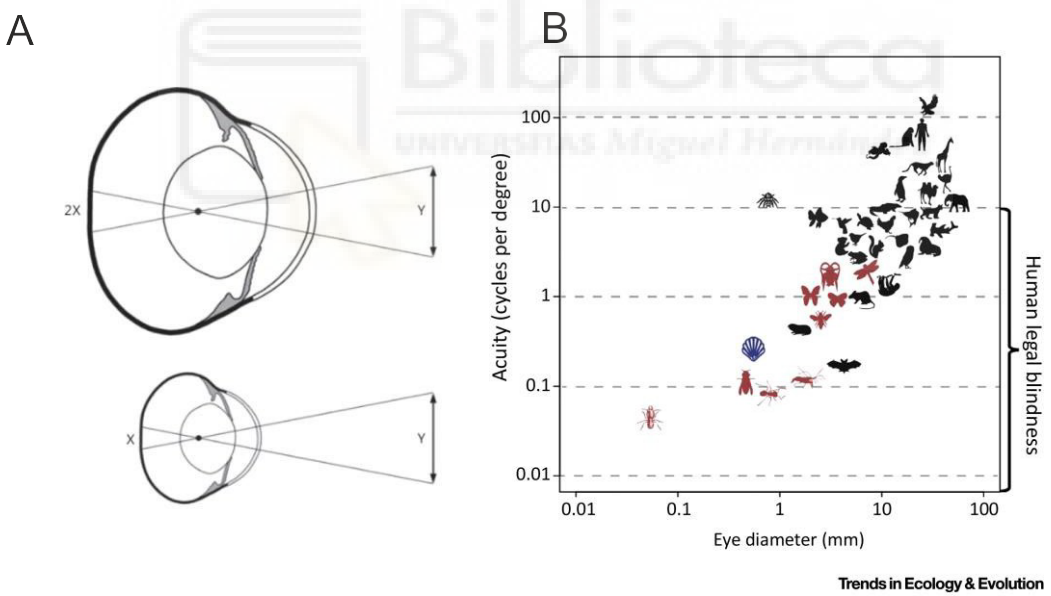

Figure 1.3. **Axial eye diameter and retinal image**. **A**. Retinal image increases with eye size ,adapted from (Veilleux & Kirk 2014). **B**. Log of visual acuity (cpd) against log of eye diameter (mm) for different species, adapted from (Caves et al 2018).

The eye is not the only structure that determines how the visual world around us is perceived. In fact, animals with similar eye sizes can have very different visual acuities (Figure 1.3), so there are certainly other elements implied in the processing of visual information.

In the case of visual acuity, these elements are the degree of binocular vision, the size of the thalamus and V1. On the one hand, animals with a higher degree of binocular view have higher visual acuities at the expense of reducing the overall size of their lateral vision (Figure. 1.4) (Kremkow & Alonso 2018, Mazade & Alonso 2017). On the other hand, as the processing capacity in higher stages is increased, that is, the number of neurons in thalamus and V1, visual acuity increases (Figure. 1.4; table 1). The fact that some primates have a higher neuron density in V1 also explains the improved visual acuity ($\mathbf{y = 5{,}4645x^{0{,}3171}\ R^2 = 0{,}99)}$, respect to other species ($\mathbf{y=0{,}6266x^{0{,}4085}\ R^2 = 0{,}79}$) (Collins et al 2010, Srinivasan et al 2015). Thus, the EVP influences heavily how the world is perceived, and may adapt to fulfill each species requirements.

The Retina

The retina can be considered a fairly stereotyped structure made up of 5 different types of neurons: photoreceptors, horizontal cells, amacrine cells, bipolar cells, and retinal ganglion cells (RGCs) (Wassle 2004). The photosensitive pigment of the photoreceptors detects the incident light and transmits that information to the other components of the retina. According to their different sensitivity to light, photoreceptors can be classified in rods and cones. Rods are more sensitive to light, and are present in a greater proportion in nocturnal and twilight animals. Cones, however, have different photo pigments less sensitive to light (which makes them more suitable for diurnal animals), but specialized in the detection of different wavelengths. Thus, it is possible to differentiate L cones (large wavelength), M cones (middle wavelength) and S cones (short wavelength) that respond to red, green and blue light respectively. The different combination in intensities of the primary colors

red, green and blue (RGB) allows to detect practically all the colors that are part of the visible light spectrum. Primates are the only trichromatic mammals, while the rest are dichromic (L and S cones) whose cones' L sensitivity varies from red to green across species. Curiously, many other diurnal vertebrates such as bone fish, reptiles, and birds are tetrachromic, in other words, they have up to four different photo pigments (Helga Kolb & Ralph 2007, Peichl 2005, Wassle 2004, Wassle et al 1981a).

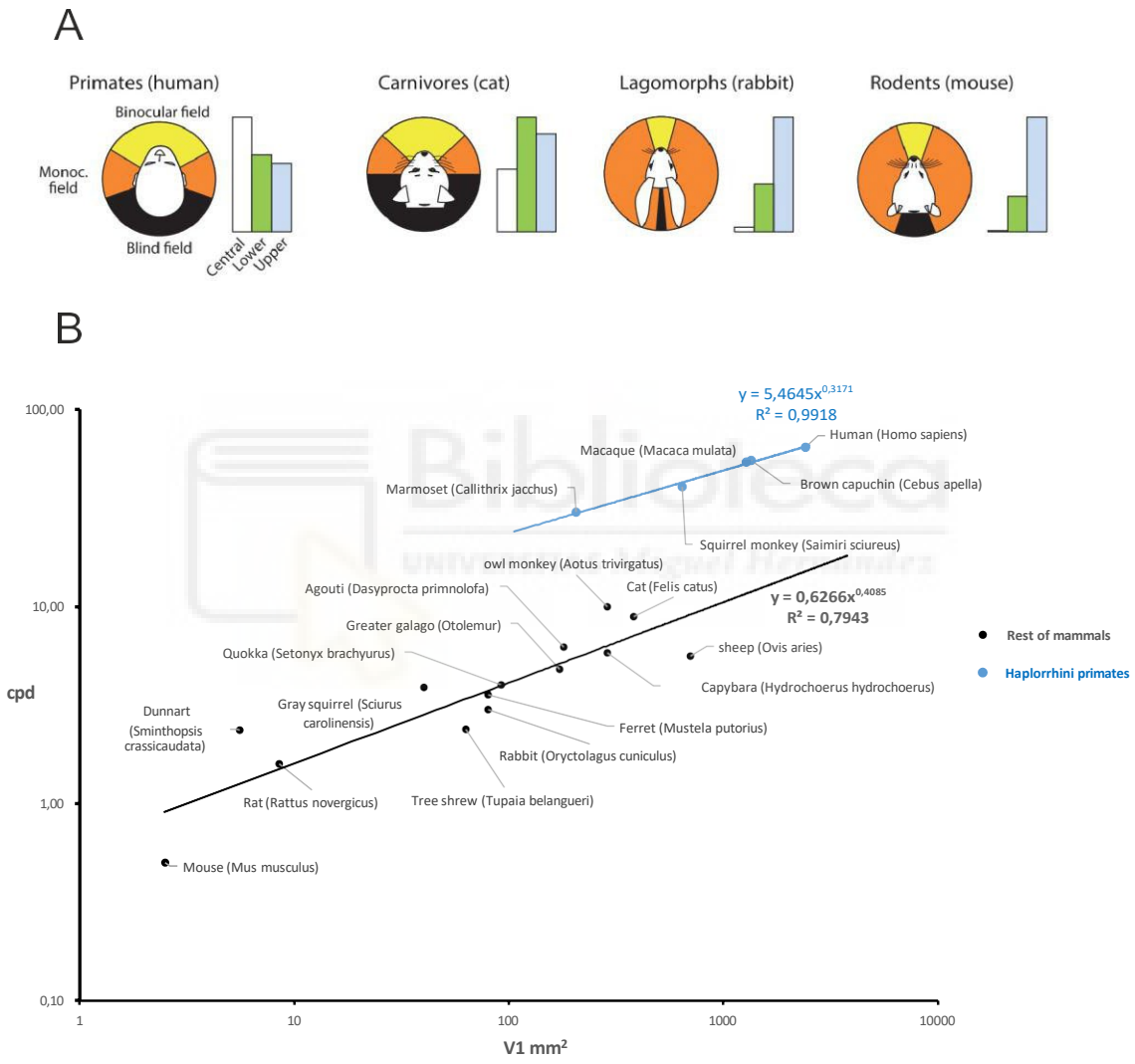

Figure 1.4. **Biological constraints that determine visual acuity. A**. Binocular and peripheral visual field varies between mammalian species, adapted from (Kremkow & Alonso 2018). **B**. Log of visual acuity (cpd) against V1 area (mm^2) for different species, data from (Table 1).

Once the light is detected, as its name suggests, by the photoreceptors, the information is processed by the circuit of horizontal, bipolar and amacrine neurons that end up generating different functional types of RGCs whose axons go to the thalamus forming the optic nerve (Figure 1.5). Horizontal cells interact with photoreceptors and bipolar cells in the outer plexiform layer (OPL). The information then travels from the bipolar to the RGCs where they interact with the amacrines in the inner plexiform layer (IPL). The operations that all of these circuit components perform to produce functionally different RGCs are widely diverse and beyond the scope of this work. More information is available in the following references (Demb & Singer 2015, Masland 2012, Nassi & Callaway 2009, Wassle 2004).

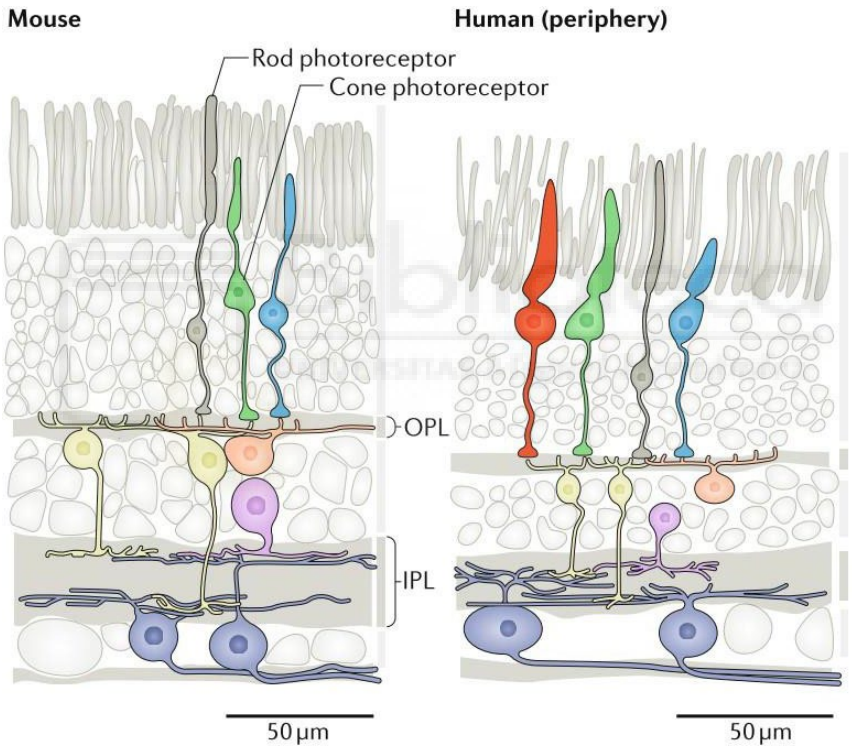

Figure 1.5. **Scheme of a segment of mouse retina and of the peripheral part of a human retina**. IPL (Inner plexiform layer), OPL (Outer Plexiform layer). Bipolar cells (yellow), horizontal cells (orange), amacrine cells (violet), retinal ganglion cells (dark blue). Adapted from (Baden et al 2020).

The different interactions between the neurons of the retina end up generating RGCs with different feature selectivities, that is, neurons which respond preferentially to a certain type of stimuli. So, the greater or lesser degree of response

of a RGC is due to the conformation of its receptive field (RF) and to the characteristics of the stimulus it receives for which it is more or less selective.

A receptive field (RF) is defined generically as "the portion of the sensory territory of an animal where a certain stimulus generates a response in the nervous system" (Gerhard 2013). In Hartline's 1938 recordings of individual axons of the optic nerve of frogs and other cold-blooded vertebrates (Hartline 1938), he observed how some nerve fibers responded to increases of light, others to decreases, and others that responded only to changes in light intensity. It was at this

time that the term RF was coined as “the region of the retina which must be illuminated in order to obtain a response in any given fiber”. Thus, the response of any given fiber of the optic nerve depends on the specific stimulation of its RF and on its different selectivity for the visual stimulus it receives.

Later, the recordings from RGCs in frogs made by Barlow 1953 (Barlow 1953a, Barlow 1953b) and in cats by Kuffer (Kuffler 1953), showed that the different responses to stimuli of different polarity, that is, "On" (bright spots), "Off" (black spots) and "On-Off" (contrast changes) are due to the RFs having a concrete center-surround spatial structure segregated in concentric subregions with opposite responses, excitation or inhibition, for a stimuli of a certain polarity (Figure 1.6). The center always has an opposite response than the periphery. In such a way that if the center is On, (a bright spot produces an excitation and a dark spot inhibition) the periphery is Off (a dark spot causes excitation and a bright spot inhibition) and vice versa. This excitation inhibition configuration is usually referred to as a Push-Pull arrangement, push for the excitation and pull for the inhibition. In the intermediate zone, we find an On-Off region that responds to contrast changes in one direction or the other. As a consequence, RGCs can be classified depending on their response to different parameters of the visual stimulation they receive on their RFs. Such as the polarity (On or Off) of the center, average luminance, stimulus size, temporality of the response... etc. Thus, the feature selectivity of a RGC, that is, its specialization to respond to a certain stimulus, its completely related to the structure of its RF.

This center-periphery arrangement gives RFs the property to respond to changes in contrast regardless of the average luminance present in the environment. The most accepted model to describe them is the DOG (difference of gaussian model). The center has more sensitivity than the surround, however, the area of the surround is larger, so that when the entire RF is illuminated homogeneously, the response is similar for different light intensities. The largest response occurs as the difference between the center and the periphery increases (Masters 2014). This ability to adapt and to generate responses depending on the context, that is, the ability of the system to operate in different light intensities is crucial for the survival in an environment where the average luminance throughout the day changes constantly.

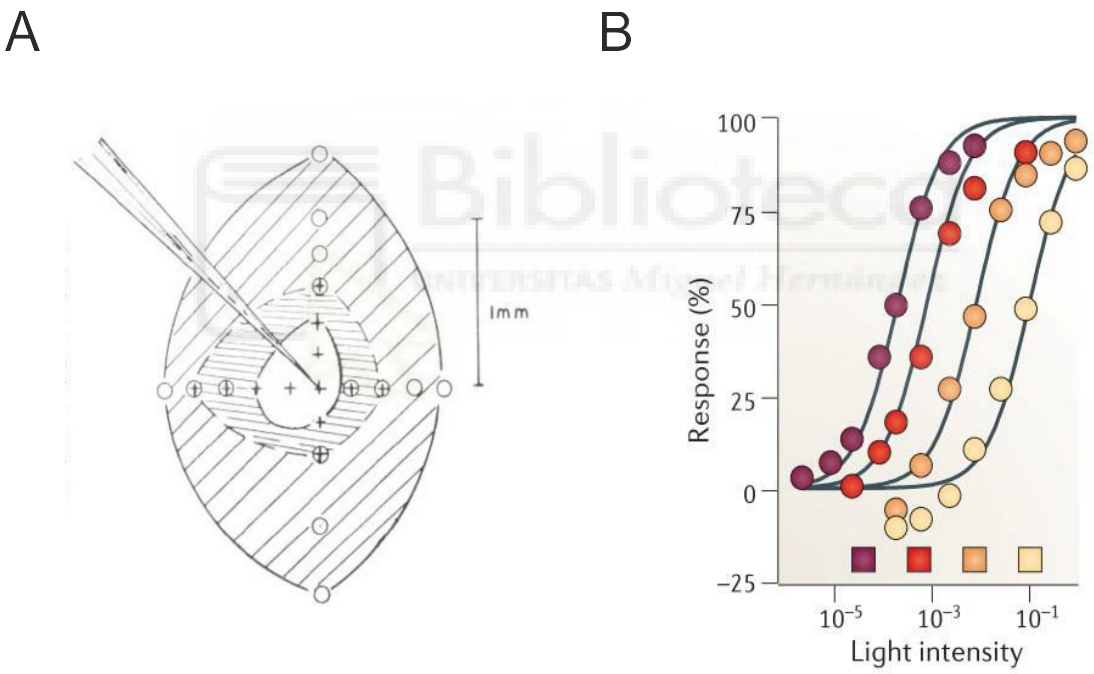

Figure 1.6. **Retinal ganglion cell RF properties**. **A**. Kuffer's recording of a center-surround RF from a cat On center RGC. The central region responded to increments in light intensity. The intermediate region (horizontal lines) had On-Off responses and the surround region (oblique lines) presented Off responses, adapted from (Kuffler 1953). **B**. Responses of a turtle cone photoreceptor at different light intensities – color coded in the figure from dark (purple) to bright (yellow) (adapted from (Carandini & Heeger 2011)).

The ability of photoreceptors and RGCs to normalize their response relative to their context is a canonical operation that appears to be performed by various regions of the brain called divisive normalization. (Carandini & Heeger 2011, Sakmann & Creutzfeldt 1969). When comparing the percentage of response of photoreceptors and RGCs at different degrees of luminance, it can be seen how the response curves shift their midpoints of response to the point of average luminance, adapting their dynamic range to different light intensities (Figure 1.6).

In addition to a more diverse set of spatial structures, RFs can also add a temporal dimension that allows them to generate a great diversity of feature selectivities to different stimuli. The most modern definition of RF is provided by Martínez, who defines it as a spatio-temporal filter that determines how the input is analyzed by each element of the visual system (Martinez, 2006). Therefore, RGCs can be classified according to their response to different types of stimuli. So, as noted before, according to their response to a stimuli of certain polarity, they can be classified as On, Off, or On-Off RFs. Regarding the temporal dimension, it is possible to differentiate between transient or sustained responses. Sustained RFs respond continuously through the duration of a stimulation while the transient RFs produce short duration responses at the beginning and with the withdrawal of the stimulus. Sustained responses are characteristic of carnivore X cells and primate parvocellular cells (P). With small center-surround RFs, they act as small spot or pixel detectors related to fine vision (Nelson & Kolb, 2004). On the other hand, transient responses are characteristic of carnivore Y cells and the primate magnocellular (M) cells; with bigger RFs, they are considered movement detectors (Masters 2014). X/P and Y/M cells are the classic and more studied retinal RFs, since there are prominently very present in the retinas of these animals (Mazade & Alonso 2017, Nassi & Callaway 2009, Seabrook et al 2017, Wassle 2004, Wassle et al 1981a, Wassle et al 1981b). However, the diversity of RFs does not end there, there are other feature selectivities for other signal components such as direction or orientation that intermingle to give 32 functionally different RGCs in mice (Baden et al., 2016) respect to the 20 functionally different RGCs found in primates (Dacey, 1999; Peng et al., 2019).

RGCs are optimally arranged to sample the environment forming functionally independent hexagonal mosaics, so that each mosaic is specialized in processing a certain feature of the visual field (Dhande et al 2015, Wassle 2004, Wassle et al 1981a, Wassle et al 1981b). Cat X cells are subdivided in two antagonistic and spatially independent On and Off tiles (Figure 1.7, A). XOn mosaics respond to bright spots and XOff mosaics respond to dark spots, both mosaics tile de retina hexagonally to cover visual space optimally. From the spatial statistical analysis of these mosaics several conclusions can be drawn. First, mosaics are quasi-hexagonal, not entirely stereotypical or crystalline structures. This implies that it is possible to predict the distance at which we will probably find the closest neuron, however, the exact position at greater distances is impossible to predict, so these tiles lack correlations at long distances. Second, the position and final structure of the mosaic is due to homotypic interactions between neurons (of the same mosaic) whose dendrites and somas compete for space (Diggle 2013, Eglen et al 2005, Wassle et al 1981a, Zhan & Troy 2000). As we will see later, this functional constraint related to optimal space coverage of two independent On and Off information channels has important consequences on the functional structure present in V1.

The types of RGCs and their arrangement along the retina varies across species whose RFs have specialized in detecting certain characteristics of the environment based on the ecological niche they occupy to extract the most relevant signals for their survival. The increased density of RGCs in different areas of the retina serves to emphasize the extraction of the most relevant information from their habitat (Figure. 1.7, B). Animals that live in plains, in open spaces, tend to have visual streak, that is, a denser strip of RGCs along the dorsal temporal axis of the retina, allowing them to oversample the horizon. This is the case of the rabbit, the cow, the agouti and the deer among other examples (Collin 2008, Hughes 1977). On the other hand, animals whose behaviors require greater visual acuities, such as chasing prey, making precise jumps, climbing trees…etc. Tend to have a higher density of concentric RGCs at some point (usually corresponding to the central axis of the visual field). Carnivores like wolves, in addition to visual streak, have an accumulation of receptors in the temporal part of the retina. Cats, on the other hand,

present an accumulation of RGCs in the central part of the retina called foveola, where the convergence between photoreceptors to RGCs is low (1: 3). Animals with a very high visual acuity such as primates and birds of prey have fovea, that is, a high concentration of RGCs in the central part of the retina where the convergence from photoreceptors to RGCs is 1:1, therefore, each RGC receives information from only one photoreceptor, which generates very small RFs, with great capacity of discrimination, favoring a high visual acuity (Baden et al 2020, Collin 2008, Hughes 1977).

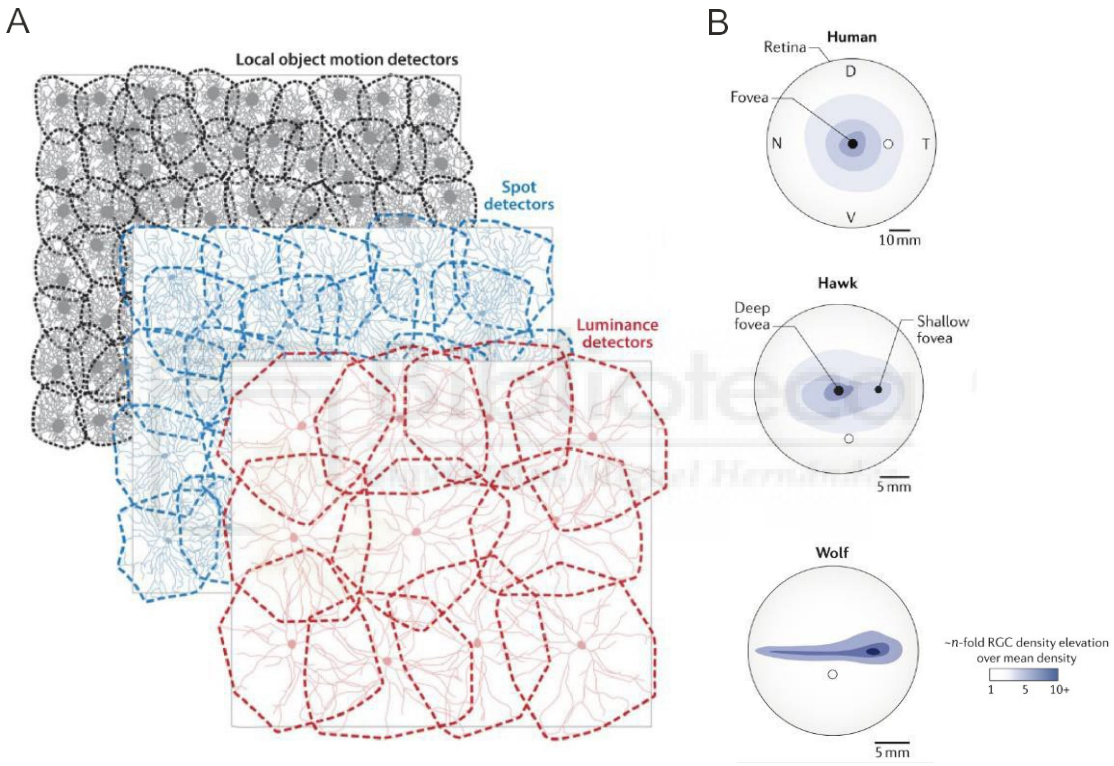

Figure 1.7**. RGCs distribution in the retina. A**. Functionally different RGCs form independent quasi-regular mosaics, adapted from (Dhande et al 2015). **B**. RGC density distribution in different species, adapted from (Baden et al 2020).

The proportion of different RGC types that tile the retina is also related to the environment of each specie. The W2 RGCs are the most numerous RGCs in mouse retina and are characterized for having fast responses to vertical stimuli. Very dense in the ventral part of the retina, they receive information from the upper visual field allowing to detect and escape quickly from aerial predators (Zhang et al 2012). On

the other hand, carnivores and primates have predominately X/P neurons sampling the central visual field and Y/M sampling the periphery. Their better visual acuity respect to mouse is also due to their overall smaller size of their X RFs compared to the functionally homologous XRFs of mice (Mazade & Alonso 2017, Nassi & Callaway 2009, Seabrook et al 2017, Wassle 2004, Wassle et al 1981a, Wassle et al 1981b).

In summary, we have different types of sensors (RGCs) distributed differently across the retina, specialized in extracting different components from the environment depending on the ecological needs of each specie.

On and Off channels

In many cases, the information transmitted by the RGCs is antagonic, that is, they extract a similar component from the environment (direction, spot detectors, orientation…etc), but of opposite light polarity (On or Off). As an example, X/P or Y/M cells can be divided in, Xon, Xoff, Yon, Yoff; forming four independent mosaics of information transmission. This is conserved across many species, including invertebrates, and the need for this split remains controversial (Gjorgjieva et al 2017, Gjorgjieva et al 2019, Gjorgjieva et al 2014, Schiller 1992, Westheimer 2007), however it is possible to find a simple and very plausible explanation to this problem.

The advantage of having antagonistic channels for a similar feature of visual space is to increase the dynamic range of the system due to the physical limitations of information transmission in neurons through the nervous system. Neuron axons are not good electrical transmitters; electrical signals cannot propagate passively a distance larger than 1mm. In such a way, that the information in the nervous system is processed differently at short and long distances. When information is passively integrated at short distances, it is done by excitatory or inhibitory graded potentials, where continuous information is integrated on-site. Thus, the neurons of some small invertebrates such as C. elegans (which do not measure more than 1 mm) and some areas of the nervous system whose components are very close to each other, such

as the retina, communicate through graded potentials. Furthermore, this is the only mechanism by which the dendrites of a neuron at any place of the nervous system can integrate the information of presynaptic excitatory and inhibitory axons.

On the other hand, the need to send fast and lossless information over long distances in larger species is done actively, consuming energy, through action potentials. The continuous information, that is, excitatory and inhibitory potentials, is integrated, and transformed into a discrete and homogeneous signal (action potentials or spikes), to send this information over long distances through its axons. However, action potentials have a clear disadvantage; they only transmit depolarizations through the axons. This means that most of the neurons of the nervous system receive information about the global level of activation of the presynaptic neuron, but the graduated inhibitory signals that have modulated the spikes get lost throughout the code. In other words, a neuron cannot transmit information in opposite directions (excitation and inhibition) through long distances, which obviously decreases its sensibility and dynamic range of information capacity and transmission. This is probably one of the main reasons why inhibition is generated de novo through interneurons at each stage of the EVP.

Since neurons can only transmit information in one direction it is easy to understand the benefits of sending similar information in channels that respond to an opposite polarity. Let us do a simple mental experiment to demonstrate this and introduce some basic concepts of information theory. Imagine a neuron of a very small organism that detects different luminance levels in a world where all the possible values of luminance are equally probable and discrete, ranging from 1 to 10. 1 for completely dark, 5 for gray and 10 for maximum brightness. Using Shannon´s information theory equation (Barlow 1961, Rieke et al 1996, Shannon 1948) we can easily quantify the information understood as the logarithm (in base 2) of all the possible states the system can occupy.

$$S = -\sum_{i=1}^{k} p_i \log_2 p_i \text{ (bits)}$$

Where p_i is the probability of appearance of each luminance value and K is the number of possible states the system can occupy. So in our case K=10 and the probability of appearance of each luminance value p_i (ranging from 1 to 10) is equally probable so $p_i=1/K$. That said:

$$S= -\sum_{i=1}^{k} \left(\frac{1}{K}\right) \log_2 \left(\frac{1}{K}\right) = \log_2 K \text{ (bits)}$$

Where one bit is the information required to choose from two equally likely alternatives. So in our world the total amount of information is $\log_2(10)$ =3.32 bits.

At the beginning our neuron could send 10 different messages (3.32 bits) based on a exciatory-inihibtory code. Excitatory (very bright=10), inhibitory (very dark=1) and silent (gray=5). However, as the organism grew the need to send information at long distances through action potentials appeared. At this point, regardless of the type of code that our imaginary neuron uses, that is, if it is a rate code or a temporal code (Rieke et al 1996), because the spikes are homogeneous, the sensitivity of my detection system will be determined by the maximum number of action potentials that can be sent in a reasonable amount of time so that the information can be processed as quickly as possible and does not harm the survival of the organism. Even neglecting this time constraint, the fact now is that it can only send excitatory information, which reduces the capacity of our neuron by half, to 5 different messages, that is $\log_2(5)$ = 2.32 bits. So clearly the system will miss a lot of details of the outside world. To overcome this problem our organism now evolves and instead uses two neurons, one specialized in detecting low levels of luminance from 1 to 5 (2.32 bits) and another one for high levels, from 6 to 10 (2.32 bits), exceeding the information capacity of the outside world (4.64 bits).

Projections of the optic nerve

The axons of the RGCs form the optic nerve and leave the retina reaching the optic chiasm. At this point many fibers cross to the other side (contralateral fibers), while others stay on the same side (ipsilateral fibers) (Herrera et al 2003, Herrera et al 2019). Once passed the optic chiasm, the contralateral and ipisilateral information projects to about 46 different nuclei (Dhande et al 2015). The functions of these nuclei can be related to the type of information they receive from the RGCs and they can be divided into two large groups. Firstly, the non-image forming pathways responsible for circadian rhythms, control of pupillary and lens reflexes, and retinal image stabilization. Secondly, the image forming pathways, formed mainly by the superior colliculus (SC)-pulvinar pathway and the dorsolateral thalamus pathway (dLGN)-V1, responsible for object recognition and correct spatial navigation in the environment (Petry & Bickford 2019, Seabrook et al 2017). In summary, visual information travels to different nuclei of the nervous system specialized in processing different components of the visual environment due to the combination of afferents received from different types of RGCs (Figure 1.8).

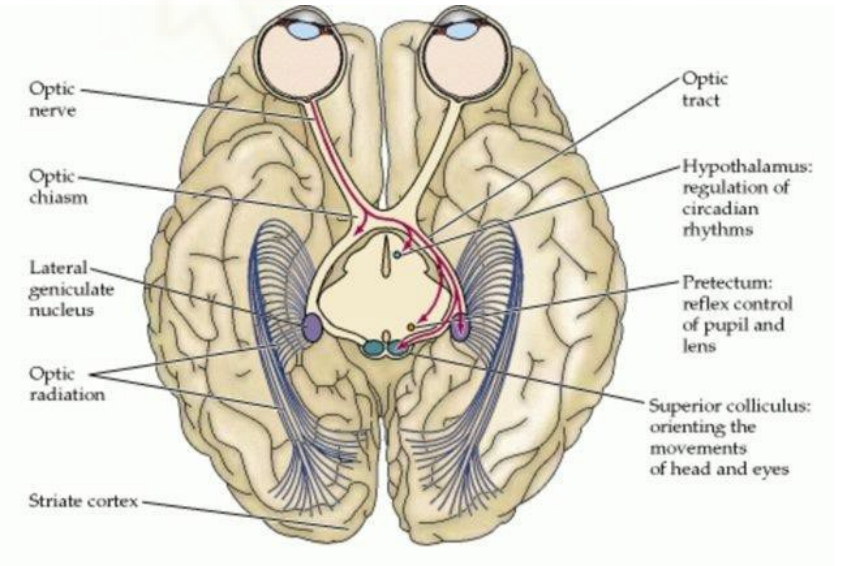

Figure 1.8. **Central projections of RGCs in humans**, adapted from (Gerhard 2013).

Crossed and uncrossed fibers

The percentage of RGC with contralateral and ipsilateral axons crossing the optic quiasm is directly proportional, at least in mammals, to the degree of binocular vision of each species. Primates, whose degree of binocular vision is superior to carnivores and rodents, are the ones with the most ipsilateral RGCs. In humans, the ratio of contra and ipsi fibers is 60:40, whether in mice is 97:3 (Figure. 1.9). Other species with a more panoramic vision such as zebrafish or chicken, totally lack ipsilateral fibers (Herrera 2018, Herrera et al 2003, Seabrook et al 2017). The information from each eye is transmitted segregated until it reaches V1 where it integrates to form binocular neurons.

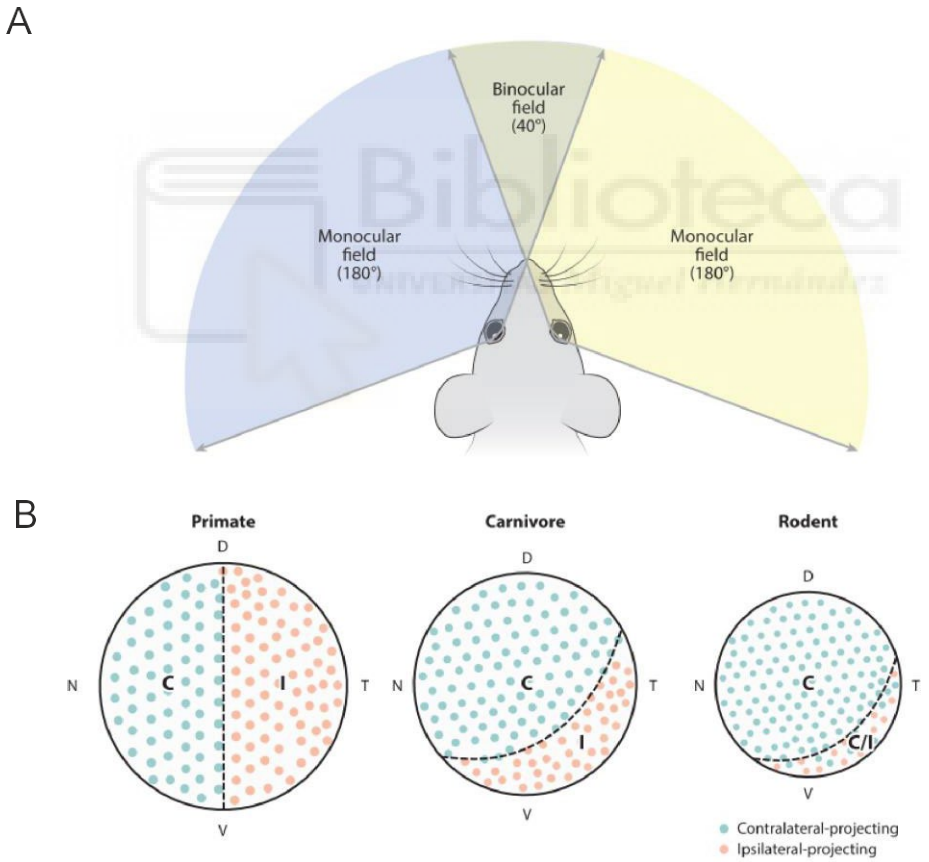

Figure 1.9. **Relationship between the degree of binocular visual field and the proportion of contralateral or ipsilateral projecting RGCs. A**. Mouse visual field. **B**. Distribution of contralateral (green) and ipsilateral (red) RGCs in primates, carnivores and rodents. Adapted from (Seabrook et al 2017).

The reason why axons cross the chiasm to finally connect with the opposite hemisphere in the cortex is an important question to address, due to the great metabolic cost of developing longer axons. First of all, it should be noted that in the vertebrate nervous system there are numerous decussations, the information from the extremities crosses to the opposite side in the medulla, and so does the motor information. In such a way that the left hemisphere governs the extremities on the right side and vice versa. Around 98% of animal species show bilateral symmetry (Herrera 2018), that is, their body organization is more or less symmetrical and many of the components of the nervous system are duplicated. It is a highly successful evolutionary trait, since it defines an axis of movement in animals and favors cephalization.

Bilateral symmetry together with the appearance of extremities that receive independent information throughout evolution, may explain the presence of the many decussations found in the vertebrate nervous system, since, at some point, the information of those duplicate components needs to be integrated (Banihani 2010, Herrera 2018). If all the connections of the nervous system were ipsilateral, we would have two separate nervous systems, our body would be governed by two independent brains with no communication between them (Banihani 2010). The multiple decussations throughout the nervous system and the large bundle of fibers that form the corpus callosum connecting both hemispheres highlight the importance of correctly integrating bilateral information in the nervous system.

However, this explanation is insufficient to understand the reason for a higher percentage of contralateral fibers in the EVP. Since there are no connections between the left and right dLGN, the information is not integrated until it reaches the cortex. Therefore, what is the reason for decussating the information of each eye in the optic chiasm and sending it to the opposite hemisphere, with the consequent energy cost? In other words, why not send everything ipsilaterally, save wire and integrate in the cortex?

A convincing hypothesis already proposed by Cajal and refined by other authors (Capozzoli 1995) is that the visual system has exerted pressure in this

direction due to the inversion of the retinal image, caused by the appearance of eyes with lenses and pupil throughout the evolution, characteristic of many chordates and invertebrates. These types of eyes impose a functional constriction that the visual system faces from the beginning, that is, the inversion of the retinal image when light passes through. The retinal image is inverted 180º, so in order to have congruent retinotopic maps, that is, continuous in the two hemispheres of V1, it is necessary for the information to cross. If not, there would be a discontinuity of the visual projection in both hemispheres (Figure 1.10). Therefore, this cross is responsible for a continuous and ordered image in V1 easier to process. Thus, this functional constriction imposed by the visual system invited the rest of the sensory and motor systems to adapt. If the visual information arrives crossed, the motor information must cross to activate the extremity closest to the eye that informs it, just as the sensory fibers of the extremities must cross to send the corresponding information to the extremity closest to the eye. Thus, integrating sensory and motor information in the same hemisphere, reduces reaction times, which will favor the survival of an individual by being able to respond quicker to changes in the environment.

Topographic maps, that is, continuous and ordered maps of sensory information, are a constant in the nervous system (Chklovskii & Koulakov 2004, Gerhard 2013): there are tonotopic (sound), somatotopic (tactile), retinotopic (visual)…etc. The importance of having maps of organized information may be due to different factors as we will see later. What is clear is that they are present in all the mammals studied, so it is obvious that it is a functional constraint for the proper functioning of the nervous system.

Finally, it is important to add that fiber crossing in the quiasm it is not the only way of integrating information in the cortex. In moles the independent information of each nostril integrates through interhemispheric connections and it is imperative for them to use this finer odor activation temporal keys to detect correctly the exact position of their food (Catania 2013). Following this line of thought, in the visual system, the corpus callosum and the anterior commissure also

seem to have an implication in synchronizing both hemispheres for the development of binocular vision (Olavarria 2001, van Meer et al 2016).

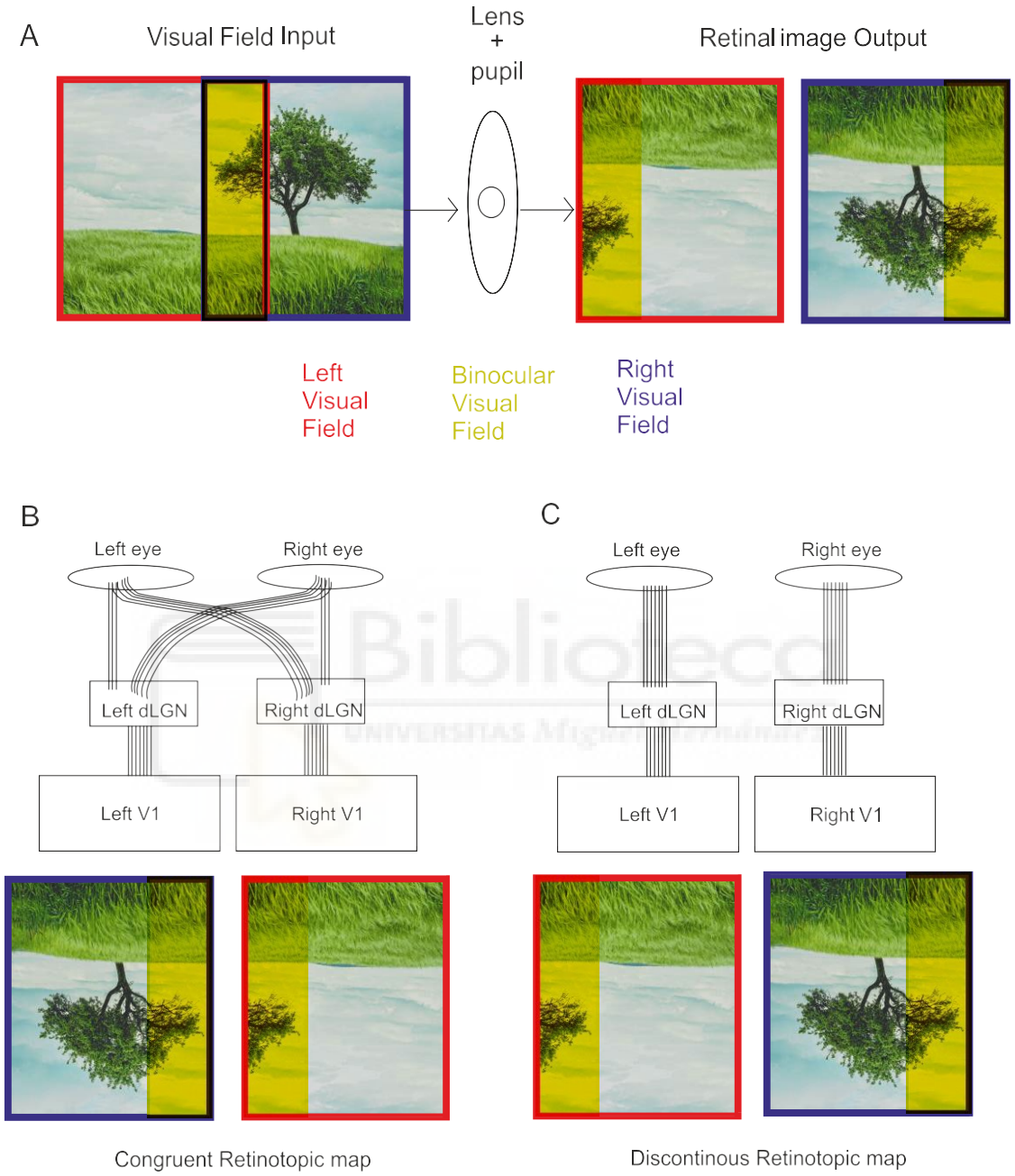

Figure 1.10. **Importance of contralateral crossing fibers in the Early Visual Pathway**. **A**. Visual field input received by the eye. The red box represents the left visual field, the blue box the right visual field and in yellow the binocular visual field. As the light crosses the lens and the pupil, the retinal image that gets to the left and the right retina is inverted 180º. **B.** Congruent and continuous retinotopic map when fibers cross to the opposite hemisphere. **C**. Discontinuous retinotopic map if all fibers where ipsilateral.

The Superior colliculus and the dorsal thalamic nucleus

The superior colliculus (SC) is a multilayered structure located below V1, derived from the optic tectum of reptiles, amphibians, and birds. (Dhande et al 2015). In the SC, the integration of ordered sensory information in each of it layers (auditory, visual…etc) is related to controlling the orientation of the head and eyes, to saccades and to rapid evasion behaviors among others functions (Dhande et al 2015, May 2006). In contrast, sensory integration in the EVP, requires more processing stages and it is done in the associative areas of the cortex.

The SC-pulvinar pathway provides general information about the environment. It serves to locate and orient respect to objects in the visual field. On the other hand, the dLGN-V1 pathway is in charge of computing specific details of the environment and serves the function of object identification and conscious development of sight (Petry & Bickford 2019). These two separate functions become clear in " Blindsight" patients. Here patients with lesions in V1 can respond to the presence of objects without being conscious of their presence (Stoerig & Cowey 1997).

As previously mentioned, there is a direct relationship between the size of the dLGN and V1 and the degree of visual acuity (Figure. 1.4; Table 1). Thus, mammals whose behavior requires a high visual acuity, such as carnivores and primates, have a larger size of V1 and dLGN in relation to their weight compared to rodents. Rodents, on the other hand, are more collicular animals, they do not focus their processing so much on solving fine details of the visual field, but on quickly detecting changes in the environment and generating rapid movements of evasion against predators (Dhande et al 2015, Mazade & Alonso 2017, Seabrook et al 2017). Thus, for example, the most numerous RGCs in mice (W3 RGCs), related to evasive behavior against aerial predators, projects mainly to SC and not to dLGN (Baden et al 2016, Roman Roson et al 2019, Zhang et al 2012). This is a big difference compared to carnivores and primates, where the retina is mainly made up of concentric RFs to solve fine details and where most of the projections go to dLGN (Alonso et al 2001, Nassi & Callaway 2009).

Another example that shows the different specialization of SC-pulvinar and dLGN-V1 can be observed when comparing the relative size of V1 and the SC across different species with different degrees of visual acuity (Table 2). The tree shrew, a prosimian of the order scadentia, has a Striatum griseum surface (SGS) - that is, the most superficial layer of the SC that together with the immediately inferior layer called stratum opticum receives all the retinal eferents-, whose volume is half the size of its V1 and 6 times greater than its dLGN. In comparison, a monkey's dLGN is 5 times the size of its SGS (Petry & Bickford 2019). Animals that put emphasis on their visual acuity have emphasized the dLGN-V1 pathway in comparison to the SC-pulvinar pathway.

Structure-function-ecological niche relationship

I would like to briefly emphasize the close relationship seen until know between the size and function of the different components that process visual information and the ecological needs of each specie. Up to know there are clear examples such as eye size, retinal area, RGCs types, dLGN and SC size. Throughout the text we will find other examples, demonstrating the important information that comparative neurobiology can provide us about the visual system.

The size of the different sensory areas in the cortex is clearly related to the biological needs of each specie (Figure 1.11). Carnivores and primates have clearly bigger visual areas in relation to their somatosensory areas compared to mice, that clearly devote their energy to their somatosensory areas. However, highly visual rodents such as the squirrel have a much bigger visual cortex. Even closely related species show clear differences due to their different lifestyles. Thus, the arboreal tree squirrel has more cortex devoted to visual areas than the terrestrial ground squirrel which in turn has larger somatosensory areas than the tree squirrel.

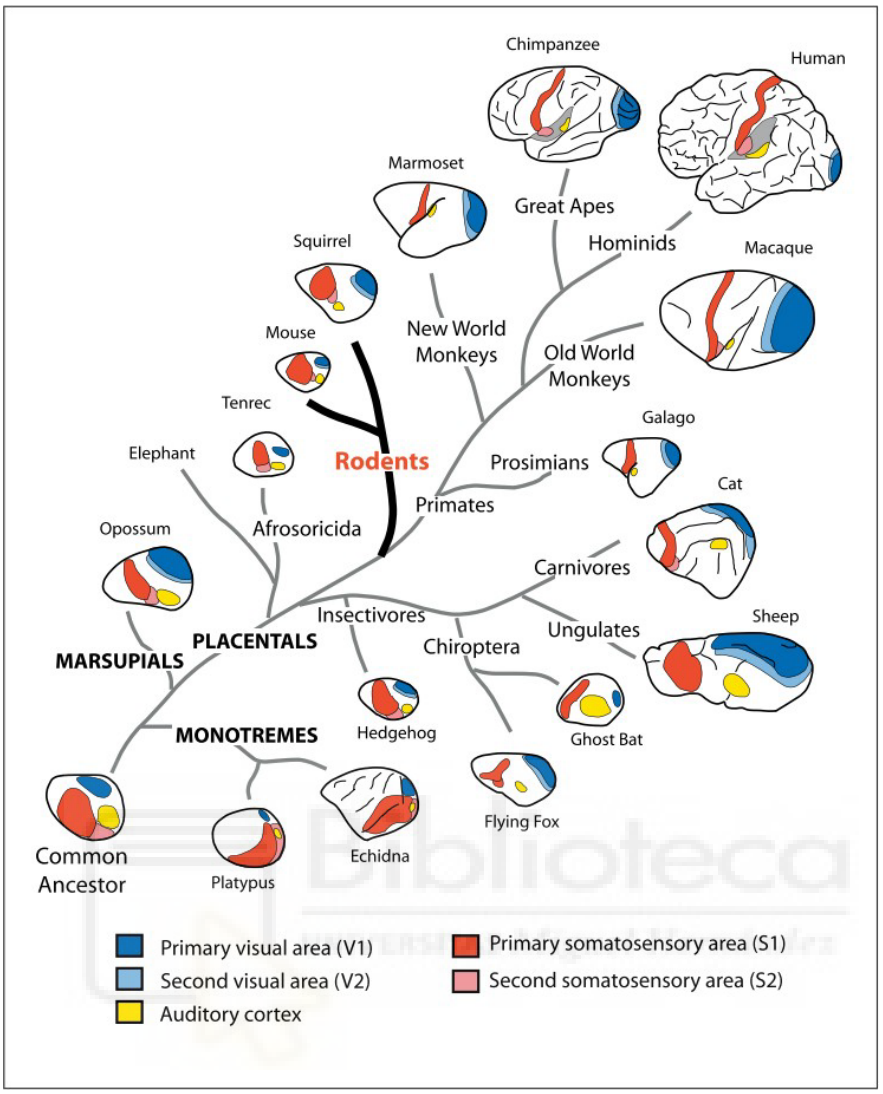

Figure 1.11. **Size of primary and secondary areas across different species**, adapted from (Krubitzer et al 2011).

Even differences between animals from the same species have been reported. The Norway laboratory rat has a bigger somatosensory cortex compared to a wild Norway rat which in turn has a bigger auditory cortex (Campi et al 2011, Campi & Krubitzer 2010, Krubitzer 1995, Krubitzer et al 2011).

These observations clearly highlight two points. First of all, the cortex is very plastic and can evolve and change swiftly. Second, these changes are not free and always come at a cost, so increasing the computation power of a sensory area is always done at the expense of another cortical region.

The lateral geniculate nucleus

The dLGN has 3 basic functions: First, by converging and diverging the information from various RGCs it generates more complex and diverse RFs. Second, by feedforward inhibition it retrieves the inhibitory information that cannot be transmitted through the axons of the RGCs. Third, it modulates the relevance of the visual information transmitted to V1.

The information from the different types of RGCs travels in parallel, with little crosstalk between functionally different channels until it reaches the visual cortex. In the dLGN the overall level of compartmentalization is higher in carnivores and primates compared to rodents. On the one hand, there is a marked citoarchitectonic segregation of the ipsilateral and contralateral fibers, that forms very marked and precise layers in carnivores and primates. Rodents, in comparison, have a laxer layering with two simple subdivisions, the shell where ipsilateral and contralateral axons arrive, and the core that only receives contralateral afferents. In fact, unlike carnivores or primates binocular cells that respond to both eyes can be found in the dLGN of mice (Rompani et al 2017).

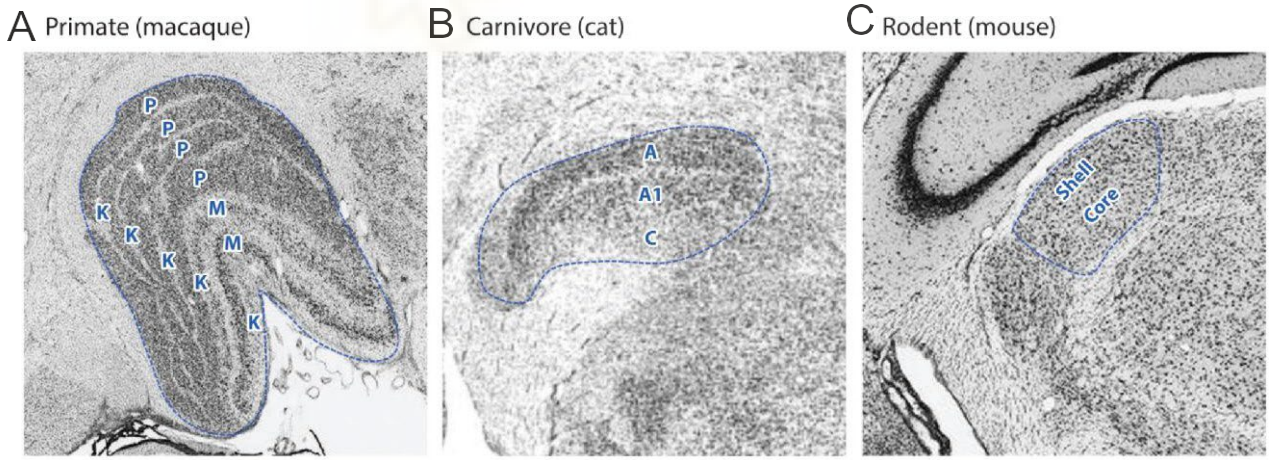

Figure 1.12. **Citoarquitecture of the dLGN A**. macaque, **B**. cat and **C**. mouse. Parvocelular (P), Magnocelular (M) and Koniocelular (K). Adapted from (Seabrook et al 2017).

On the other hand, the functional types of RGCs (X/P, Y/M…etc) that innervate dLGN are also compartmentalized in marked cytoarchitectonical layers (Figure 1.12). The macaque has a clear lamination of its main RGCs, that is, a parvocellular (P), magnocellular (M) and koniocellular (K) layers. (Gerhard 2013, Nassi & Callaway 2009) - the latter related to trichromatic vision of primates-. In cats there are fewer layers, although they are still very marked and segregated for its main RGCs types. Layers A and A1 receive most of the X RGCs and some Y RGCs. Layer C receives mainly Y RGCs and W RGCs (all those RGCs that have RFs different from X or Y cells are classified as W) (Martinez & Alonso 2001). Despite the weak lamination observed anatomically in mice, the different types of RGCs are arranged in separated layers, this can be functionally checked by the fact that each lamina of functionally different RGCs has its own retinotopic map (Seabrook et al 2017).

The crosstalk between different excitatory RGCs types in the dLGN is practically null in carnivores and primates, whereas there is convergence between different types of RGCs in rodents. In cats, the X RGC: dLGN convergence ratio is 1:3, that is, each neuron of the dLGN receives an average of 3 contributions from similar X RGCs (Martinez et al 2014) . In mice, however, the convergence ratio is 1:5. The response of a dLGN neuron can be modulated as a combined response of 5 different RGCs types (Roman Roson et al 2019). Furthermore, it is possible to differentiate in mouse between relay mode neurons, which receive inputs of the same type of RGCs, and combination mode neurons that mix information from different types of RGCs (Liang et al 2018). However, the convergence between excitatory X cells of the same polarity in cat generates a richer diversity of RFs that improves coverage of visual space, visual acuity and signal-to-noise ratio. Thus the linear interpolation of inputs from RFs with similar functional properties can improve information transmission in the EVP (Martinez et al 2014). In summary, both the greater diversity of RGC types in rodents, together with their lower specificity of connections to the thalamus, generates a greater diversity of RFs in the dLGN compared to carnivores and primates (Figure.1.13), that instead have a lower diversity of RFs in the retina where most RFs are concentric, small and with transient or sustained responses

(X/P, Y/M), as an evolutionary strategy to develop high visual acuities (Nassi & Callaway 2009, O'Brien et al 2002, Rathbun et al 2016).

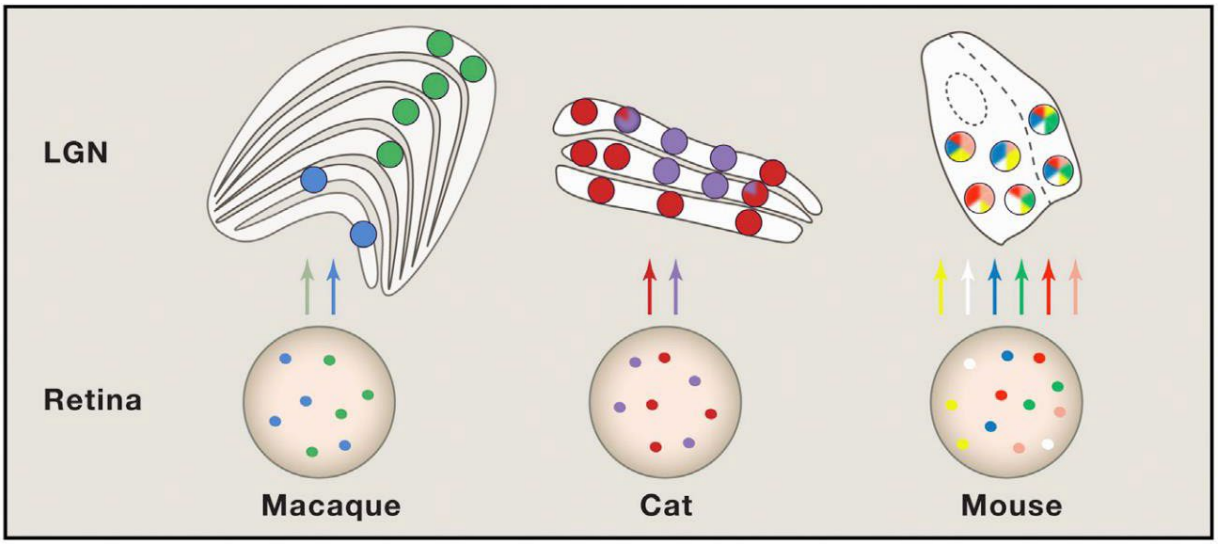

Figure 1.13. **Organization of Visual Streams in Different Species**. Mouse has a higher diversity of RFs types in the retina and the dLGN in comparison to the cat and macaque. Adapted from (Chen et al 2016).

dLGN inhibition

As the Pull cannot be transmitted along the axon, the inhibition must be generated de novo in each EVP station, that is, in the dLGN and in the cortex by means of feedforward inhibition. To generate a new push-pull structure of the RF using feedforward inhibition, it is very useful to have two similar channels with antagonistic information whose RFs of different polarities overlap in space and sample the space in a regular way. Thus, in cat, XOn and XOff RGCs, can once again generate a push-pull structure in the relay cells by crosstalk between the On and Off pathways mediated by interneurons. The push, is transmitted directly and parallel to the dLGN. From here the interneurons of the dLGN connect with the relay neurons of opposite sign but with overlapping RFs in visual space resulting in a closed push-pull circuit (Hirsch et al 2015, Martinez et al 2014) (Figure 1.14). The push-pull

structure has the function of increasing the dynamic range of the signal, to enhance visual sharpening and to reduce the redundancy of the message (Hirsch et al 2015).

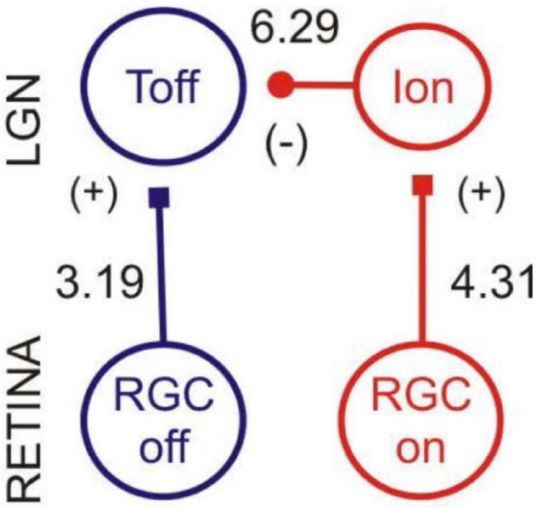

Figure 1.14. **Scheme of push-pull circuit in the dLGN for a relay off neuron** (Toff). Numbers represent the mean convergence from RGCs to excitatory relay cells and interneurons (Ion) of opposite sign. Adapted from (Martinez et al 2014).

Finally, the dLGN can modulate the way the signal is transmitted as a function of the behavioral state. Thus, the dLGN can switch between tonic and bursting mode. In tonic mode, the neurons of the dLGN fire replicating the signal from the RGC input. On the other hand, high-frequency action potential trains are called bursts. This type of modulation is related to the transition between sleep (bursting mode) and wakefulness (tonic mode), or to accurately signal and transmit relevant changes in an individual's visual field through bursts (Hirsch et al 2015, Sherman 2016, Sherman & Guillery 1998).

Driver and Modulatory synapsis

In the retinothalamic circuity and in other parts of the nervous system, synapsis can be classified as drivers or modulators. Sherman (Sherman & Guillery 1998) defines as drivers the inputs that define the basic RFs properties of a postsynaptic cell, while modulators alter the probability of certain aspects of transmission. In the case of the visual system, the inputs from the RGCs innervating the dLGN act as drivers, while the modulating inputs can come from layer 5 and 6 of the cortex, the reticular nucleus of the thalamus, and other nuclei of the nervous system. Modulatory synapses make up the bulk of the circuit while RGC drivers generate only 7% of all synapses. However, it is the drivers that have more weight in the transmission of the function to V1 because their synapsis are located closer to the soma. Thus, inactivation of small areas of the dLGN can silence V1 activity, despite the fact that most of the modulatory connections are still intact (Martinez & Alonso 2001).

The Primary Visual Cortex

The primary visual cortex combines and integrates sensory information generating RFs with new spatio-temporal characteristics. This is achieved thanks to the increase in the number and diversity of excitatory and inhibitory neurons as well as a greater interconnectivity between the components.

Anatomy

The mammalian telencephalon is made up of 80% of excitatory neurons and 20% of inhibitory cells (Harris & Shepherd, 2015). Unlike the quasi-regular structure of the retina, the cortex is intrinsically more variable, with many differences across species and between different cortical areas. Furthermore, it is

made up of a great diversity of excitatory and inhibitory neurons whose morphological, genetic, functional and connectivity criteria are broad and difficult to define (Binzegger, Douglas, & Martin, 2004; DeFelipe et al., 2013; Harris & Shepherd, 2015) which makes it quite impenetrable to have a clear drawing of it. However, despite this high complexity, its anatomical structure can be described by the location of each of these components and their connections. Its structure, despite varying between different species and orders, has certain common features that are repeated throughout the phylogeny.

First of all, most excitatory neurons are glutamatergic, have a pyramidal morphology (basal short dendrites in the soma and a long apical dendrite) and generate local and long-range connections. On the other hand, interneurons are GABAergic and tend to have a more local and nonspecific degree of connectivity. (Harris & Mrsic-Flogel, 2013).

Secondly, there is a clear columnar and laminar structure. Vertically and within a radius of about 50 um, we find strongly connected neurons forming minicolumns (DeFelipe et al 2002, Kaas 2012a). Each of these small columnar units repeat and clump together, generating fundamental processing units throughout the cortex. On the other hand, the different neurons, inputs and outputs of the minicolumns are distributed in a stereotypical way, allowing them to be generically grouped in 6 layers along the horizontal and vertical axis (Douglas & Martin 2004).

Layer 4, also called granular layer, is very characteristic of primary sensory areas such as V1 and is the main thalamorecipient layer (J. A. Hirsch & Martinez, 2006b; Kremkow & Alonso, 2018; Smith & Populin, 2001). It is made up of essentially two types of excitatory neurons; pyramidal and stellates (Harris & Mrsic-Flogel, 2013; Smith & Populin, 2001). Stellates are more compact and are generated from pyramidals that lose their apical dendrites during development (Callaway & Borrell, 2011). The proportion and total amount of these neurons varies depending on the cortical area and across species. Primate and carnivores' V1 layer 4 is populated by stellate cells, while rodent layer 4 is made up of pyramidal cells (Smith & Populin, 2001). In addition, layer 4 varies a lot across different species due to the different

ways it integrates the thalamic afferents, with clear distinctive anatomical features between species and across different regions of the cortex.

Third, there is a stereotyped flow of excitatory information between layers in carnivores, rodents and primates (Figure 1.15). The dLGN fibers innervate mainly layer 4 and 6. Layer 4 neurons, in turn, send information to layer two 2/3 (J.-M. Alonso & Martinez, 1998). From there, layer 2/3 neurons send long-range connections to other layer 2/3 neurons, to other cortical areas and to layer 5. From layer 5 information flows to other layer 5 neurons, to layer 2/3, to diverse subcortical nuclei and to layer 6. Layer 6 sends feedback connections to the thalamus and to the other cortical layers. For more details, see (Douglas & Martin, 2004; Harris & Mrsic-Flogel, 2013; S. D. Van Hooser, 2007).

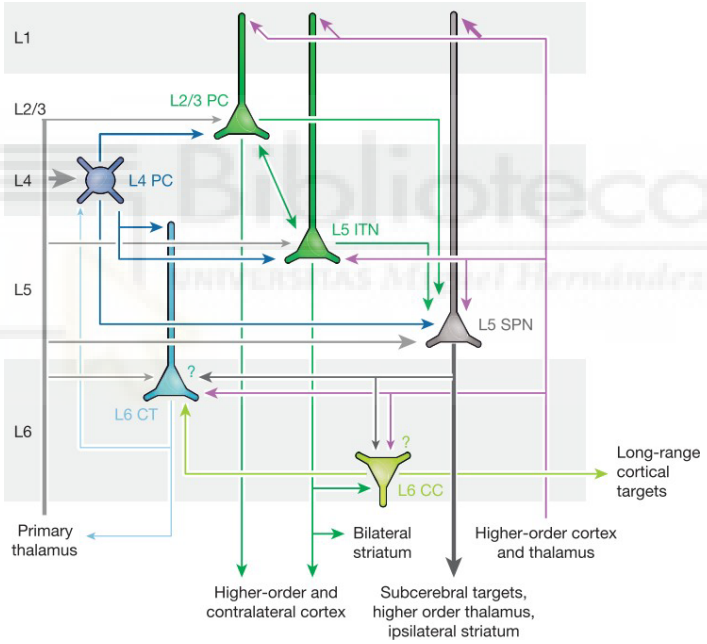

Figure 1.15. **Flow of information from main types of cortical excitatory neurons**. The width of the arrows relates to the more dominant connections. Adapted from (Harris & Mrsic-Flogel 2013).

Despite this series of distinctive features, there are differences in the lamination pattern and width of each of these layers between different species. So, on the one hand, there are certainly differences in the anatomical subdivisions of

each layer across different mammalian orders and suborders (Figure 1.16). (DeFelipe et al., 2002; Kaas, 2012b). On the other hand, the relative width of each layer is different in carnivores, rodents and primates and variations can be observed even across different cortical areas. Thus, for example, the sensory areas that receive a greater amount of thalamic input have a larger layer 4 size compared to motor regions (DeFelipe et al., 2002; Hutsler, Lee, & Porter, 2005).

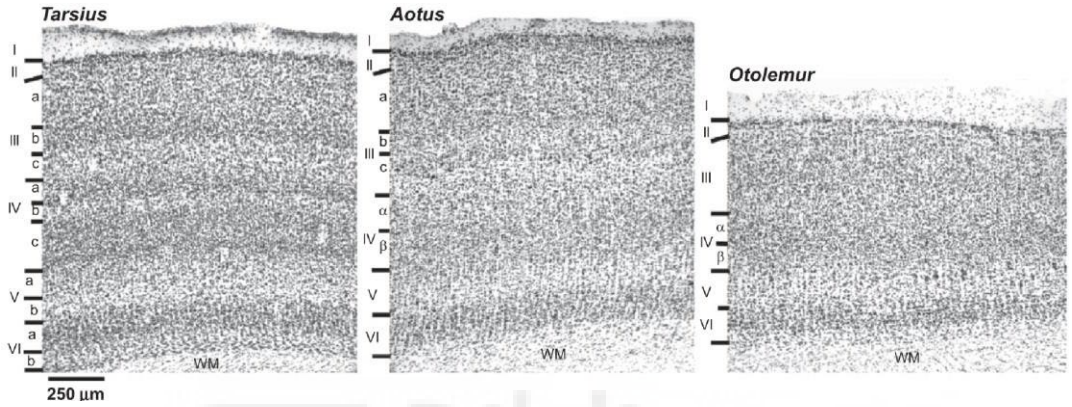

Figure 1.16. **Different lamination patters from different primate species**. Adapted from (Kaas 2012b).

There is an intense debate regarding the homogeneity or heterogeneity of the cortical structure in different mammalian species. The question is not trivial at all and the answer has very important consequences to explain if the differences between function and behavior of each species are due to a different cortical assembly or rather to an increase or decrease in the number of neurons grouped in stereotyped functional blocks (columns).

On the one hand, there are experiments that maintain that the total number of neurons under 1 mm^2 of cortex remains stable in mammals, whereas what increases the thickness of the cortex in different species is the number glial cells (Carlo & Stevens, 2013; DeFelipe et al., 2002; Rockel, Hiorns, & Powell, 1980). This uniformity supports the direct relationship between the total number of neurons and the speed by which information is transmitted along the axons with the level of intelligence of

each specie (Roth & Dicke, 2005). It also relates to evolutionary theories that postulate that the evolution of the neocortex is due to the radial addition of similar functional modules, that is, of columns (Rakic, 1988).

On the other hand, other studies, contradict this uniformity regarding the number of neurons and the degree of connectivity between them. The number of neurons under 1 mm^2 of cortex may be different across mammalian species (DeFelipe et al., 2002; Herculano-Houzel, Collins, Wong, Kaas, & Lent, 2008), which totally contradicts the previously mentioned studies.

Also, the ratio between white matter and gray matter is higher in rodents compared to primates. Rodents have a greater amount of fibers interconnecting the components of the cortex while primates, on the other hand, save wire and manage to compact a greater number of neurons in a smaller volume (Ventura-Antunes, Mota, & Herculano-Houzel, 2013). This has consequences in the overall organization of the circuit. Rodents are organized as uniform or dense networks, where all components tend to be connected to each other. While primates are organized as small world networks, with a majority of short-distance connections and sparser long-range connections (Kaschube, 2014; van den Heuvel, Bullmore, & Sporns, 2016; Ventura-Antunes et al., 2013).

Finding similarities and differences in the cortex of different species is essential to describe the basic elements and the connections that compose it. The biggest problems when extracting the canonical elements from the cortical circuitry come from the difficulty of classifying the great diversity of its components, as well as their intrinsic variability. To classify it, it is essential to distinguish between variability and real differences. For this, it is necessary to observe the cortex at different scales and determine what level of detail is adequate to explain a certain phenomenon. It is very difficult, if not impossible, to describe and classify the elements of the cortex anatomically without taking function into account. Relating the anatomical structure with the electrical response of the neurons allows to distinguish between variability and clear anatomical differences, making it possible to generate models that explain the basic computations that the system is carrying

out. It is in these search of these differences, where we can find answers to what is common and describe how the cortical circuit works.

Parallel pathways in rodents, carnivores and primates

The great diversity of RFs can be classified into 3 large parallel and homologous routes of information transmission that reach V1; The P, M and K pathways in primates, related to the X, Y and W pathways in carnivores and rodents (Kremkow & Alonso 2018, Van Hooser 2007). The X/P and Y/M pathways are made up of concentric RFs with transient or sustained responses respectively. The W/K has neurons with RFs that respond to a much more diverse set of feature characteristics. They can range from RGCs selective to direction and/or orientation to blue opponent cells related to primate trichromatic vision (Seabrook et al 2017, Van Hooser & Nelson 2006). These pathways are different between species because they clearly have a different diversity and proportion of RFs. However, there are certain neurochemical and functional homologies that allow them to be grouped into 3 well-defined homologous groups (Kremkow & Alonso 2018, Seabrook et al 2017).

On the one hand, despite the lower lamination of the dLGN in mice, the Core receives concentric RFs (larger than those from carnivores and primates) with transient and sustained responses. This allows to group these channels into the X/P and Y/M pathways (Roman Roson et al 2019, Seabrook et al 2017). In all mammals, the axons of these pathways lead mainly to V1's layer 4 and to a lesser extent to layer 6. In carnivores there is a large part of Y fibers that project directly to V2, which makes some authors to consider it a primary visual area (Van Hooser & Nelson 2006, White et al 1999).

On the other hand, the tremendously diverse W/K pathway in mouse projects to the dLGN shell and relates to the C and K layers of the dLGN of carnivores and primates respectively (Baden et al 2016, Chen et al 2016, Roman Roson et al 2019, Seabrook et al 2017, Van Hooser & Nelson 2006). The W/K, unlike the X/P and Y/M, projects

to the upper layers of the cortex (Layers 2 and 3). In carnivores and primates these afferents form dense “blobs” rich in cytochrome oxidase, while in rodents these projections to the superficial layers are more diffuse (Van Hooser 2007).

Finally, layer 4 shows certain differences in how it segregates its inputs. In primates, there is a clear segregation of the M afferents that project to a more superficial zone of layer 4 (4Cα), while the P afferents project to deeper zones (4Cβ). In carnivores there is some X/Y segregation, but it is clearly more diffuse. In tree shrews there is no segregation of the M or P pathways, but there is a clear segregation in On/Off polarity neurons. Off cells occupy the deepest layer and On cells the upper layer 4. (Hirsch & Martinez 2006b, Van Hooser 2007). In rodents, on the other hand, there are no marked segregations, which is consistent with a greater crosstalk between pathways already present at the dLGN level.

V1 function

When classifying the components of the cortex functionally, we are faced with the same problems as when doing it from an anatomical perspective. That is, deciding which criteria we to use to describe them to correctly define the relevant differences between neurons.

Kuffler's (Kuffler 1953) studies related the functional microstructure of the RFs, obtained using simple stimuli, that is, small points of light, with the overall function of the neuron when faced with more complex visual stimuli. Following this line of thought, in 1962 Hubel and Wiesel mapped the cat´s V1 RFs (Hubel & Wiesel 1962) with simple stimuli and saw that the RFs functional structure was different from the concentric RFs present in the dLGN. These new RFs form elongated subregions of On and Off polarities that gives them a new feature selectivity, the ability to respond to a preferred orientation (Figure 1.17). In such a way, that the strongest response appears when stimulating the RF with a bar positioned over the subregion with a similar polarity. So, for example, a white bar triggers the firing of the neuron when positioned over the elongated On subregion of the RF and

decreases the activity when positioned over the elongated Off subregion of the RF. Thus, the RFs respond to a bar of a certain orientation located in a concrete region of visual field, and the response decreases when the stimulus moves away from that orientation. They named these neurons "simple cells", since their response could be predicted from their RFs functional structure.

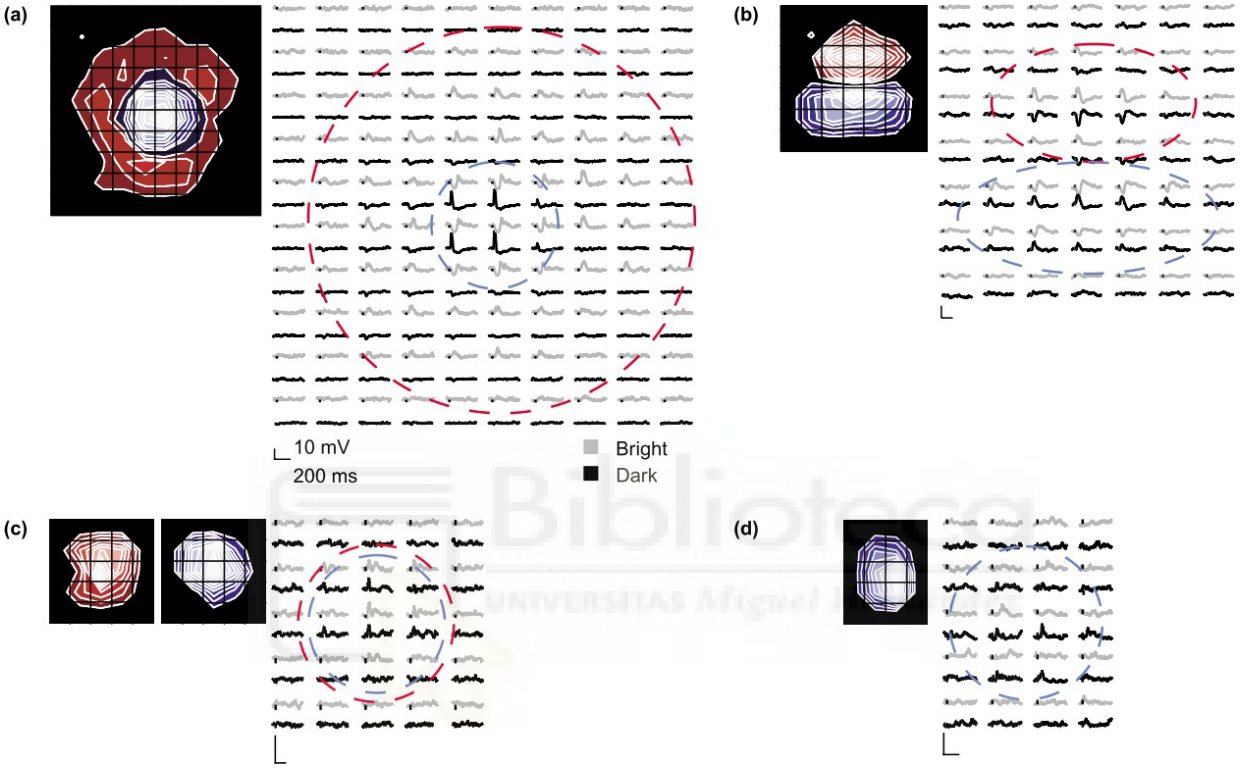

Figure 1.17. **Mapped receptive fields in the dLGN and V1.** The receptive fields are shown in two ways: First, as contour plots where brightness indicates response strength. Second, response averages of the corresponding responses to small dark (black traces) and bright (gray traces) squares. Red represents On subregions and blue represents Off subregions. **A**. dLGN neuron RF. **B**. Simple cell. **C**. Complex cell that fires for both bright and dark stimuli. **D**. Complex cell where dark but not bright squares excite the cell, adapted from (Hirsch & Martinez 2006a).

On the other hand, they found many other neurons whose response patterns could not be predicted from the spatial structure of their RF, which they named "complex cells". These cells no longer have elongated RFs of different polarity, however they respond to a preferred orientation regardless of the specific position

of the bar covering the RF, in other words, the polarity of the bar (black or white) does not affect the degree of response.

These facts reveal two basic principles that condition the way we approach our understanding of visual information processing in V1. First of all, it is a hierarchical system where as we move up, neurons develop more specific feature selectivities. As a consequence, the functional classification of neurons has to be done with increasingly complex stimuli and the description we make ultimately depends on the stimulus we use for their classification. Thus, in addition to simple and complex cells, neurons can be classified by another series of feature selectivities such as response to direction, preferred frequency, eye preference, polarity, modulation by the periphery and the linearity of the response, among others.

As expected, at this point in the text, the distribution of the different types of RFs varies through the cortical layer (Figure 1.22) and across different species, however, there are certain shared common design features.

First, the complexity of RFs increases at higher processing layers compared to the thalamorecipient layer. In all species we find RFs in layer 4 whose response can be predicted from their spatial structure. Thus, in carnivores and rodents most layer 4 neurons are simple. In primates like the macaque, the functional topolology is different. The 4Cα magnocellular layer has simple RFs, while the parvocellular 4Cβ has concentric RFs similar to those of dLGN. The trew shrew, on the other hand, lacks simple RFs and the segregated On and Off RFs in layer 4 are concentric like in the dLGN. As we follow the flow of information to other layers, RFs selective to more complex characteristics appear (Heimel et al 2005, Hirsch & Martinez 2006a, Hirsch & Martinez 2006b, Martinez 2006, Martinez & Alonso 2001, Martinez & Alonso 2003, Van Hooser 2007).

Second, all mammals have RFs that respond to a preferred spatial frequency. Here, clear niche specializations can be observed. Those animals whose behavior requires a high visual acuity have smaller RFs in retina, dLGN and cortex, in addition to RFs that respond to higher spatial frequencies in V1 (Heimel et al 2005, Mazade & Alonso 2017). On the other hand, mice have RFs that respond to a higher spatial frequency

in the retinotopic portion of V1 corresponding to the upper visual field, probably to defend themselves from aerial predators (Zhang et al 2015, Zhang et al 2012).

Third, there is a columnar organization for certain feature selectives such as the response of one eye or the other, orientation selectivity and a clear retinotopic organization.

Orientation columns

All mammals have columns of bigger or smaller diameter whose response to orientation is similar on the vertical axis (Heimel et al 2005, Hubel & Wiesel 1962, Kaas 2012a, Kaschube et al 2010, Ringach et al 2016, Van Hooser 2007). However, the columnar organization on the horizontal axis varies across species. In carnivores and primates, V1 cells with similar orientation preferences tend to cluster together in an orderly fashion giving rise to the renowned cortical orientation-preference maps (OPMs) (Blasdel 1992a, Blasdel 1992b, Bonhoeffer & Grinvald 1991, Kaschube 2014, Kaschube et al 2010, Ohki et al 2006, Van Hooser 2007). On the other hand, in rodents and lagomorphs these clusters of cells are more decorrelated and smaller, giving rise to a "salt and pepper" configuration in V1 (Figure. 1.18) (Jimenez et al 2018, Liang et al 2018, Ohki et al 2005, Ohki & Reid 2007, Van Hooser 2007, Van Hooser et al 2005).

Classical electrophysiology techniques, where able to describe how orientations change gradually and continuously along the horizontal axis in OPMs (Clarke & Whitteridge 1976, Hubel & Wiesel 1962, Kremkow et al 2016). Later, the development of the technique of optical imaging of intrinsic signals allowed to record the joint activity of large areas of the cortex, elucidating the global columnar organization of OPMs. This technique relates oxygen consumption to neuronal activity. With a high resolution camera, large cortical areas of up to 2 cm^2 can be recorded, where the activity of the cells appears as dark spots as hemoglobin is transformed into deoxyhemoglobin, which absorbs the incident light of a determined wavelength (Blasdel 1992a, Blasdel 1992b, Bonhoeffer & Grinvald

1991, Grinvald et al 1999, Kalatsky & Stryker 2003). Finally, calcium imaging revealed the microstructure of OPMs at the cellular level (Ohki et al 2005, Ohki et al 2006, Ohki & Reid 2007).

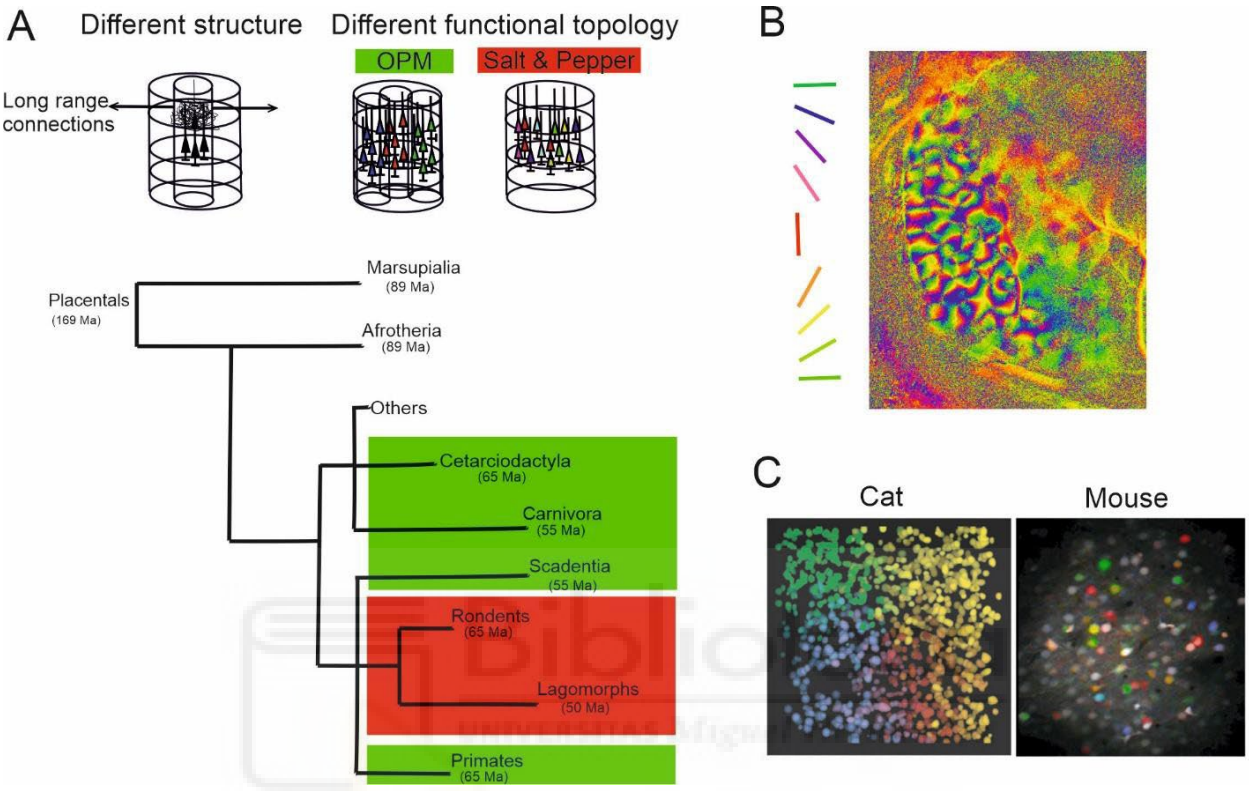

Figure 1.18. **Cortical functional topology is different across mammals. A.**Scheme of the different functional topologies found in V1 across mammalian species (salt and pepper in red; OPM in green; for the rest of species there is no available functional data). **B**. Ferret OPM obtained in the laboratory using optical imaging. C. Functional microstructure of the cortex of a cat (OPM) and a mouse (salt and pepper), adapted from (Ohki & Reid 2007).

Kaschube (Kaschube et al 2010) analyzed the OPMs of various species demonstrating that the maps of carnivores and primates follow common design standards preserved throughout the phylogeny (Figure 1.19). Thus, orientation columns are distributed continuously and periodically. The change from one orientation to another occurs gradually and the columns that respond to a similar orientation (isoorientation) are separated by a fixed average distance (Schottdorf et al 2014). Furthermore, these quasiregular patterns are interrupted by two types of singularities, where the orientations change rapidly; linear zones and pinwheels. A

linear zone is straight strip in the map with an abrupt change in orientation. Pinwheels are regions of rapid orientation change arranged in a circular fashion rotating clockwise or counterclockwise. Interestingly, although the mean size of the orientation columns varies between species as well as the number of pinwheels/mm^2, if a hypercolumn (λ) is described as the mean area between iso-orientation columns, dividing the pinwheels/mm^2 by λ results in a dimensionless magnitude named pinwheel density (ρ), constant in all species with OPMs and whose value is 3.14 (Kaschube 2014, Schottdorf et al 2015).

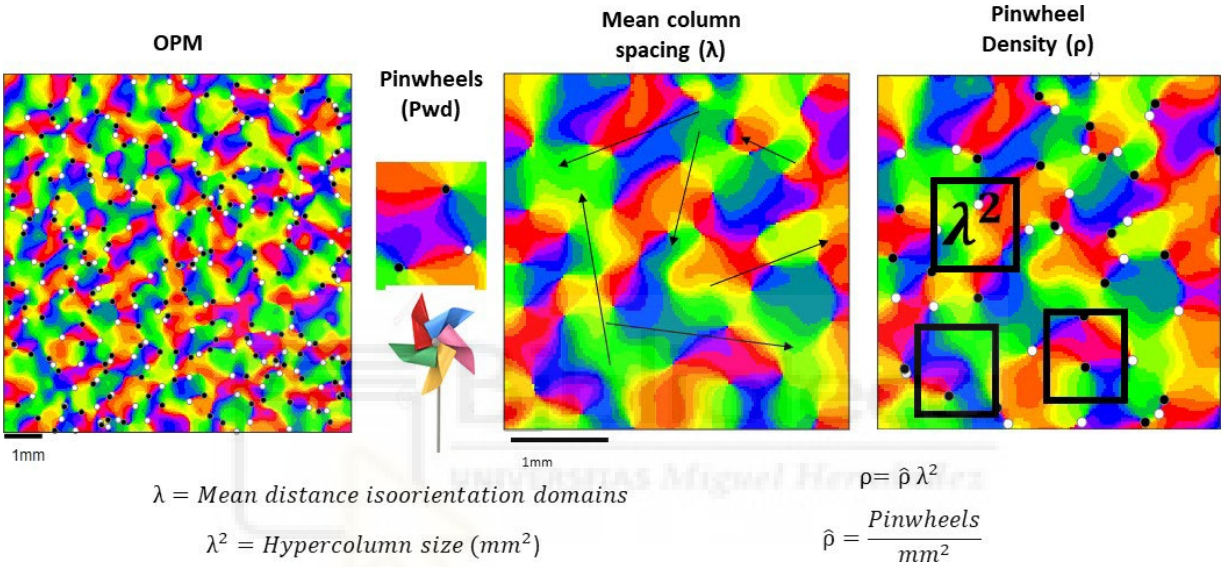

Figure 1.19 **Quantification of computationally obtained OPMs**. Pinwheels can rotate clockwise (white) or counter clockwise (black). Once calculated the mean column spacing (λ) the pinwheel density (ρ) can be computed. OPMs color coded for orientation as in Figure 1.18.

Ocular dominance columns

The inputs of each eye innervate layer 4, giving rise to neurons that respond preferentially to the contralateral, ipsilateral eye or to both (binocular neurons). The percentage of contralateral and ipsilateral RGCs in each specie clearly relates to the topological function observed in V1. In carnivores and primates, there is a clear segregation of neurons that respond preferentially to one eye or the other, giving rise to so-called ocular dominance maps (ODMs) (Binzegger et al 2004, Blasdel 1992a, Swindale et al 2000, White et al 1999). Mice, on the other hand, lack ODMs

since the majority of fibers reaching the cortex are contralateral and only a minority are ipsilateral, therefore, they have a big area of contralateral response, and a small region of binocular response (see results; Figure 3.20; Figure 3.22, for examples) (Cang et al 2005a, Kelly et al 2014, Sato & Stryker 2008). Unlike OPMs, ODMs are not so stereotyped and their topological arrangement varies widely across species (Weigand et al 2017a). Thus in cats, ferrets, and primates there is a fairly marked modular organization in columns, but much more stereotyped and defined in primates (Muller et al 2000, Weigand et al 2017a). In ferrets, however, the final region of V1 and all of V2 is completely monocular, so the columnar organization disappears in the V1/V2 border completely and, instead, two big irregular regions of ipsilateral neurons form V1 and a big band of contralateral neurons that form all of V2 populate de cortex (White et al 1999). Recall that in carnivores, unlike other species, the Y path innervates with great force V2, so that carnivores can be considered to have two primary visual areas (Hirsch & Martinez 2006b, Van Hooser 2007, White et al 1999). In the case of ferrets, a fully monocular V2 representing the central part of the visual field could be related to the detection of rapid movements, not as associated with the precision required for binocular vision, which is preferentially computed in V1.

Retinotopic maps

Retinotopy is a functional constriction present in all mammals studied up to date. The development of topologically ordered RFs tiling the visual space may be due to several factors.

First, the "minimum wiring" principle postulates that the brain tries to use as less wire length as possible to reduce the metabolic cost. The retinotopic disposition of RFs forces neurons that encode similar spatial information to be close to each other and, therefore, saving wire when connected (Chklovskii & Koulakov 2004, Chklovskii et al 2002).

Second, it is important to have a continuous and congruent map of visual information in both hemispheres. (Murcia-Belmonte et al 2019). Disruptions in this congruence cause deficits in behavior (Sperry 1943).

Third, for multisensory integration it seems reasonable to have sensory information topographically organized. Thus, for example, in the SC where the sensory information of the retina and ear is integrated in its different layers, an ordered tonotopy and retinotopy may be essential to integrate the information correctly enabling to relate a noise with a certain region of the visual field. (May 2006, Seabrook et al 2017). Likewise, for depth perception it is essential for RFs to be retinotopically aligned to receive slightly different information from each eye and develop binocular disparity (Parker 2007).

Fourth, noise reduction. Biological information channels have extrinsic noise, due to the properties of the signal, such as photon noise (Masters 2014) and other intrinsic ones due to the neurons themselves. RFs that receive similar spatial information increase the redundancy of the system making it possible to average the signal and reduce noise. So, the same mechanism the RGCs use in the retina, that is averaging the signal from several photoreceptors to eliminate photonic noise (Faisal et al 2008), might be used in the cortex in the same way, especially in the fovea of primates where the photoreceptor:RGC convergence is 1:1. Thus, increasing redundancy is a good way to increase the signal to noise ratio of the visual system.

Certain ecological needs can be associated with the anisotropy of the retinotopic maps present in V1. Retinotopy is not homogeneous throughout V1. The cortical magnification factor (Cmag), understood as the mm of V1 dedicated to a certain area of the cortical visual field (Schottdorf et al 2014, Swindale 1996), varies throughout the cortex and in different species. Such is the case of carnivores and primates, whose high visual acuity in the central portion of the visual field relates to the fact that the number of RFs dedicated to central vision is much higher compared to the periphery. In mice and rabbits, on the other hand, the Cmag factor is higher in the upper axis of the visual field where the need to discriminate objects at larger distances is greater (Kremkow & Alonso 2018, Swindale 1996).

Retinotopy implies that the quasiregular arrangement of RGCs is exerting a clear functional constriction in the RFs that form in the cortex. Moreover, differences in cortical retinotopy can be associated with differences in the density of RFs that anisotropically sample different regions of the visual field in the retina, like the fovea of primates for example (Baden et al 2020, Kremkow & Alonso 2018, Liang et al 2018). This functional constraint that the retina imposes on the cortex has clear implications for developing models that explain the emergence of the characteristic functional topologies of V1.

Models of cortical functional topology

Knowing the transformations that RFs undergo at each station of the EVP is essential to develop models that explain the emergence of new feature selectivities and, therefore, explain the basic mechanisms that the EVP may use to process information. Of all the functional characteristics present in V1, the ones that have received the most attention, due to their high prevalence in the mammalian cortex, are the emergence of orientation-selective RFs and the mechanisms required to orderly wire such a large number of neurons to develop stable retinotopic maps.

Orientation selectivity models

Models describing the emergence of orientation preference can be classified in two different groups; hierarchical models or intracortical (or recurrent) models. Hierarchical models are based on adaptations and updates of the model proposed by Hubel and Wiesel in their influential 1962 paper (Hubel & Wiesel 1962). Each layer 4 neuron receives an average of 20-80 afferents from thalamic neurons with concentric RFs and different On or Off polarity (Alonso et al 2001, Lien & Scanziani 2018). The combined integration of this information generates RFs with two elongated sub regions of different polarity (Hirsch & Martinez 2006a, Martinez

2006, Martinez 2011), which gives these neurons a new feature selectivity, the ability to respond to an edge with a certain orientation in the visual field (Figure 1.20). In turn, complex cells are formed by integrating single cell inputs, which gives them the property of response regardless of the polarity of the stimulus (Alonso & Martinez 1998). Highlighting an ascending and therefore hierarchical flow of information from the thalamoreceptor layers to the more superficial layers.

The classical version of the model proposed by Hubel and Wiesel required greater determinism and order in the afferents that reached layer 4. So that to generate simple RFs, it is necessary for the connections of different polarity arriving from the dLGN to be aligned in visual space. The most modern version of the model does not require so much specificity in the connections. It is based on experimental data supporting that the orientation of a V1 column can be predicted from the population field of the thalamus of retinotopically aligned neurons in the visual field (Jin et al 2011, Martinez 2011). Therefore, if the orientation of a column in V1 is determined by a retinotopically aligned pool of RFs of different polarity, where does the structure of the thalamic population RF come from? How can the characteristic periodic structure of OPMs emerge?

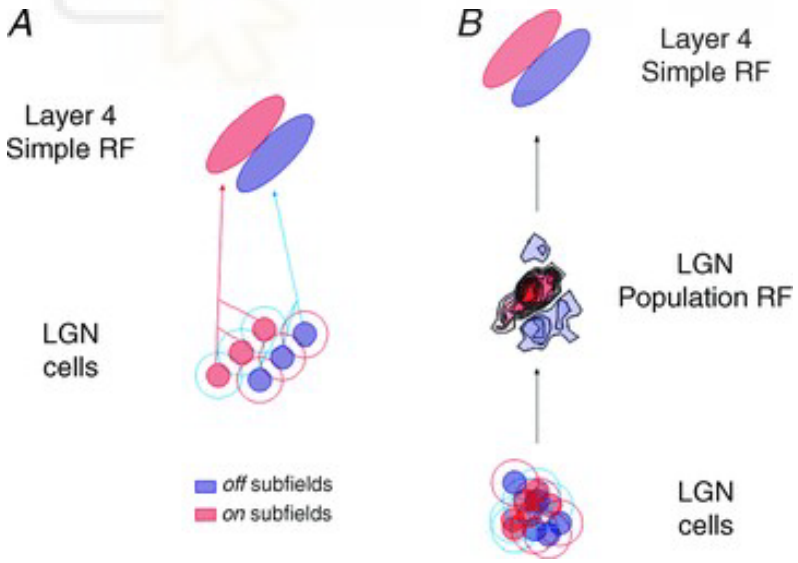

Figure 1.20. **Hierarchical model hypothesis**. **A**. Classical model by Hubel and Wiesel (Hubel & Wiesel 1962), simple cells are generated from dLGN neurons aligned in visual space. **B**. Modern view, simple cells are generated from a large pool of dLGN afferents that together form the dLGN population RF, adapted from (Martinez 2011).

The On and Off concentric RFs that reach layer 4 are arranged in the retina forming independent hexagonal mosaics (Eglen et al 2005, Wassle et al 1981a). The spatial statistics of these mosaics favors that the closest neighbor of a RGC neuron is another one of opposite polarity, giving rise to dipoles that, by linear sum of their RFs, can generate neurons selective to orientation in V1 (Figure 1.21). This statistical property of the mosaics is enough to bias the development orientation selectivity without depending on very strict connectivity rules (Soodak 1987), which finally derived in the Ringach´s model of statistical connections (Ringach 2004, Ringach 2007). Here the neurons of the retina connect to the cortex following a Gaussian function, in such a way that, the closer they are to each other in the circuit, the greater the probability of connection between them will be. This simple rule is capable of generating many of the qualitatively relevant features of OPMs. However, the long range correlations that are generated are not as strong as in experimentally obtained maps, since the retinal mosaics from which they come from lack long range correlations (Diggle 2013, Eglen et al 2005, Wassle et al 1981a, Zhan & Troy 2000). Because spatial data on retinal mosaics is scarce, if the mosaic structure were more regular than experimentally reported, marked long range correlations can emerge with a simple statistical connection model (Paik & Ringach 2011). The main criticisms that hierarchical models receive are that none of them are capable of generating OPMs quantitatively similar to those reported experimentally (Kaschube et al 2010, Schottdorf et al 2015), that retinal dipoles cannot generate the typical circular correlation profile characteristic of OPMS (Schottdorf et al 2014), and that to generate strong long range correlations one would have to start from retinal mosaics whose spatial statistics are not supported by experimental data (Figure 1.21).

Contrary to such a simple approach to the emergence of orientation, there is an undeniable need of intracortical connections to generate many of the characteristics of V1 RFs. When mapping RFs with bright and dark spots along the different cortical sheets, simple neurons of the thalamorecepient layers (4 and 6) respond with a depolarization to a stimulus (push) and with a hyperpolarization to a stimulus of opposite polarity (pull) in each of its subregions. This inhibition (pull)

is generated de novo in V1 (Figure 1.22). It is developed by mechanisms mediated by cortical interneurons and is essential for neurons to remain selective to contrast. Clearly, the linear sum of RFs in the hierarchical model cannot explain the mechanisms of contrast invariant tuning (the capacity to maintain orientation selectivity regardless of the strength of the stimulus contrast) present in V1(Hirsch & Martinez 2006a, Hirsch & Martinez 2006b, Martinez 2006).

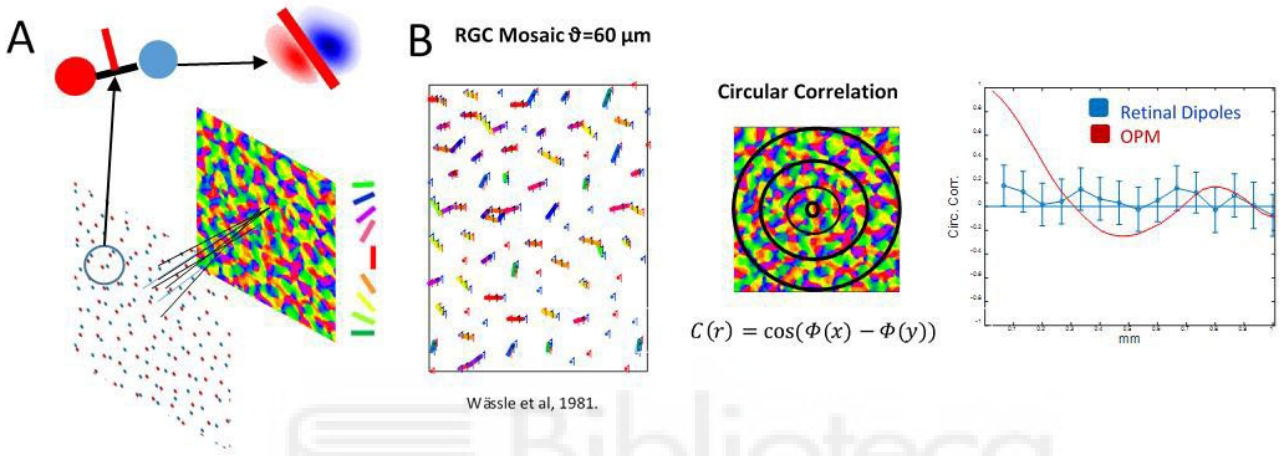

Figure 1.21. **Dipole model**. **A**. Simple cells are generated from retinal dipoles. **B**. Dipole mosaic replicating the exact spatial location from the real RGC mosaic from (Wassle et al 1981a) , ϑ= Maximum distance for the formation of dipoles. **C**. Circular correlation function for de retinal dipoles mosaic and for a computer simulated OPM.

Also, the fact that only approximately 10% of the synapsis in V1 belong to the connections arriving from the dLGN (Martinez & Alonso 2003), supports intracortical models in which the inputs of the thalamus are considered to have little strength in the cortex, instead intracortical interactions are responsible of amplifying these weak thalamic signals endowing the RFs with orientation selectivity (Kaschube 2014, Kaschube et al 2010, Martinez & Alonso 2003).

However, most of layer 4 and layer 2/3 cortical activity disappears by silencing a small region of the dLGN (Martinez & Alonso 2001), which reveals a similar relationship between drivers and modulators in the retinothalamic and thalamocortical circuits, where a minority of excitatory synapses are responsible of

the basic characteristics of the RFs (Sherman & Guillery 1998). This highlights again the difficulty of relating structure to function if only the total number of connections are taken into account.

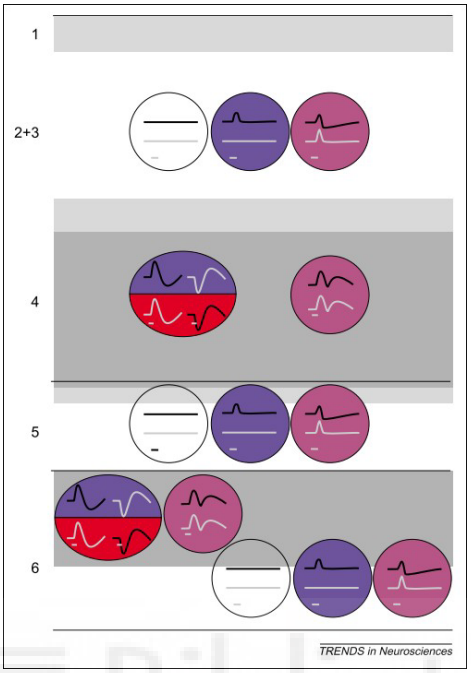

Figure 1.22. **Laminar distribution of spatio-temporal mapped RFs in cat visual cortex**. Note that simple cells (oval shape) respond positively to a stimuli of positive contrast and with a hyperpolarization for a stimuli of opposite polarity, push-pull arrangement. On the other hand, many complex cells have a push-push arrangement, they respond equally for stimuli of the same polarity (purple). Blue (complex neurons that respond exclusively to one contrast), white (complex neurons that do not respond simple spatial stimuli). Black and white lines correspond to the intracellular response to bright and dark spots respectively, adapted from (Hirsch & Martinez 2006a).

Retinotopy Models.

The spatially ordered arrangement of RFs in V1 is essential to obtain a consistent and congruent image of the visual field in the two hemispheres (Cang et al 2008, Godement et al 1984, Lemke & Reber 2005), and it is the basis on which the rest of the functional topologies of V1 emerge. In order to understand the mechanisms by which such a large number of connections are arranged so precisely, it is important to understand the phases in the development of the EVP.

The development of the main functional maps in V1 occurs in a staggered way. First, the retinotopic map is established in the dLGN and later in V1. The geniculocortical afferents do not go directly to layer 4, they are maintained and remodeled in the subplate until it degrades, enabling connections to layer 4 and 6. In addition, the afferents of the contralateral eye arrive first and later come those of the ipsilateral eye, establishing an initial continuous retinotopic binocular map in space (Huberman et al 2008, Kremkow & Alonso 2018).

In second place, the strengthening of the contralateral and ipsilateral connections ends up segregating the inputs according to the eye, giving rise to neurons with a contralateral, ipsilateral and binocular response. Finally, conformational changes in the inner plexiform layer of the retina allow information to be segregated into antagonistic On/Off channels, causing orientation-selective neurons to emerge in V1 (Figure 1.23) (Huberman et al 2008, Kremkow & Alonso 2018).

The mechanisms that allow the correct development of retinotopic maps are molecular guidance cues for the initial establishment of connections and gross retinotopy, followed by activity dependent mechanisms that refine them. The molecular guidance cues work thanks to Eph receptors gradually and differentially expressed in different RGCs that, in turn, interact with an ephrin gradient that is also gradually expressed in the target tissue to which they are directed (Herrera et al 2003, Herrera et al 2019, Huberman et al 2008, Swindale 1996). Once the gross retinotopic map is established, the activity-dependent mechanisms come into play. Activity dependent mechanisms change the weights of the connections of the circuit following hebbian rules (Hebb 1949). Hebbian plasticity is based on the fact that when two neurons fire synchronously they tend to strengthen their weights. Moreover, the synchronous or asynchronous firing between two neurons can induce changes in their internal structure, increasing or decreasing neurotransmitter release and thus, strengthening or weakening their weighs through activity dependent mechanisms (DeFelipe et al 2013, Markram et al 1997).

There are mainly two types of activity dependent mechanisms that take part for the development of retinotopy. On the one hand, there are those that occur by the spontaneous activity mediated by retinal waves, which take place before the photoreceptors are fully formed and, therefore, are prior to the visual experience. (Ackman et al 2012, Crair et al 1997, Huberman et al 2006). On the other hand, after the eye opening, the so-called critical period is entered and a finer remodeling of the axons occurs. It is important to note that the retinotopic map is already formed prior eye opening, and therefore, its formation is independent of the visual experience (Huberman et al 2008, White et al 2001, White & Fitzpatrick 2007).

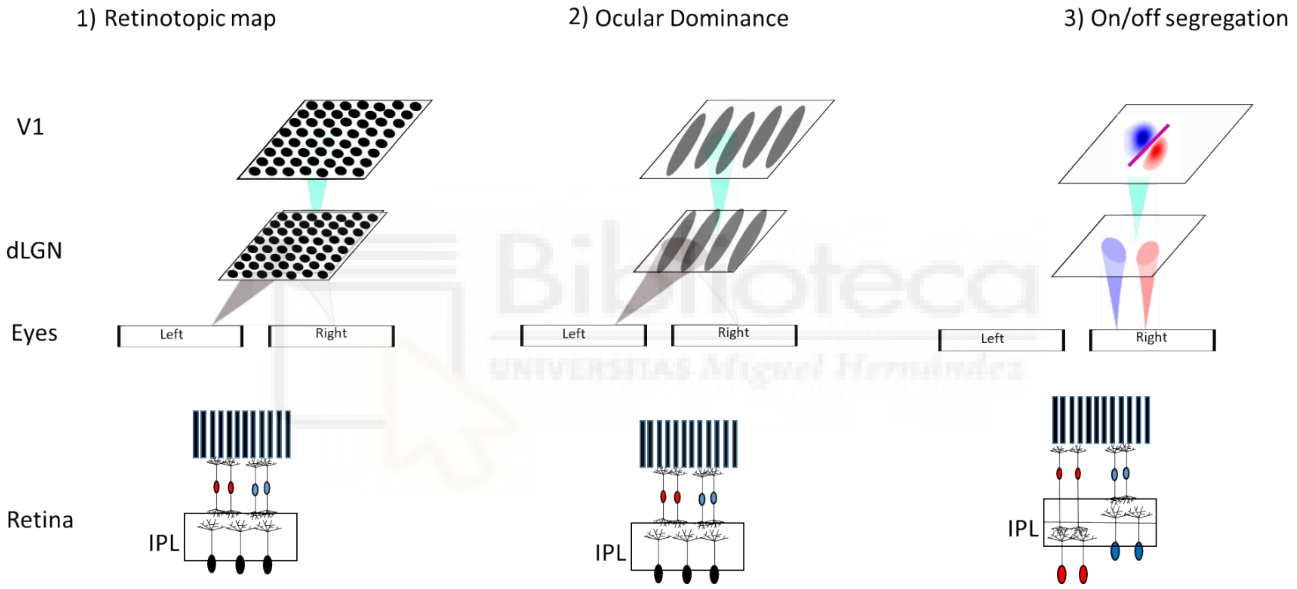

Figure 1.23. **Phases in the development of the Early visual pathway development**.

Until recently there was no evidence of what guided the activity-dependent mechanisms acting before eye opening. However, Crair (Ackman et al 2012) has shown that retinal waves generated spontaneously in the retina are transmitted to the postsynaptic layers (superior colliculus, dLGN and V1) synchronously in both hemispheres governing their spontaneous activity. On the other hand, Retino-retinal (R-R) connections have been seen in many species at the beginning of development, these fibers seem a good candidate for the synchronization of the

activity of both retinas since there are no functional connections between hemispheres at the level of the dLGN or the SC (Murcia-Belmonte et al 2019).

Many theoretical and computational models have been applied to understand how activity dependent mechanisms shape the formation of retinotopic map development (Eglen & Gjorgjieva 2009, Hjorth et al 2015). A particular class of models, that is, input driven self-organization models, introduced initially by Willshaw and von der Marlsburg (Willshaw & von der Malsburg 1976) with the modifications introduced by Kohonen, give a clear and beautiful answer to how these mechanisms work (Kohonen 1982, Kohonen 2013b).

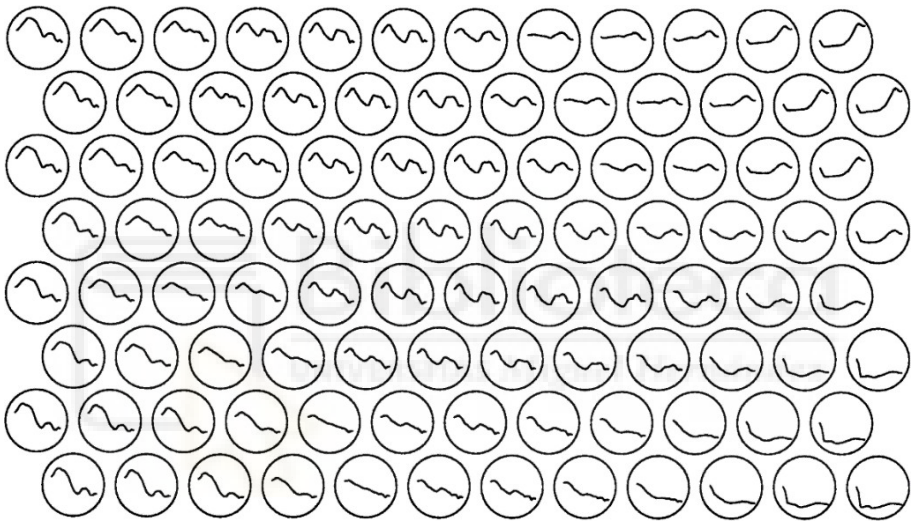

Figure 1.24. **Kohonen algorithm used to classify a short interval of natural speech.** Each circle represents a neuron whose RF is specialized in detecting a precise speech interval. Note how they are arranged in topographical order, adapted from (Kohonen 1998).

The self-organizing model (SOM) elaborated by Kohonen proposes that the weight of the connections of a neural layer can be self-organized by the input and a function that propagates the activity in the surrounding neighborhood following simple hebbian rules. Thus, when two neurons fire synchronously in the developing circuit they strengthen their weights. As the neuronal layer keeps receiving different types of input, their weights update over time specializing in the detection of a certain stimuli. This simple rules make neurons that are close in the circuit to

develop RFs that respond to similar features, generating ordered retinotopic maps where each neuron´s RF is specialized in detecting the position of a stimulus in visual space. In other words, neurons develop RFs with feature selectivities for a precise stimuli using a self-organizing algorithm based in a simple hebbian rule, a function that enables the propagation of the activity of the activated neurons to their neighbors, and some degree of plasticity to allow the actualization of their weights over time. The SOM algorithm was initially built to explain the correct development of ordered retinotopic maps in the visual system. However, this algorithm is so powerful that it is still used nowadays to process and classify any multidimensional signal in a topographical order (Figure 1.24) (Kohonen 1998, Kohonen 2013a).

What do receptive fields do?

So far we have described the structure of the EVP and have made an effort to relate the feature selectivity of the RFs to the ecological needs of each specie. In fact, there is a clear relationship between feature selectivity and the topological disposition of the RFs, with the ecological niche that each species occupies. Therefore, comparative biology is a useful approach for finding common and uncommon elements between species and generating hypotheses about the fundamental operations that the EVP is performing.

To test these hypotheses, computational models can be used in which the way the system physically performs the operations as well as the specific algorithm it uses to carry them out is left aside, to instead focus on the main operation that it has to carry out (Marr & Poggio 1976). In computer science, is perfectly known that, different algorithms can arrive to the same solutions (Van Hooser 2007). So, it should be noted that all theoretical hypothesis must be carried out under the important premise that, despite the fact that the underlying machinery/algorithm that carries out this operation may be different, the resulting functional architecture to solve the problem will be similar. This allows to confirm

or not a certain hypothesis when comparing modeling results with experimental data.

Extracting the most relevant components of the environment for the survival of an individual marries the efficient coding hypothesis postulated by Barlow in 1961 (Barlow 1961). Shannon's "Information Theory" (Shannon 1948) was born out of the need to minimize the cost of sending information over long distances with the lowest possible energy cost in artificial systems. Following these line of thinking, Barlow understands sensory systems as communication channels whose main characteristic is to extract the most relevant information from the environment with the lowest energy cost. Sensory systems act as filters that maximize the entropy of the message to be transmitted in the system, eliminating its redundant components. The criterion to optimize is, therefore, the reduction of redundancy and the way to do it biologically is through spatiotemporal filters (RFs) that extract the most important components (or those with more information) from the environment.

This hypothesis relates with the fact that natural images are highly redundant, that is, highly correlated and with a 1/f statistic. This basically means that if you divide an image into small pixels the probability that a pixel is similar to its neighbor is very high (Simoncelli & Olshausen 2001). Thus, the elements that contain more information are those where there is a rapid change of contrast, in other words, a border. Therefore, the edges of an image are the elements that contain the most information from the statistics of a natural environment.

Neuroscience has been applying many of the principles of information theory with more or less success (Rieke et al 1996). Starting from the premise of efficient coding, computational models based on "sparse coding" have been developed. They work by searching for a series of base functions that minimize the dimensionality of the signal and that describe it with the least number of components (neurons) as possible (Babadi & Sompolinsky 2014, Martinez-Garcia et al 2017, Olshausen & Field 1996, Olshausen & Field 1997, Rehn & Sommer 2007, Simoncelli & Olshausen 2001). These base functions can be extracted using different optimization algorithms such as ICA, PCA, TICA …etc. (Beyeler et al 2019, Martinez-Garcia et al

2017). Curiously, these types of algorithms are capable of generating the characteristic simple RFs present in V1(Olshausen & Field 1996), indicating that V1 in part, and not totally as we will see, is maximizing the transmission of the most relevant information from the environment.

However, experimental data does not fit totally with the hypothesis of complete redundancy reduction (Rehn & Sommer 2007, Ringach 2002). There are low spatial frequency RFs in V1 increasing redundancy, therefore there is an overcomplete set of RFs that filter the information of the environment (Olshausen & Field 1997). In other words, there are more spatio-temporal filters than those required if the main operation carried out by the system is redundancy reduction. Furthermore, the population response of the neurons varies between the different cortical layers, where the thalamorecepient layer has a denser code compared to the sparser code of the superficial layers (Faisal et al 2008) .

Why does the EVP need to be redundant? Redundancy can be essential, among other reasons, to increase the signal-to-noise ratio in the SVT. Thus, averaging the activity of several neurons that receive a similar input eliminates noise (Faisal et al 2008). Also, coming from Barlow himself (Barlow 2001), it becomes especially relevant when we think of the brain as a Bayesian decoder that handles probability distributions to make its decisions. In this context, because we live in a constantly changing environment, adaptation consists on the ability to generate robust probability distributions of the environment. For this, it is necessary to understand the statistics of the redundant components of each new environment encountered by an individual.

In summary, the application of certain principles of information theory for the transmission of information in artificial sensory channels has had relative success in neuroscience. However, the EVP is not optimizing only this problem of channel capacity, there are other tradeoffs that it has to assume and that remain to be discovered.

Aims

Understanding the developmental rules that give rise to a cortical structure through evolution is useful to identify the basic elements and their interactions in the formation of a system. Many computational models are able to simulate the development of several features of V1 neurons (Kaschube 2014, Kaschube et al 2010, Schottdorf et al 2015, Swindale 1996, Weigand et al 2017b). However, to understand the role the structure has in the system we have to move a step further and relate these interacting elements to a concrete function or objective that the cortex has to achieve (Marr & Poggio 1976). To these end I have focused in resolving the following questions:

- What are de main operations performed by V1?
- What can we learn from the early visual system with the available functional data in mammalian species?
- Do these species share common developmental wiring rules? If so, are they optimizing or solving the same problem? Do they solve it in the same way?
- Are the functional differences due to different biological constraints?
- What are the advantages of these connection strategies for information processing in the brain?
- What is the relationship, if any, between the functional architecture and the main operations the system is performing? In other words, do OPMs serve a specific function or operation V1 performs?
- Can we extract any canonical features governing the development of cortical circuits and function?

Materials and methods

Statistical Wiring Model of the Early Visual Pathway.

A Feedforward 3-Layered Neural network of the excitatory part of the early visual pathway was constructed based on previous experimental and theoretical work (Martinez et al 2014, Ringach 2004, Ringach 2007, Schottdorf et al 2015, Wassle et al 1981a). However, because the size of V1 differs between species (Table 1), a parameter was added that enables to increase or decrease the area of V1 with respect to the retina, that is, to explore the different divergence-convergence ratios (DCr) between species. The area of the dLGN was considered to be the same as the retina, and the density of the excitatory relay cells was 1.5 times bigger than the RGCs density. Our retinal and thalamic mosaics each simulate a square patch of tissue of 15mm^2, that is, the area of a mouse retina (Table 1). To avoid boundary effects, only those relay cells that were separated from the edges of the mosaic by at least 100 microns, were considered for further analysis.

Divergence-convergence Ratios (DCr) between layers

We defined the convergence-divergence ratio between two consecutive layers as [1]:

(1) $$DCr = \frac{N_{pos}}{N_{pre}} = \frac{div}{conv}$$

Where N_{pos} and N_{pre} are the number of postsynaptic and presynaptic neurons respectively, and div and conv represent the average divergence and convergence connectivity between layers.

The number of cells in each layer is given by the product of the cell density and the area of the corresponding layer. From this we can derive that [2],

(2) $$DCr = \frac{pos_d * A_{pos}}{pre_d * \omega * A_{pre}} = \frac{div}{conv}$$

Where pos_d and pre_d are the density of neurons (cells/mm^2) in the retina and V1 layer 4 respectively. A_{pos} and A_{pre} represent the area (mm^2) for each layer. The factor ω represents the upsampling of the LGN (nº of LGN neurons/nº RGC neurons) in the model.

Retinal Layer

To simulate the spatial statistics of the position of RGCs of the retina we used the pairwise interaction point process (PIPP) algorithm (Eglen et al 2005, Schottdorf et al 2014), to simulate a RGC mosaic that resembled the distribution reported for the cat using the parameters from (Schottdorf et al 2014) for the w81S1 mosaic by (Wassle et al 1981a). The density of the RGCs was fixed to 98 Off cells/ mm^2 and 90 On cells/mm^2 for 7° of eccentricity as in cat (Wassle et al 1981a).

dLGN Layer

Thalamocortical cells were regularly distributed forming a hexagonal compact mesh of sensors that covers a surface of the same size as the thalamic layer. The area of the LGN was the same as the one used for the retina and only the density of cells was varied by a factor ω = 1.5 respect to the number of RGCs. The polarity (On or Off) of each thalamocortical neuron was inherited from its nearest neighbor in the antecedent RGC mosaic, following a minimum wiring paradigm (Chklovskii et al 2002).

Arrangement of layer 4 cortical cells

The cortical neurons were arranged as in the dLGN but with a higher density, 2200 cells/mm^2. However, to simulate the different DCr across species, the coordinates of the peak RFs of the neurons of the previous layer were re centered and proportionally expanded or compressed to fill the postsynaptic layer following equation [3] before connecting the neurons from the next layer,

$$r(x,y) = [1 + \frac{x - X_{min}}{X_{max} - X_{min}}\ ,\ 1 + \frac{x - Y_{min}}{Y_{max} - Y_{min}}]\,\kappa \tag{3}$$

Where x and y are the coordinates for the neurons position and κ is the factor that expands or compresses the coordinates conserving the retinotopy in the final layer. X_{min}, X_{max}, Y_{min},, Y_{max},, stand for the minimum and maximum x and y coordinates.

Connectivity between layers

The probability of connection between layers (Pr) was modelled as a Gaussian function of the x-y distance. Where x is the coordinate of a neuron in the previous layer and y the coordinate of a neuron of the next layer from x.

The weight of connections was also assumed to be a Gaussian function of the distance between the receptive-field centers. The function for both connection probability and strength was as in [4],

$$Pr = min\{q * \exp(-\frac{\|x-y\|^2}{2*\sigma_l^2}), 1\} \tag{4}$$

The area of influence of each neuron is determined by σ_l (simulating dendrite and axonal coverage) and the strength of each connection could be varied changing the free parameter q. The connections between the retinal and thalamic layer where done between same sign neighbors however V1 neurons inherited a combined polarity pooling from the On and Off pathways.

The connections also followed a winner takes all mechanism (Kohonen 2013b, Willshaw & von der Malsburg 1976). In the sense that the connection with the bigger strength inherited the activity of the RF from the previous layer and the rest of possible connections are then calculated from this new peak of activity. That said, to connect each layer with the next the following steps were always made:

1) Calculate the probability of connections between all neurons from the pre and postsynaptic layer.
2) Connect to the neuron with the strongest weight, that is, the "winner neuron".
3) The "winner neuron", inherits the activity of the RF of the previous layer.
4) The probability of the rest of possible connections is calculated from this new coordinate of peak activity.
5) The weights for each neuron are normalized so that the sum of all the weights of each neuron is equal to 1. In other words, all neurons have the same weight in the model.

Due to the different convergence ratios between layers in the model, a small number of unconnected presynaptic cells are sometimes present. To overcome this problem those neurons were connected to their nearest neighbor and the strength of their connection was obtained with the same function as in [4].

To summarize, this way of performing the connections assumes that all neurons in the circuit have the same weight and it assures a "fire together, wire together" hebbian mechanism favoring the connections of neurons with similar RFs, that is, with RFs that respond to similar regions of visual space, rather than just connecting according to the spatial coordinates of their soma.

Model RFs

RGCs and the excitatory part of thalamic RFs where modelled as in (Martinez et al 2014). The RFs of V1 layer 4 cells where constructed by linearly combining all their pooled thalamic inputs [5], weighted with the same Gaussian function we used [4] to calculate connection probability

(5) $$RF = \sum_{i \epsilon N} Pr_i \cdot RF_i$$

Where Pr is the weight of each RF from the previous layer that receives a total of N different connections.

Population receptive field

To obtain the structure of the thalamic population receptive field we computed the On-Off linear combination of all thalamocortical receptive fields (Jin et al., 2011), following equation [6]. The results are shown as color maps in which areas where On and Off responses are coded in red and blue, respectively.

(6) $$cov = \frac{1}{N} \sum_{i=1}^{N} On_{RF_i} + Off_{RF_i}$$

Preferred Orientation and spatial frequency

The preferred orientation, spatial frequency and tuning curve for each layer 4 RF was computed based on the Fourier spectrum of the RF ($RF(fx, fy)$) as in (Ringach 2007, Schottdorf et al 2015).

(7) $$\mu = \frac{\iint RF(fx, fy)\, e^{2i\,\mathrm{atan}(fy/fx)}\, dfx\, dfy}{\iint RF(fx, fy)\, dfx\, dfy}$$

Where the preferred orientation is

(8) $$\vartheta_{pref} = \arg(\mu)/2$$

And the preferred spatial frequency was obtained using the Center-of- Mass Method (Ringach 2007)

(9) $$k_{pref} = |\mu|$$

Tuning curves and orientation selectivity index

For each layer 4 RF its tuning curve (TC) and orientation selectivity index (OSI) where calculated as in (Ringach 2007, Schottdorf et al 2015). Where the TC for a given spatial frequency (k) and a given orientation (ϑ) is

(10) $$TC(\vartheta, k) = |RF(k\cos(\vartheta), k\sin(\vartheta))|$$

and where the TC was extracted for the k_{pref} of each RF,

(11) $$TC(\vartheta, k_{pref}) = |RF(k_{pref}\cos(\vartheta), k_{pref}\ \sin(\vartheta))|$$

ϑ took values from 0 to 2π. As seen in Figure 2.1 the model returned neurons poorly tuned, that is, broadly selective to o nd others more selective to a specific orientation, as denoted by the shap uning curves.

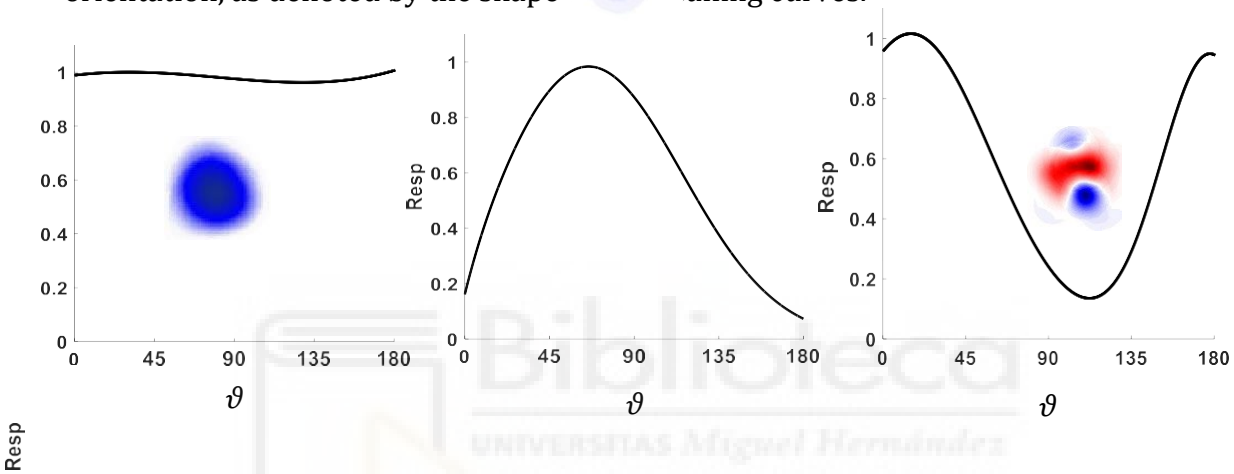

Figure 2.1. **Tuning curves from model V1 RFs.** Example of a broadly tuned neuron (left) and two orientation selective neurons (middle and right). Seen as the degree of response (Resp) for each orientation (ϑ), given a preferred spatial frequency (k_{pref}).

Once obtained the TC the OSI was calculated as

(12) $$OSI = \frac{|\int_0^{2\pi} TC(\vartheta, k_{pref}) e^{2i\vartheta}\ d\vartheta\ |}{\int_0^{2\pi} TC(\vartheta, k_{pref})\ d\vartheta}$$

to describe how narrow or broad the tuning curves are for the RF of each V1 neuron, in other words, how selective is a neuron to its ϑ_{pref} . As reported by (Ringach 2007), there is a clear relationship between OSI and k_{pref} . The more selective a neuron is to a ϑ_{pref} the higher the k_{pref} (Figure 2.2).

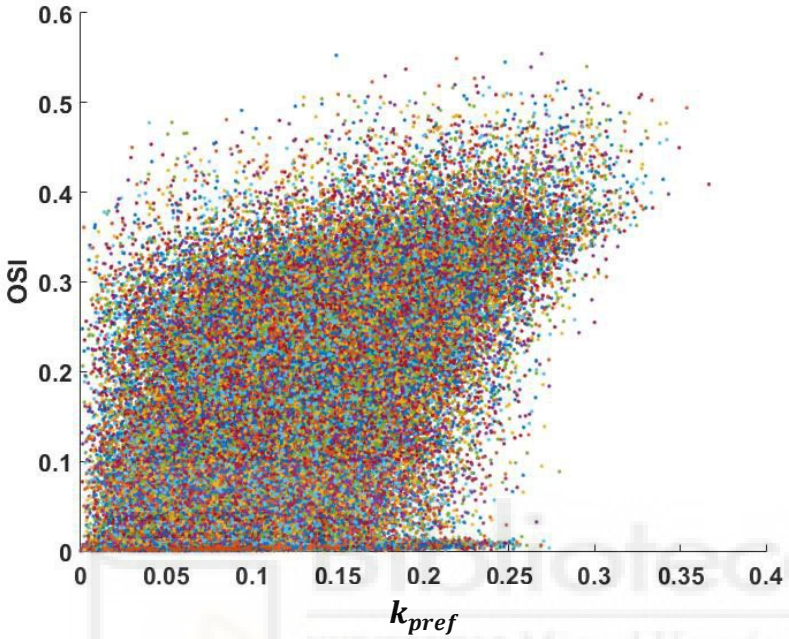

Figure 2.2. **Orientation selective increases with preferred spatial frequency.** Neurons with a high k_{pref} tend to have a high OSI. Each color represents a different V1 neuron.

Cortical magnification factor and local connectivity matrix

The Cmag was understood and computed as the area of V1 that receives information from a similar RF. Taking into account formulas [1,4], the Cmag is completely related to the levels of thalamocortical divergence and, therefore, completely linked to the DCr. Thus, the final levels of divergence are computed as the area of the resulting connectivity Gaussian function (Pr) which in turn depends

on the value of σ_l from [4]. In summary, as the DCr value increases, so does the size of (Pr), the levels of divergence, the Cmag and vice versa (Figure 2.3)

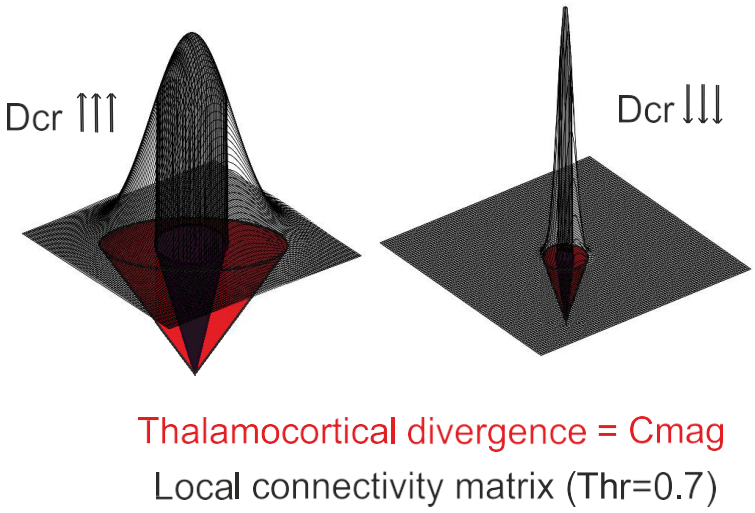

Figure 2.3. **Connectivity Gaussian functions (Pr) for different DCr.** The area occupied by the extent of the mean thalamocortical divergence determines Cmag. The extent of local connections between V1 neurons is determined by a local connectivity matrix whose area is thresholded at 70% of peak response from Pr.

V1 local connections

Local connections between V1 neurons were simulated using a thresholded Gaussian filter convolution where the local connectivity matrix (Lc) used to simulate the extent of local connections was determined as the area of Pr>0.7. In other words, only those neurons whose probability of shared response was above 70 % where considered to form local connections (Figure 2.3).

(13) $$Lc(x, y) = 1 * \exp\left(-\frac{\|x - y\|^2}{2 * {\sigma_{cor}}^2}\right) > 0.7$$

Where $\sigma_{cor} = \sigma_l$ (as in [4]) so that the size of the filter is completely related to the levels of divergence required to reach a fixed value of convergence, for each DCr value between layers.

Once obtained the Lc, the coordinates of the neurons selective to orientation (OSI>0.25) where transformed to form an image f(x,y), that was convoluted using the Lc as the mask for the convolution [14],

$$(14) \quad g(x,y) = Lc * f(x,y) = \sum_{dx=-a}^{a} \sum_{dy=-b}^{b} Lc(dx,dy)(f(x+dx, y+dy)e^{2i\vartheta})$$

Where g(x,y) is the OPM obtained interpolating the orientation from the influencing local connections and $-a \leq dx \leq$ a and $-b \leq dy \leq$ b.

Circular Correlation

The circular correlation between al pairs of neurons with an OSI>0.25 was computed as a function of increasing concentric circles, as in (Schottdorf et al 2014)

$$(15) \quad C(r) = \cos(2(\vartheta(x) - \vartheta(y)))_{(r-b/2)\leq|x-y|\leq(r+b/2)}$$

Where r are the values of increasing radius up to a r_{max} of 1.8mm_c (mm_c for mm of cortex) and b= r_{max}/80. So that the total length of the maximum radius is divided into 80 independent bins where the circular correlation is computed. The same function can be used for calculating the correlation between dipoles of the retina or the dLGN. However, in this case, b=r_{max}/17 and rmax=1.8 mm/Cmag. Where the Cmag= 1.7 mm_c/mm_r (mm_r for mm of retina) as for the w81S1 mosaic by (Schottdorf et al 2014, Wassle et al 1981a).

Once $C(r)$ is computed a series of parameters where extracted to describe the circular correlation function across models with different DCr. First, the local column diameter of OPMs was extracted as the first point in the function that reaches a value of 0. Furthermore, the anticorrelation point was extracted searching for the next inflexion point after the local column diameter point. The hypercolumn size (λ), that is, the mean distance between isoorientation domains (Kaschube et al 2010), was estimated as the position of the highest peak of positive correlation after the function reaches a value of 0. The strength of the periodicity, termed as periodicity robustness, was calculated as the area of positive correlation under λ (Figure 2.4).

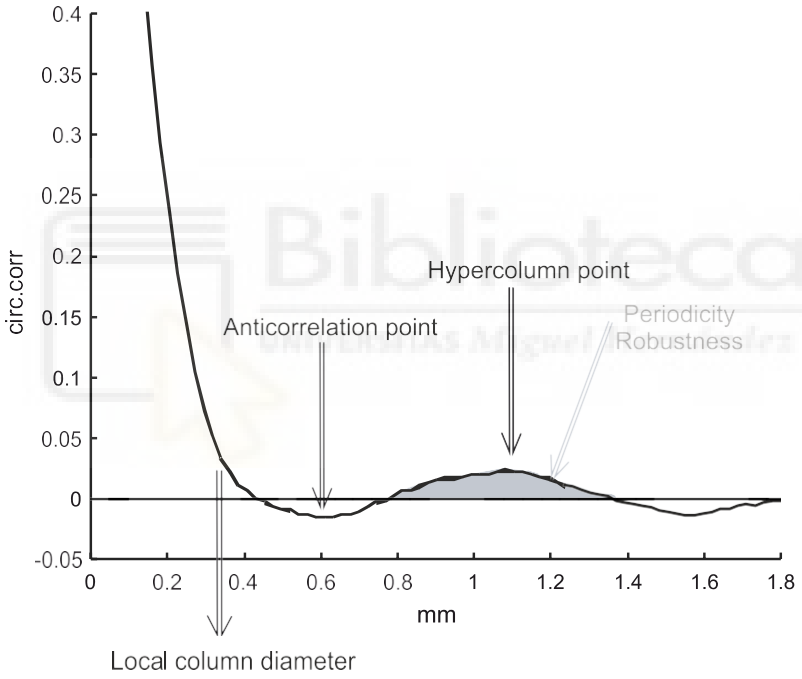

Figure 2.4. **Parameters extracted from the circular correlation function.** For each circular correlation function calculated, the local column diameter, anticorrelation, hypercolumn size (λ) and periodicity robustness where extracted.

Orientation Bias

Orientation Bias (OBias) was calculated as in (Molano-Mazon 2013, Ringach 2007) by reconnecting each neuron of the circuit 20 independent times and calculating the resulting dispersion in the orientation of the resultant vectors in the unitary circle, as in eq [16],

(16)
$$OB = \frac{1}{N}\sum_{i=1}^{N} e^{2i\vartheta}$$

Where N=20 independent connections and ϑ is the orientation obtained for each N_i independent iteration. So, for each OPM, the orientation can be predicted through the thalamic population RFs. One the one hand, clear stable regions, with a high orientation bias, where present at locations with a high contrast change in the thalamic population RF. On the other hand, regions of low stability, where located at

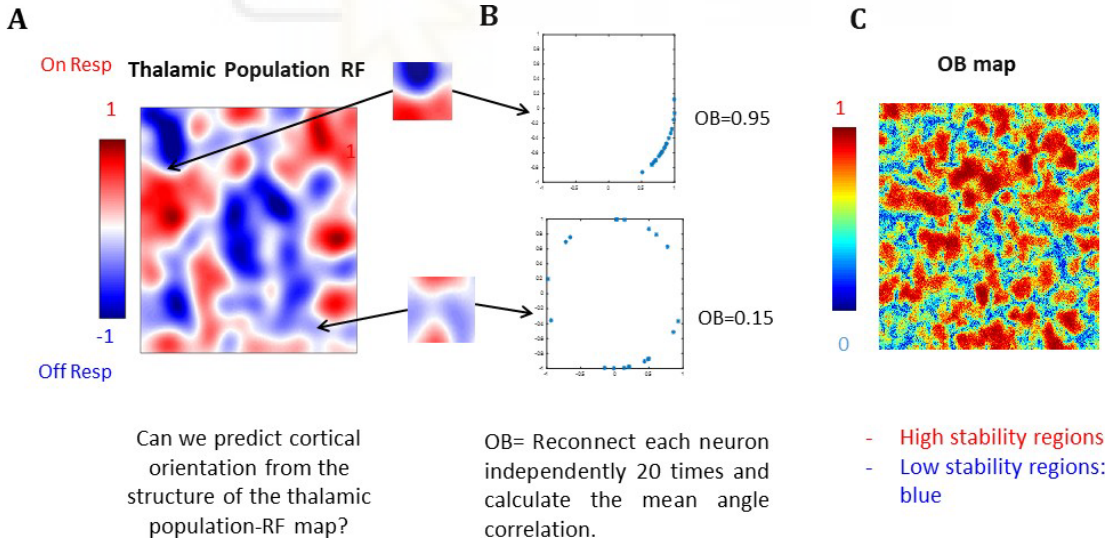

Figure 2.5. **OBias computation. A.** Population RF computed as in eq [6]. **B.** Example of 20 independent reconnections and OBias values from two different regions of the population RF map. **C.** OBias map of the whole region.

low contrast locations. Finally, an Obias map can be computed where it is possible to see how stable regions intermingle with low stability regions (Figure 2.5).

RF coverage of visual space and redundancy

Coverage of visual space in V1 was computed as in (Martinez et al 2014) for a square window of 2.25 mm^2. The area of visual space covered by the RFs in V1 was calculated independently for the On and Off pathways and the area covered by each RF was computed as the region of the RF whose response was above a threshold of 90% of its peak response.

Redundancy was calculated as in [17] and defined as the proportion of overlapping RFs covering visual space for the same window where coverage was computed.

(17)
$$Red = \frac{\frac{1}{N}\sum_{i=1}^{N} Peak_{RF_i}}{\bar{P}_{resp}}$$

Where the mean population response of all RF peaks covering V1 is summed and divided by the individual mean response of a single RF peak.

SOM model

We used a simplified and modified version of the self-organizing map (SOM) as described by (Kohonen 1982, Kohonen 2013b, Willshaw et al 1976). The topography of the RGCs is represented by a regular square mesh of size 11 by 11 with the cells in the nodes. Those cells project to a postsynaptic layer of the same size, initially with synapses between all the cells in a non-specific manner. A representation of the location of the center of mass (CM) of the normalized weights, *w*, of the synaptic connections results in a mesh contained in a unit square.

By stimulating the retina with different stimuli the synaptic weights change in according to a Hebbian rule, so that they are changed according to the expression [18],

(18) $$\delta w_i = \lambda \cdot e^{-\frac{t}{\tau}} \cdot e^{-\frac{(X-x_w)^2+(Y-y_w)^2}{2\sigma^2}} \cdot (r_s - w_i)$$

Where δw_i is the change in the i synaptic weight w_i. λ is the weight decay term, t is the time expressed in number of iterations. τ is the time constant for the λ decay. X and Y are the arrays holding the coordinates of retinal cells. x_w and y_w are the coordinates of closest cell to the stimulus location, *i.e.*, the coordinates of the *winner*. σ gives the extent to which the activation propagates to neighbouring cells, and finally, r_s is the vector position of the stimulus.

Figure. 2.6 shows the development of a map over time. Starting from a condition in which all cells are connected with almost equal weights, thus the position of all CM is very close to the center, the stimuli make it to deploy in a way that by the end of 12000 iterations the synaptic connections have been greatly refined and the receptive fields of each post-synaptic cells is centred around the position of the topographically corresponding retinal cell.

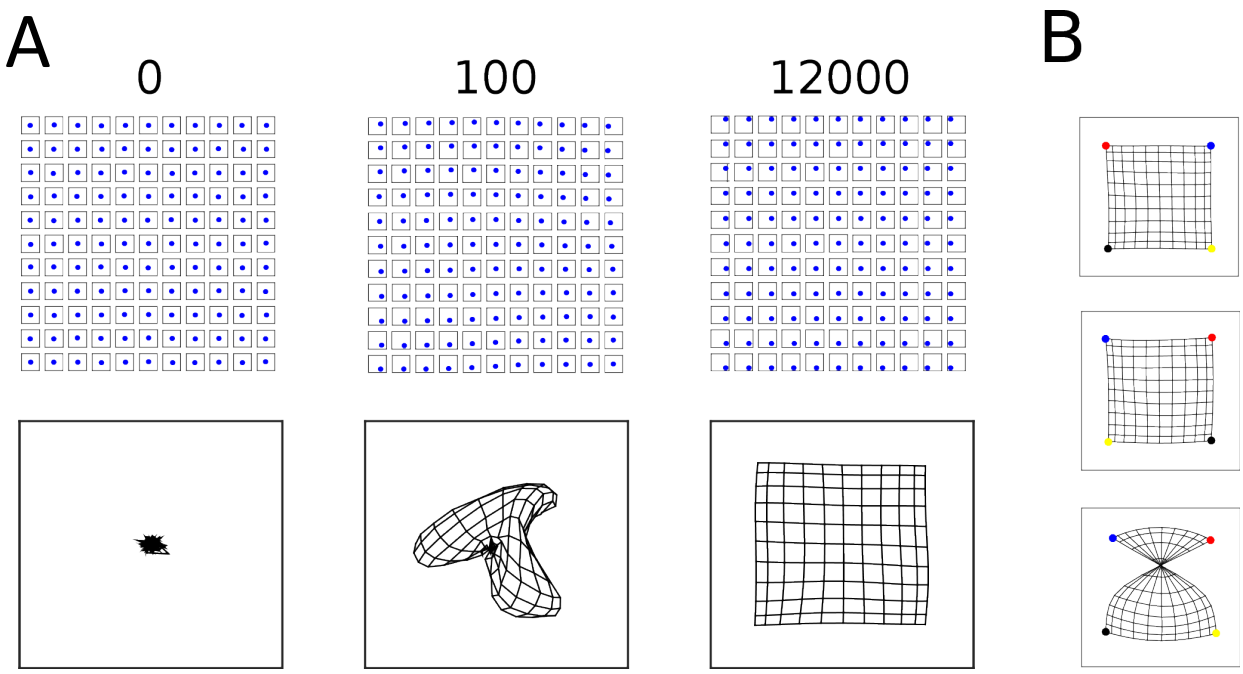

Figure 2.6. **The SOM model generates topographic maps. A**. Top row: position the receptive field centre for each postsynaptic cell. Bottom row: position of the CM of synaptic connections. Left panel: initially, at time 0, all synaptic weights are distributed equally, so that postsynaptic neurons response is unspecific. Centre panel: at time 100 postsynaptic responses and weights become more specific. Right panel: at time 12000 an ordered topographic map has been generated. **B.** The model returns different final results after 12000 iterations. Top: the postsynaptic sheet develops the same orientation as the presynaptic sheet, as indicated by the location of the coloured corners. Centre: the map unfolds but with incorrect orientation, different from the retina. Bottom: The postsynaptic weights did not unfold properly (the retinotopic map is disrupted).

On the other hand, another parameter allowed us to study how the strength of the Ephrin gradient or other molecular mechanisms are involved in the formation of topographic maps. Molecular guidance was modelled as a Gaussian function which increased the strength of the initial weights in the model based on the proximity of the presynaptic and postsynaptic neurons [19],

(19)
$$MG = e^{-\frac{\|(r_{\underline{pre}}+r_{\underline{noise1}})-(r_{\underline{post}}+r_{\underline{noise2}})\|^2}{2\cdot\sigma^2_{molecular}}}$$

Where *MG* is the weight of the molecular gradient for each presynaptic neurons respect to all of the postsynaptic neurons, $\sigma_{molecular}$ determines the specificity or strength of the molecular gradient and r_{noise} introduces a level of normally distributed noise between connections, with mean 0 and standard deviation σ_{noise}. The final synaptic strength for each presynaptic neuron N_i is the normalized average of all of its weighted connections.

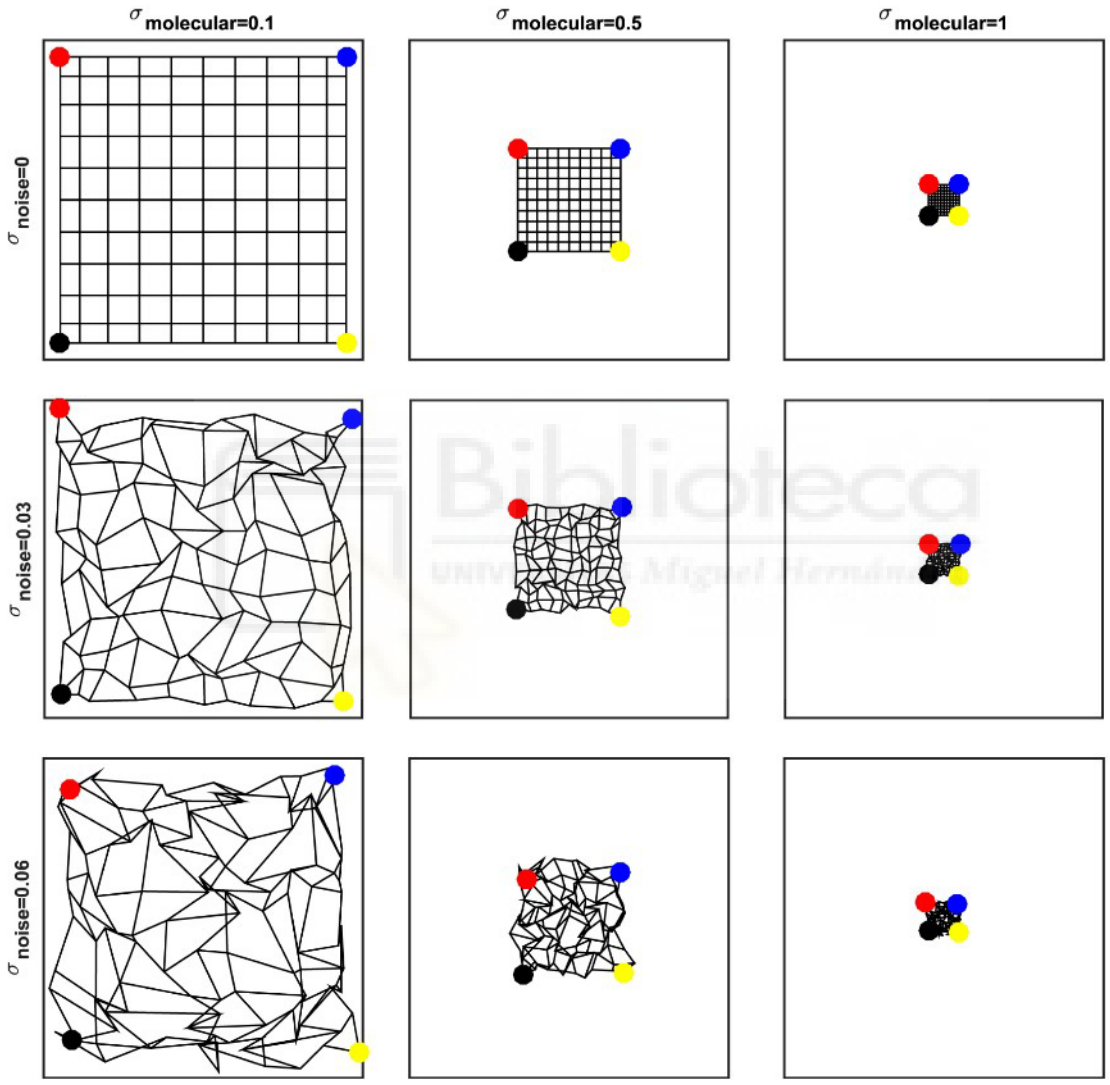

Figure 2.7. **Effect of molecular gradient and positional noise in the development of retinotopic maps.** Initial maps for all combinations of $\sigma_{molecular} \in [0.1, 0.5, 1]$ and $\sigma_{noise} \in [0, 0.03, 0.06]$.

The effect of the model parameters $\sigma_{molecular}$ and σ_{noise} is illustrated in Figure.2.7. A low value of dispersion in the molecular gradient and noise level gives an initial mesh very close to a perfectly deployed topographic map (upper left panel in Figure.2.7). Furthermore, an increasing the value of σ_{noise} (going from the front top to bottom in Figure.2.7) produces more disorganized initial maps. And increasing the value of $\sigma_{molecular}$ (going left to right in Figure.2.7) produces less predetermined initial maps, with receptive fields for all cells very close to a uniform response, therefore with the positions of the center of mass of the weights close to the center.

The different types of retinal activity used are shown in Figure 2.8. First, random patterns activate each retina with a sequence of independent uniform random stimuli. This stimulus class models the emergence of retinotopic topography in the absence of R-R projections. Second, locally coupled stimuli activate synchronously a small subset of RGCs retinotopically matched in both retinas for the first few iterations (100) of the model. Afterward, the activation of both retinas followed a sequence of independent uniform random stimuli as in the previous scenario. Last, binocularly matched retinal waves were triggered near the center of a retinal mesh and travel toward the periphery at the same speed in both retinas. The radius of the wave of stimulation increased at a rate of $2\ 10^{-4}$ (per iteration), and stimuli were applied randomly around that radius following a Gaussian distribution of mean 0 and sigma 0.04. In each case, the final synaptic strength onto each postsynaptic neuron Ni is the normalized average of all of its weighted connections.

By modeling the development of the right and left postsynaptic targets simultaneously, we were able to study how the presence or absence of R-R connections, and the different patterns of coordinated activity that they afford, could affect the establishment of bilaterally congruent retinotopic maps in visual structures receiving direct retinal inputs (Figure 2.8. C). The model returns correct results, i.e., perfectly matched left and right retinotopic layouts, only when the unfolding and orientation of both postsynaptic sheets is the same as the orientation

in the presynaptic RGC layer. On the other hand, incorrect results could come in the form of different orientations between pre and postsynaptic sheets or incorrect unfolding, which produce disruptions on the topographic map. Model parameters used are provided in Table 2.

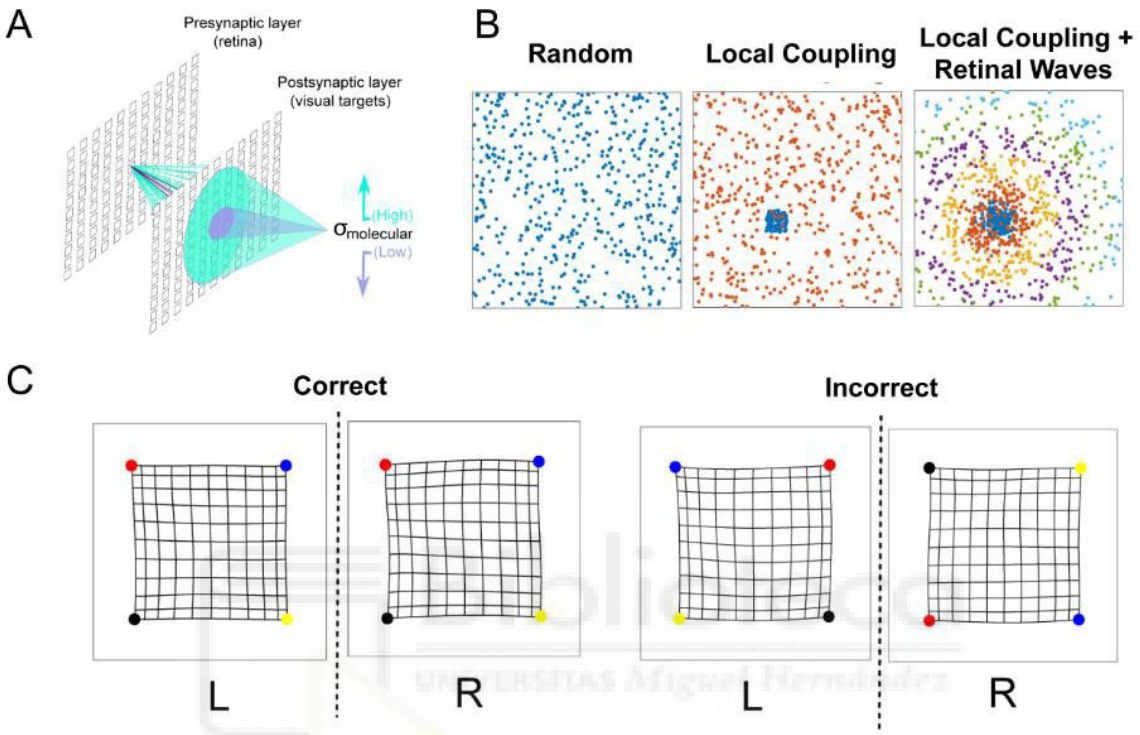

Figure 2.8. **Effect of molecular and activity-dependent mechanisms on the development of bilaterally congruent topographic maps. A**. A gradient of different guidance molecules instructs initial targeting in the postsynaptic layer. **B**. Left panel: To model the absence of R-R connections, a set of completely random stimuli was applied. Center and right panels: The presence of R-R connections was modeled in two different ways: Local coupling - an initial region of stimulation (shown in blue) is followed by random activity. Local coupling + retinal waves - local coupling followed by a retinal wave traveling at a constant velocity. **C**. Retinotopic maps in mice have bilateral congruency, thus both topographic maps are arranged in the same orientation. By modelling the development of the right and left postsynaptic targets simultaneously, we were able to study the role of molecular guidance cues and synchronous activity in the development of bilateral congruency. Examples of two simulations. Left: Correct bilateral congruency, i.e., left (L) and right (R) postsynaptic layers develop the same orientation as the presynaptic sheet as indicated by the order of the colored dots in the corners. Right: Incorrect bilateral congruency, in which, neither of the postsynaptic sheets coincides with the orientation of the retina nor coincide with each other as indicated by the order of colored dots.

SOM parameters

Table 2: Numerical values of model parameters.

Parameter	Description	Value
Λ	Weight decay term	0.1
T	Time constant of λ decay	5555
Σ	Lateral interaction influence decay	2
Nn	Number of cells	11 × 11
Nt	Number of iterations	1200
σ_{noise}	Standard deviation (SD) of position noise	[0,0.21]
$\sigma_{molecular}$	SD of the molecular gradient gradient	[0.1,10]

Experimental procedures

A total of 9 Brn3b-Zic2 and 11 WT mice were anesthetized with isoflurane (4-5%) and supplemented with chlorprothixene (2mg/kg s.c) to gain stability in the OI signal (Kelly et al 2014). Atropine (0.3-0.5 mg/kg s.c) was also used to reduce secretions. Temperature was maintained at 38º through the whole surgery and lactate 5% glucose (10ml/kg/h S.C) was infused to avoid dehydration. For imaging ISO levels where lowered to 1 - 0.75%. Mice were treated according to Spanish and European Union regulations, and experimental protocols were approved by the Institutional Animal Care and Use Committee of the University.

For visual stimulation, a high refresh tv monitor (*Mitsubishi Diamond Pro 2070sb)* was placed in front of the mouse and separated by 25 cm. The stimulation protocol consisted of trials of drifting square gratings oriented at 0, 90, 45 and 135, panned back and forth in both directions at a frequency of 1Hz. The total duration of the stimulation was of 4 seconds preceded by a 1 second baseline (a grey screen) and data was acquired in trials of 10 seconds binned in 500ms frames followed by another 10 seconds of inter stimulus interval, allowing the hemodynamic values of the cortex to return to baseline levels. Separated contralateral or ipsilateral stimulation was done by plugging each eye with a sterile patch. Finally,

experimental data was averaged over 10 trials to increase signal to noise ratio (SNR).

Data analysis

A digital image can be considered as a function f (x, y) where x, y and f (x, y) are finite and discrete (Gonzalez & Faisal 2019).The signal, binned as 500 ms data frames, was divided by the mean of the first 1.5s of prestimulus frames following equation [1],

(1) $$f(x,y)_i = \frac{f(x,y)_i}{\sum_{i=1}^{3} f(x,y)/_3}$$

To reduce high frequency noise, images where convoluted by a 5 by 5 median filter and frames between 2.5 and 6 seconds (frame 7 and 12) after the onset of the signal where collapsed and averaged for each orientation for further processing. This range of frames (2,5 - 6 seconds) was constantly selected for two reasons; First, due to characteristics of the OI signal, the SNR in those frames is at its peak (Figure 2.9). Second, this range of frames contains the accumulated temporal information of the cortical response for the two directions of the stimulation of each grating.

The SNR was computed as in eq [2],

(2) $$SNR = \frac{sig - back}{\sigma_{back}}$$

Where *sig* is the signal, *back* is the response of the prestimulus frames and σ_{back} the standard deviation of the background prestimulus frames. Only experiments with a mean global response for the 4 orientations above 2std from the background where used for further processing.

Once this collapsed image was computed ocular dominance response regions of activity for contralateral and ipsilateral eye stimulation were segmented and delimited at a threshold of 70% of their maximum peak response as in (Sato & Stryker 2008).

Finally, the ODI was calculated using a contrast index as in (Cang et al 2005a, Sato & Stryker 2008) following eq [3],

(3) $$ODI = \frac{C - I}{C + I}$$

Where C and I correspond to the contralateral and ipsilateral regions of response respectively.

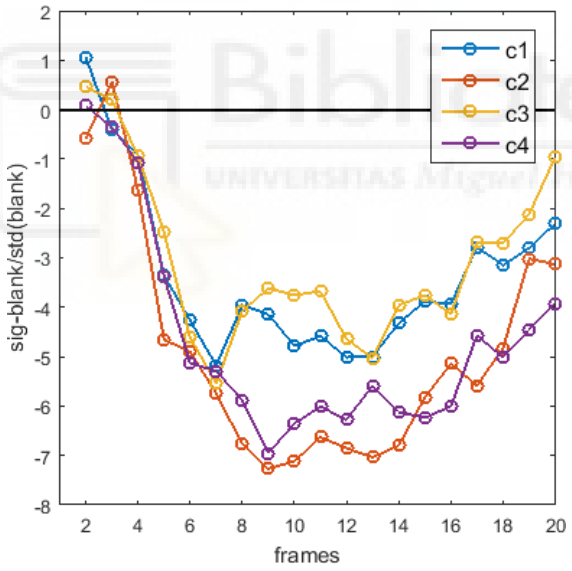

Figure 2.9. **SNR timecourse of an OI experiment**. C1, C2, C3, C4 correspond to 0 90 45 and 135 degrees of response respectively.

Mann Whitney test where performed for area of response comparisons and an ANOVA o control the confounding influence of weight against different response areas. All simulations and statistical analysis where performed with Matlab, Python or Graphpad softwares.

Results

Compression-Decompression Feedforward Network Model generates neurons with a preferred orientation

To study the wiring rules and operations the early visual pathway performs we built a compression-decompression feedforward network model that allows to explore the different functional topologies that emerge in V1 as the divergence-convergence ratios (DCr) between layers change. As it can be observed in Figure 3.1, neurons are connected between layers following a Gaussian function, so the closer two neurons are in the circuit the most probable the connections will be. The On and Off information travels in parallel from the RGCs to the dLGN and it finally converges the information from both pathways in layer 4 of V1, generating the classical RF that responds to a preferred orientation.

The connectivity between layers for a fixed value of σ_l, that determines the width of the Gaussian function, is determined by the DCr formula (see methods). The degree of thalamocortical divergence is correlated with the Cmag and computed as the thalamocotical divergence area. As a final step, intralayer short range connections between neurons in layer $2/3$ are simulated following a Gaussian thresholded local connectivity matrix (at 70 % of peak response from the global Gaussian connection matrix). In other words, the strength and area of local connections are determined by the size of the Gaussian field required for a fixed level of convergence of inputs in the cortex and the DCr across layers. That way we can differentiate from the raw input that reaches layer 4 neurons and the output, in which the size of local connections, which interpolate the final orientation, is constrained by the DCr. So as the DCr increases, so does the number of neurons that share a common input as well as the size of the local connectivity matrix. Finally, different functional topologies of orientation selective neurons can be explored by modifying the DCr across layers.

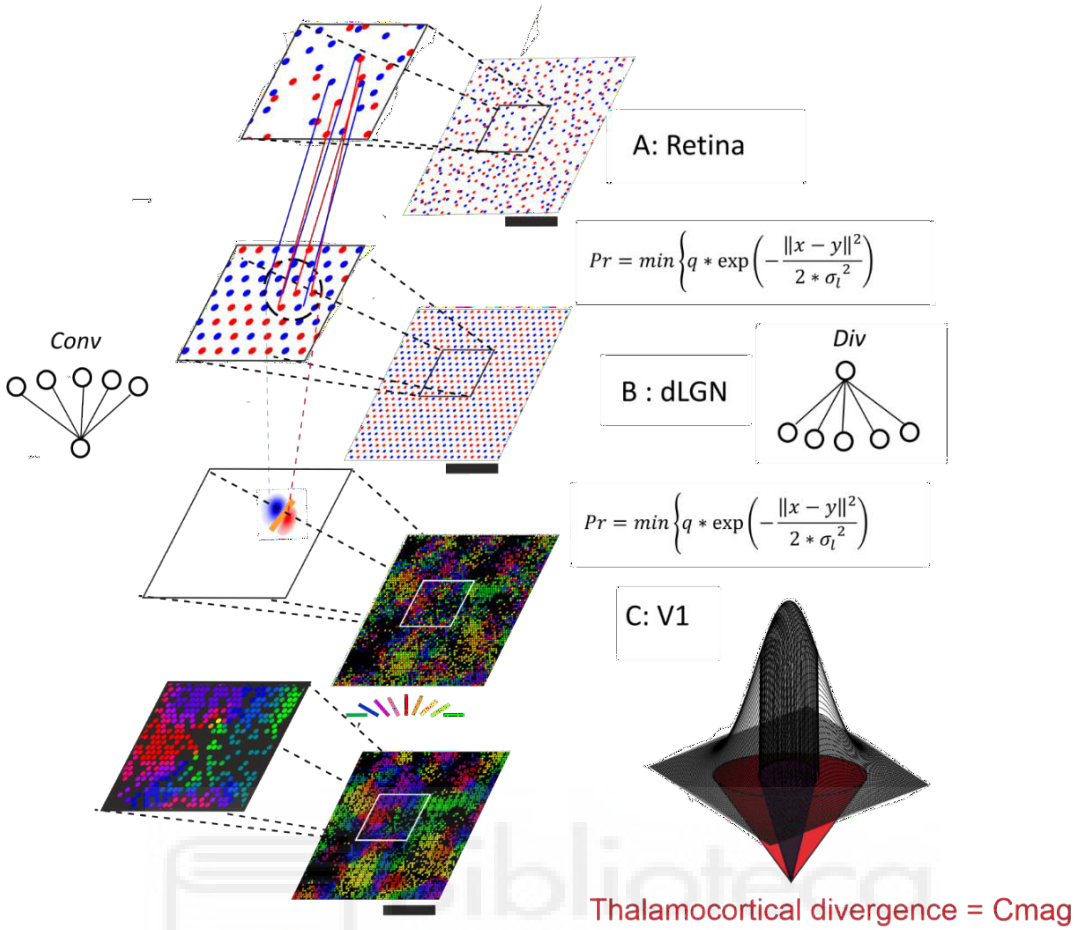

$$DCr = \frac{Divergence}{Convergence} = \frac{Pos_n}{Pre_n} = \frac{Pos_A * Pos_D}{Pre_A * Pre_D}$$

$$X_n = layer\ number\ of\ neurons$$
$$X_D = layer\ denstity$$
$$X_A = layer\ area$$

Figure 3.1. **Compression-Decompression Statistical Neural Network Model.** Connections between the retina (**A**), the dLGN (**B**) and V1 (**C**) are able to generate simple RFs that respond to a preferred orientation in V1. At the first stage (**A**), the on/off RGCs are placed following the PIPP algorithm simulating the spatial statistics of real data (see methods). In the second stage (**B**) the dLGN neurons are arranged as a hexagonal regular mesh of sensors and only neurons that share the same polarity are connected with the previous layer. The third step, (**C**) corresponds to converging connections from both polarities (On and Off) from the thalamic layer, that are able to generate the classical receptive field of a layer 4 cortical neuron that responds to a preferred orientation. As a final step, a local connectivity matrix thesholded at 70% of the peak response from the final layer connection matrix, determines the intralayer short range connections between V1 neurons.

Thalamocortical convergence modulates the structure of OPMs and receptive fields

High values of convergence are necessary to generate the characteristic RFs and topographic layouts of oriented neurons of V1. As the convergence values increase from 4 to 60 connections per neuron as reported by experimental results (Alonso et al 2001, Lien & Scanziani 2018), the proportion of neurons with a high OSI increases (Figure 3.2).

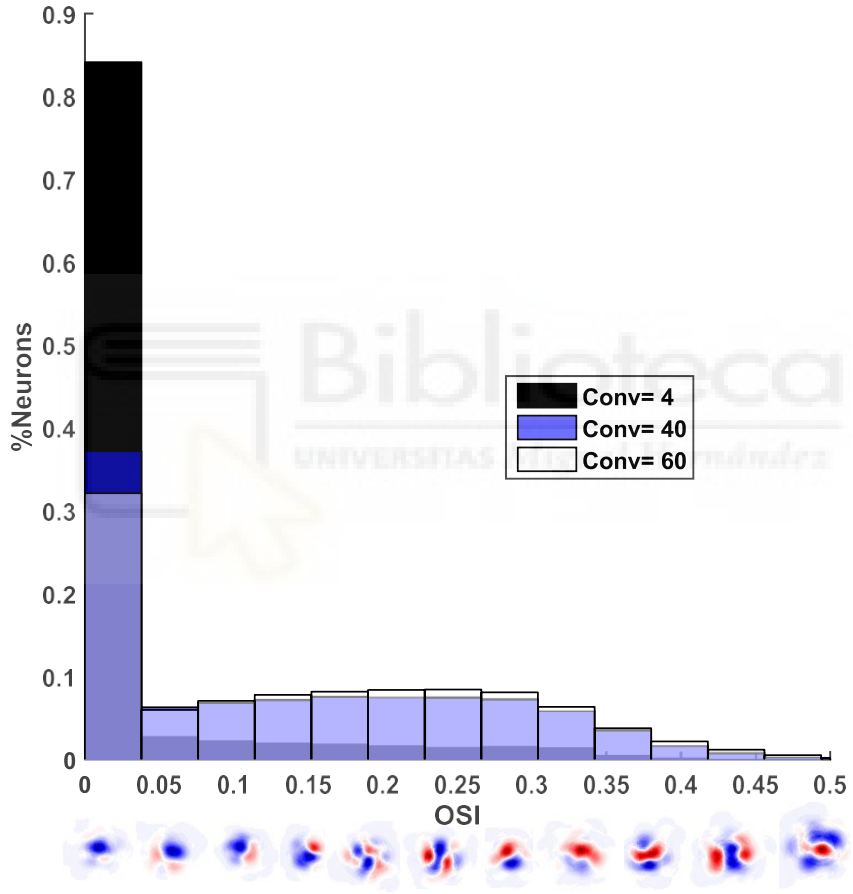

Figure 3.2. **Thalamocortical convergence modifies the proportion of OSI neurons of V1.** As thalamocortical convergence increases the proportion of neurons with high OSI values rises. Bellow, example RFs for different OSI values.

This high values of convergence allow to predict the orientation of a V1 neuron by looking at the thalamic population RF, that is, the sum of all the On and

Off spatially distributed receptive fields (RFs) of the neurons. When the convergence values are low neurons clearly selective to orientation (OSI>0.25) are clustered in small domains dispersed randomly over the cortex. However, as convergence increases, OSI neurons start to cluster in the borders of the thalamic RF population map, making it possible to predict the orientation of a V1 neuron by visual inspection of the thalamic population RF (Figure 3.3).

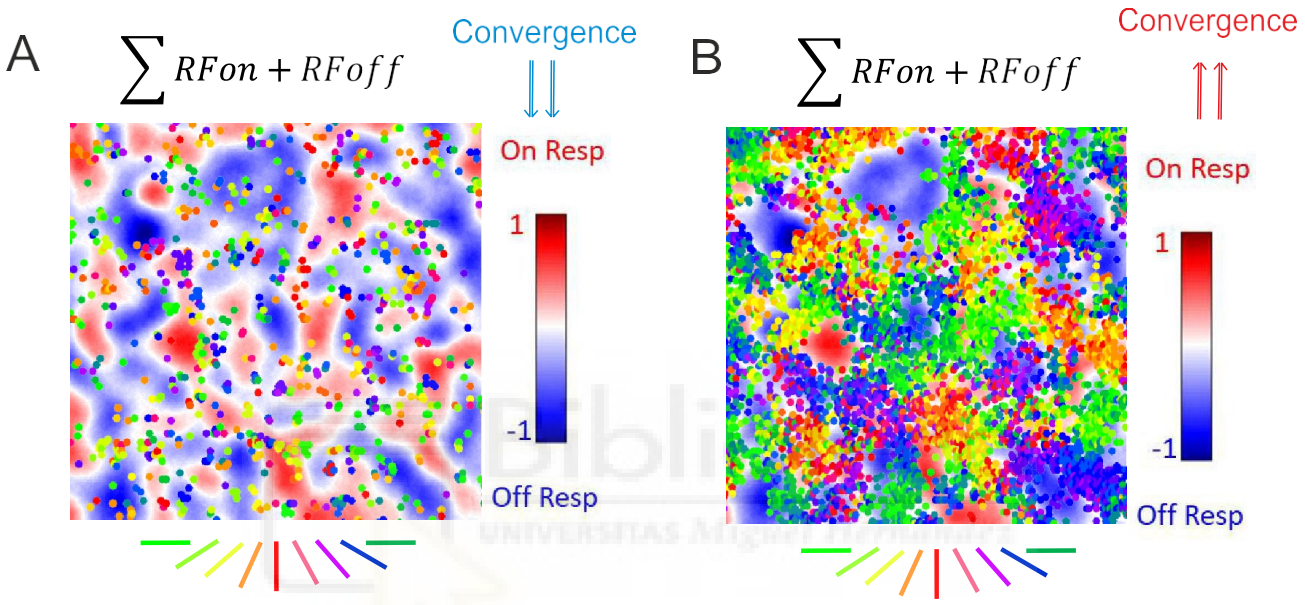

Figure 3.3. **Thalamocortical convergence increases the correlation between the thalamic population RF response and the topological disposition of orientation selective neurons in V1. A**. Low values of thalamocortical convergence generate small random clusters of orientation selective neurons in V1 that do not follow any apparent order respect to the thalamic population RF map. **B**. High values of convergence make OSI neurons to cluster in the borders of the thalamic population RF map. Thalamic population RF maps are represented as the superimposed activity of all On RFs (red) and Off responses (blue). Superimposed neurons selective to orientation are color coded as a function of their preferred response to orientation.

Finally, this high values of convergence seed the typical circular correlation signature of OPMs (Schottdorf et al 2014). When measuring the circular correlation at concentric circles of increasing radius from all neurons strongly tuned for orientation (OSI>0.25), the typical circular correlation signature of OPMs,

characterized by strong local correlations, intermediate distance anticorrelations and long range correlations, emerges (Figure 3.4). Thus, high values of thalamocortical convergence are important for the functional topology of layer 4 V1 neurons.

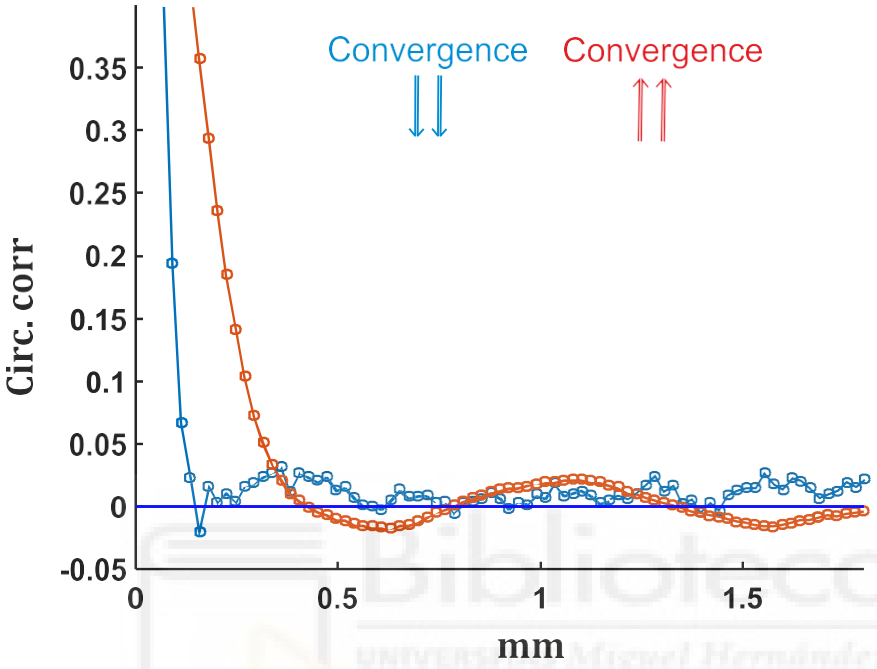

Figure 3.4. **Circular correlation as a function cortical distance**. In blue a model obtained with low convergence values from 4-5 connections per cortical neuron. In red high convergence model with a mean 60 connections per cortical neuron.

Divergence-Convergence ratios are tuned to recover as much visual information as possible and as a consequence the proportion of orientation selective neurons in V1 increases

What is the role of this high convergence values taking into account the high metabolic cost required? The conclusion that we can extract from the model is that the function these high values of convergence have is to recover the maximum level of spatial information as possible from On and Off RGCs through interpolation of inputs. To explore the maximum level of spatial information, understood as the

coverage of space with different degrees of convergence, we took the final On or Off RFs of all V1 neurons, cut the RFs at 90% of their peak response and calculated the area that they covered, normalized respect to the initial area covered by the RGCs in the retina. With the density of V1 neurons fixed, we varied the number of V1 neurons by increasing or decreasing V1 area and the degree of thalamocortical convergence (Figure 3.5).

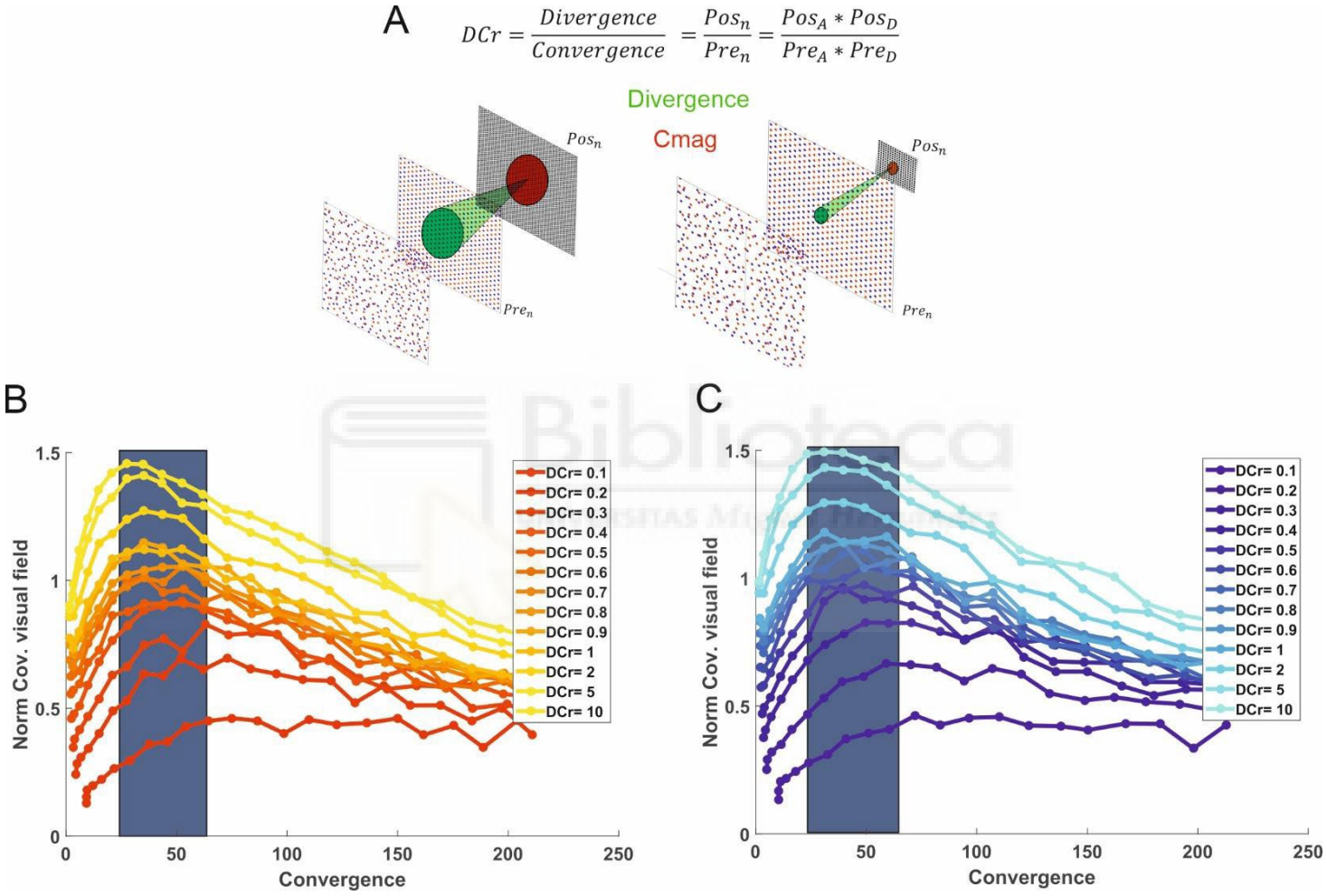

Figure 3.5. **Coverage of visual space as a function of retinothalamic convergence. A**. Coverage of the visual field is analyzed by cutting the On or the Off RFs at 90 % of their peak response for different DCr values at different thalamocortical convergence values and V1 areas. If the size of V1 increases so does the divergence and the Cmag across layers and viceversa. **B.** Coverage of visual space in V1 as a function of convergence for On RFs. **C.** Coverage of visual space in V1 as a function of convergence for Off RFs. Blue rectangle, optimal coverage values for different DCrs. Different DCr values are color coded.

There is an optimal thalamocortical convergence value of around 20-60 connections per layer 4 cortical neuron depending on the final size of V1 (or to the final DCr) in which the maximum percentage of normalized covered visual field is reached respect to the initial coverage of the retina. This means that the joint distribution of On and Off convergence values generates high overall values of convergence which in turn increase the number of OSI neurons present in V1 (Figure 3.2). Thus, there is an optimal coverage of visual space principle operated in V1 by interpolation of inputs through high values of thalamocortical convergence.

As noted by the DCr formula, as Pos_n or V1 area increases, the levels of divergence required to reach a fixed value of convergence also increases. Which in turn implies that the levels of divergence required to reach the optimal values of coverage of visual space also increase with the DCr (Figure 3.6). As we will see later, these different levels of divergence will have clear consequences in the overall topological function of V1 cortical neurons.

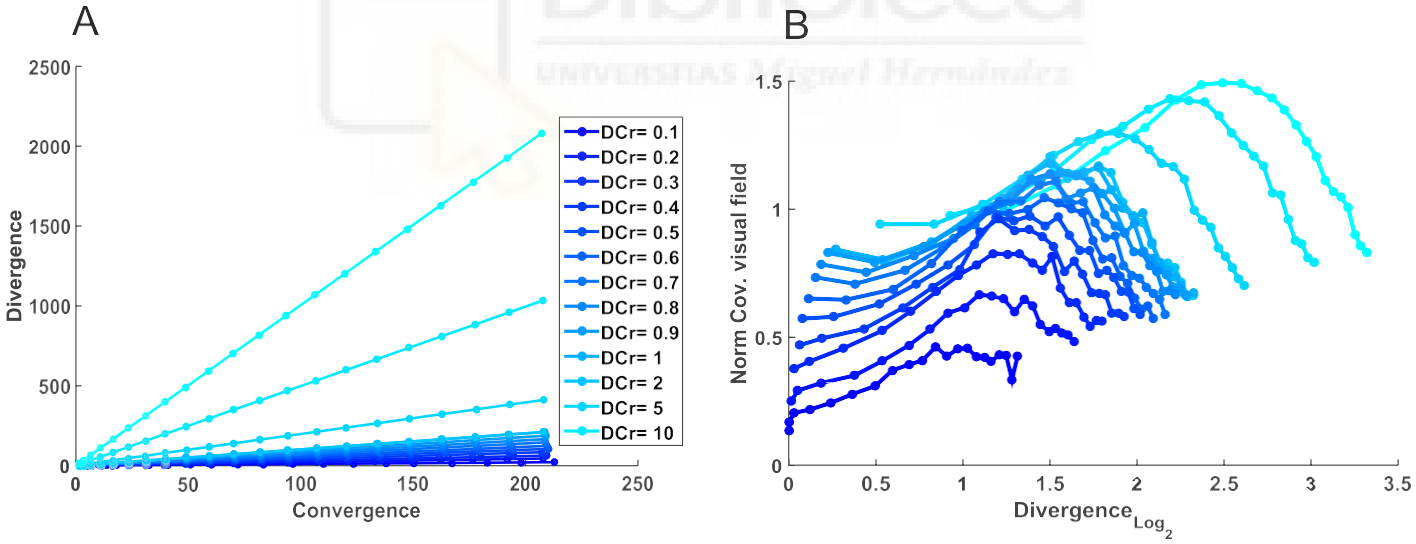

Figure 3.6. **Divergence-converge ratios relationships for V1 Off neurons**. **A**. Divergence as a function of convergence and different DCrs. **B**. Normalized covered visual field as a function of divergence (in logarithmic scale) and different DCr. Different DCr values are color coded. Similar results are obtained for On RFs.

Also, as Pos_n increases in V1, due to an increasing V1 area, so does de DCr and the maximum covered visual field reached for the optimal thalamocortical convergence value, as there are more neurons computing information in the final layer (Figure 3.7). However, when DCr>2 the coverage effectiveness mediated by interpolation of inputs starts to diminish and stabilizes at a plateau following an exponential function ($y = 1.42\ (1 - e^{-1,71x})$). Thus, there is a maximum level of coverage that can be reached, that cannot be surpassed by increasing more the number of neurons in the final layer.

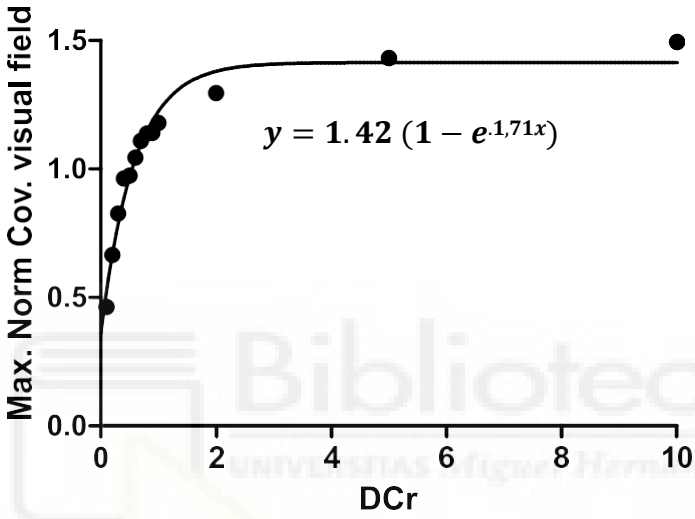

Figure 3.7. **Maximum normalized coverage of visual field as a function of V1 divergence-convergence ratios**.

Finally, it is important to mention that this increase in coverage is not simply mediated by an increase in size of V1 layer 4 RFs, it is reached at an intermediate point where the increase in RF size is combined with the final position occupied in space by the RFs.

First, as thalamocortical divergence and convergence increases so does the final area of each On or Off RF (mm^2) that each cortical neuron develops (Figure 3.8). The different levels of DCr do not affect the final size of the RF, however, as noted earlier in the DCr formula, as the DCr increases the divergence levels must increase to reach a determined value of RF size and thalamocortical convergence.

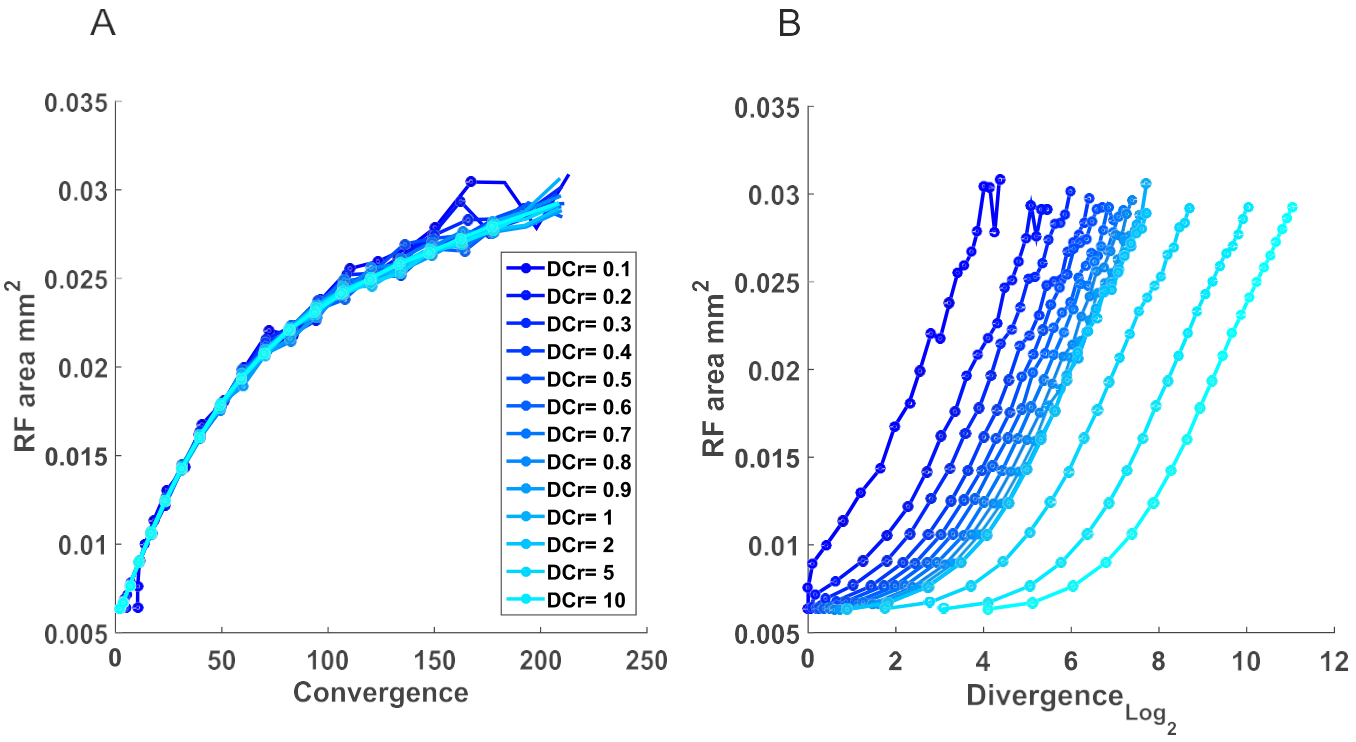

Figure 3.8. **Off RF size as a function of DCr. A.** RF area (mm^2) as function of convergence and different DCr**. B.** RF area (mm^2) as function of divergence (in logarithmic scale) and different DCr. Different DCr values are color coded. Similar results are obtained for On RFs.

An increase in RF size will certainly decrease visual acuity because as RFs grow bigger the discrimination between two different elements close in the visual field becomes more difficult. As noted by (Hirsch et al 2015, Martinez et al 2014), this upsampling and interpolation of RFs will certainly cause image blurring, however inhibitory circuits may compensate this mechanism enhancing contrast borders and reducing the blur. Nevertheless, RF size increase due to interpolation of inputs it is not the only the factor that increases coverage in visual space, in fact, the RFs peaks reallocate in visual space so that the region maximum coverage its obtained at an intermediate level of RF size (Figure 3.9). However, for very high levels of thalamocortical convergence the RFs peaks cluster in very defined points of visual space decreasing coverage in favor a highly redundant message.

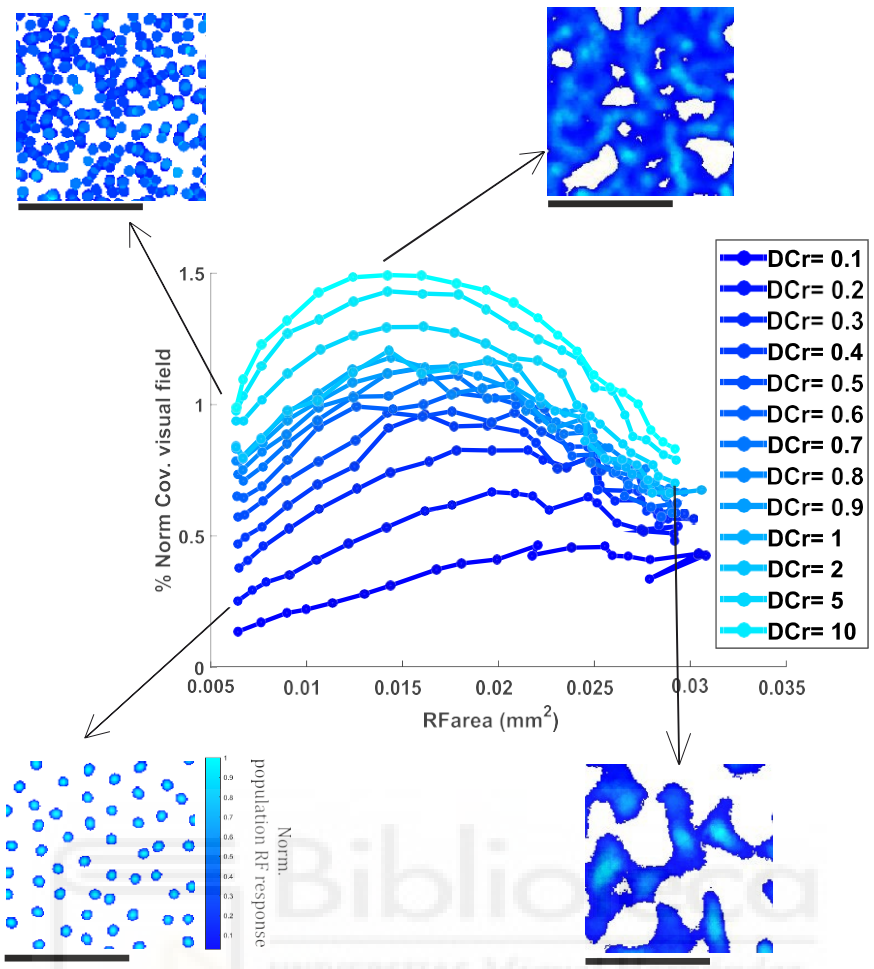

Figure 3.9. **Normalized coverage of visual field for Off RFs as a function of RF area**. Small boxes are examples of RF population peaks covering a cortical area of 2.25 mm^2 (scale bar 1mm), normalized by the population maximum response. Different DCr values are color coded. Similar results are obtained for On RFs.

In fact, by measuring redundancy, understood as the proportion of RF peaks overlapping similar regions of the visual field (see methods), it can be seen how as divergence and convergence levels increase as well as the final size of V1, redundancy increases since the proportion of neurons sharing similar RFs rises (Figure 3.10). And, more importantly, that optimum values of coverage of visual space are reached at intermediate redundancy levels. Thus, RFs do increase their overlapping at increasing DCrs, however as the optimal thalamocortical levels of convergence are surpassed, RFs start to cluster in definite points of visual space, increasing redundancy, but decreasing coverage of visual space (Figure. 3.11).

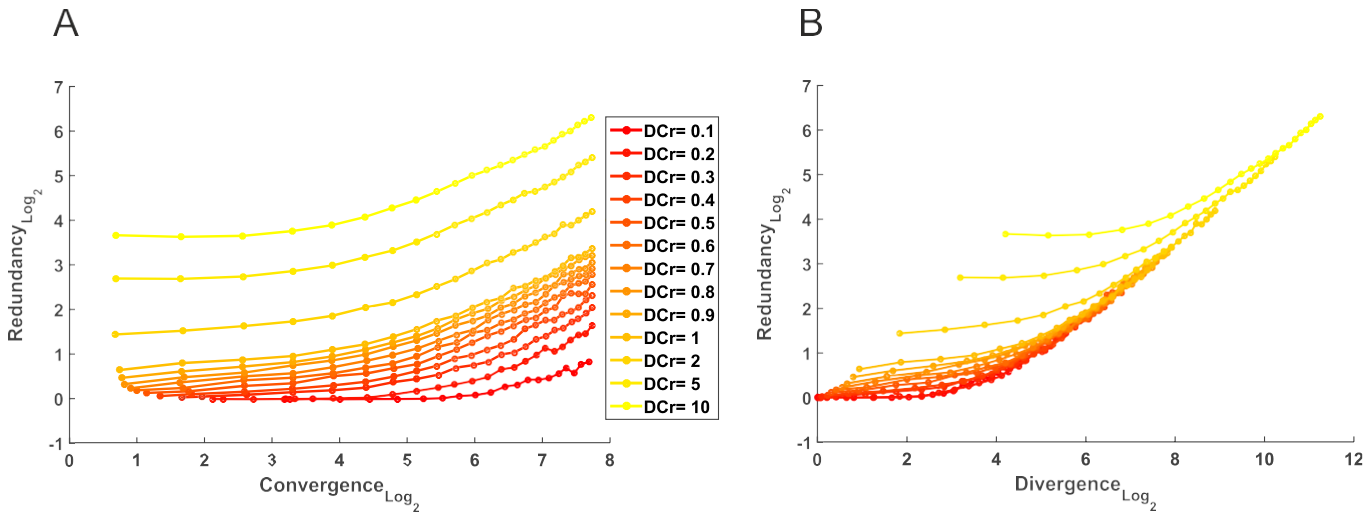

Figure 3.10. **Redundancy as a function of divergence-convergence ratios for On V1 RFs**. **A.** Redundancy as function of convergence and different DCr. **B**. Redundancy as function of divergence and different DCr. Plots are in logarithmic scale and different DCr values are color coded. Similar results are obtained for Off RFs.

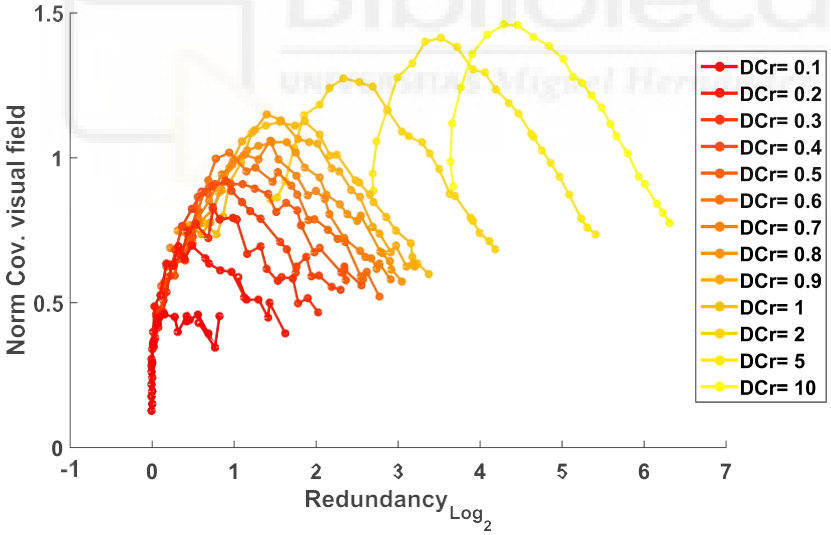

Figure 3.11. **Normalized coverage of visual field for On RFs as a function of V1 redundancy levels**. Redundancy axis is in logarithmic scale and different DCr values are color coded. Similar results are obtained for Off RFs.

These simulations demonstrate that the main operation that V1 layer 4 neurons are performing is to interpolate information from the On and Off pathways

to recover as maximum information as possible through convergence of thalamocortical inputs to optimally cover visual space with intermediate levels of redundancy. As the convergence increases, RFs realocate in visual space enhacing coverage, and as the DCr increases (bigger V1 size) smaller RFs tile better the visual field which will certainly enhance visual acuity. Finally, these high convergence values are the cause for the high proportion of orientation selective neurons in V1 due to the integration of On and Off inputs to optimally cover visual space.

Cortical functional topology is consequence of a universal coverage optimization principle and different biological constraints determined by the DCr

The fact that different functional topologies appear across different mammalian orders, salt and pepper in rodents and lagomorphs and OPMs in carnivores, primates, scadentia and cetarciodactyla, together with the antagonistic view of some authors that consider similar the cortex across mammalian species (Carlo & Stevens, 2013; DeFelipe et al., 2002; Rockel, Hiorns, & Powell, 1980), while others claim that is clearly different (DeFelipe et al., 2002; Herculano-Houzel, Collins, Wong, Kaas, & Lent, 2008). Suggests some kind of common biological constraints, that may be dominating the development of the cortical circuitry through evolution causing differences in closely related species (primates and rodents) and similarities in more dissimilarly related species (carnivores, primates, cetarciotactila) (Figure 3.12. A).

If we now assume that all these species follow the same coverage optimization principle, the convergence value of the DCr formula can be fixed to high values of around 40 to 60 of mixed On and Off inputs per layer 4 neuron as experimentally reported (Alonso et al 2001, Lien & Scanziani 2018) to explore the different functional topologies that may emerge at different DCr values.

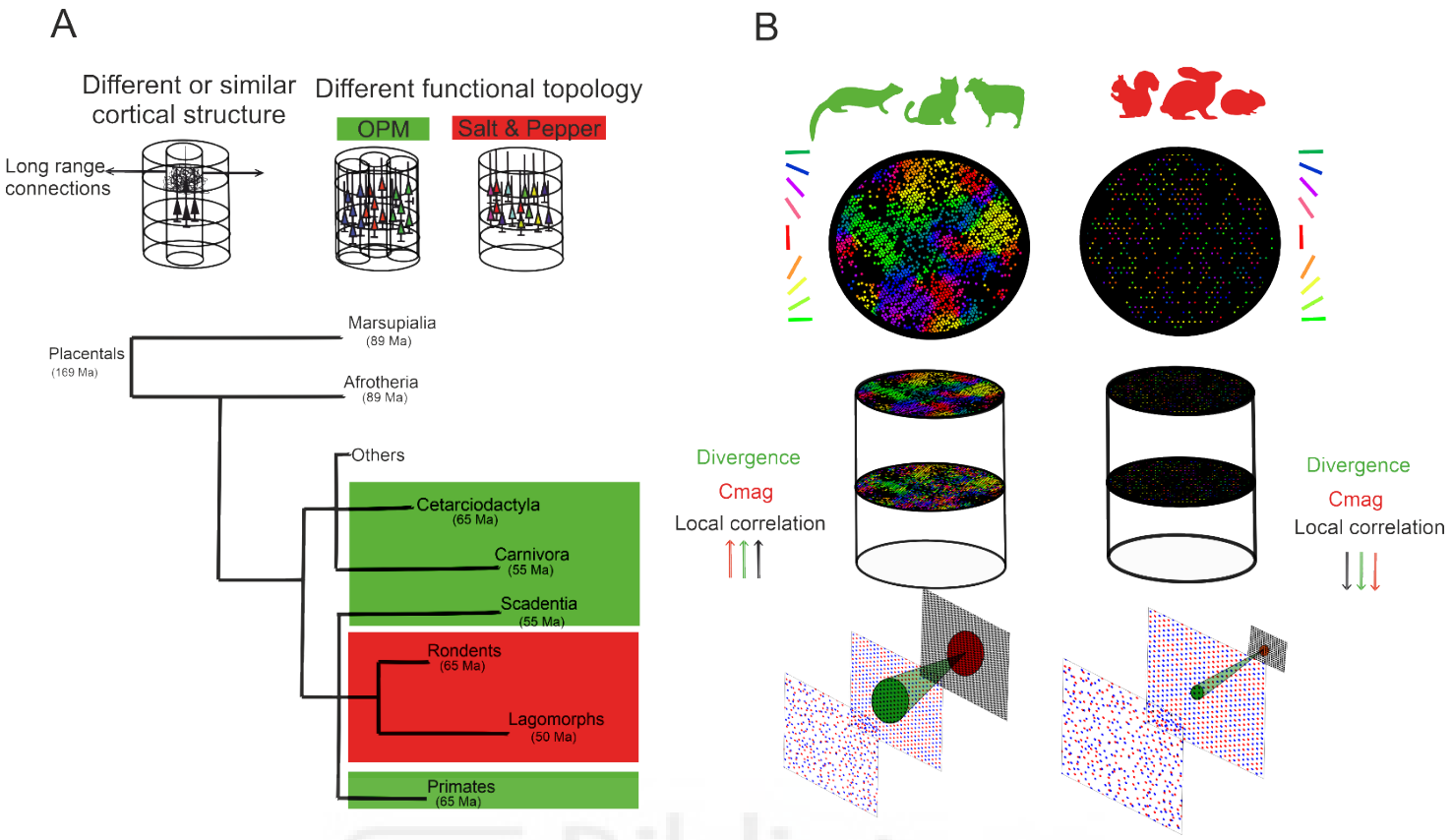

Figure 3.12. **Cortical functional topology as a function of Divergence - Convergence ratios. A.** Scheme of the different functional topologies found in V1 across mammalian species (salt and pepper in red; OPM in green; for the rest of species there is no available functional data). **B.** DCr values for a fixed connectivity profile determine the salt and pepper or OPM configuration found across phylogeny.

The model predicts that when the number of neurons in V1 is low enough, to maintain the optimum levels of convergence, the divergence lowers to a value of around 4-10 efferents per LGN neuron, following the DCr formula (Figure 3.13). This in turn generates low local correlations (>50 μm) and small Cmags (< 0.1 mm^2) giving birth to a salt and pepper decorrelated functional topology (Figure 3.12. B).

On the other hand, when the number of neurons in V1 is big enough, to maintain the optimal levels of convergence, the divergence values need to be really high (>100 afferents per neuron), which in turn increases the cortical magnification factor (>0.1 mm^2), as well as the size of the local correlation domains (>150 μm),

thus creating an OPM (Figure 3.12. B, figure 3.13). So when the DCr >2 an OPM starts to emerge.

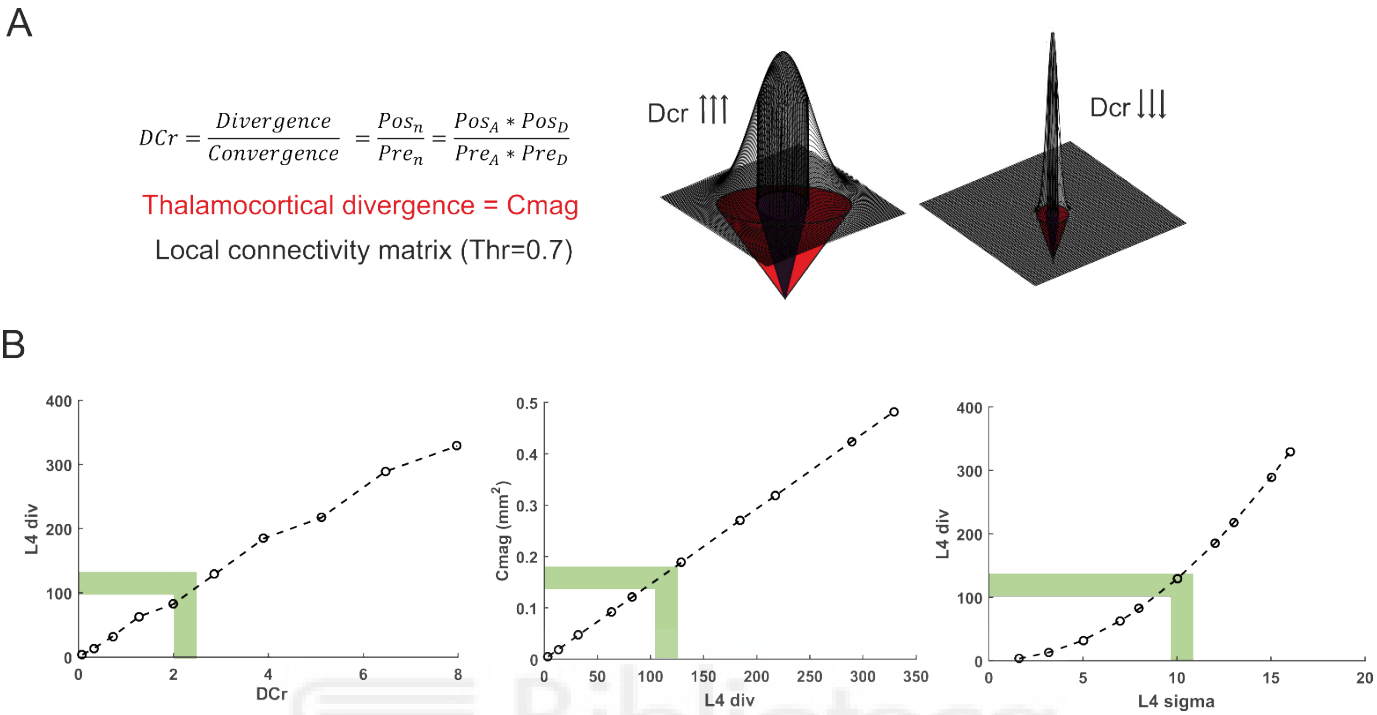

Figure 3.13. **Parameter relationships for high convergence values and different DCrs. A.** As DCr increases so does the thalamocortical divergence, which in turn increases the Cmag (Cortical magnification factor) understood as the mm² of V1 devoted to a similar RF. **B.** Relationships for L4 divergence, cortical magnification factor and σ_l. In green OPM threshold.

These results can be summarized by looking at the circular correlation function at increasing DCr values (Figure 3.14). As DCr increases, local correlations, anticorrelations and long range correlations also increase. In other words, the larger the DCr value, the larger the mean diameter of the cortical columns present in V1 as well as hypercolumn size (λ), determined by the long rage correlation peaks (see methods).

To test the hypothesis that the functional topology of V1 is mainly due to the biological constraints generated by the difference in size of V1 respect to the retina

and a common optimization principle of coverage, we compared our results to anatomical data (Fig. 5 and Table 1).

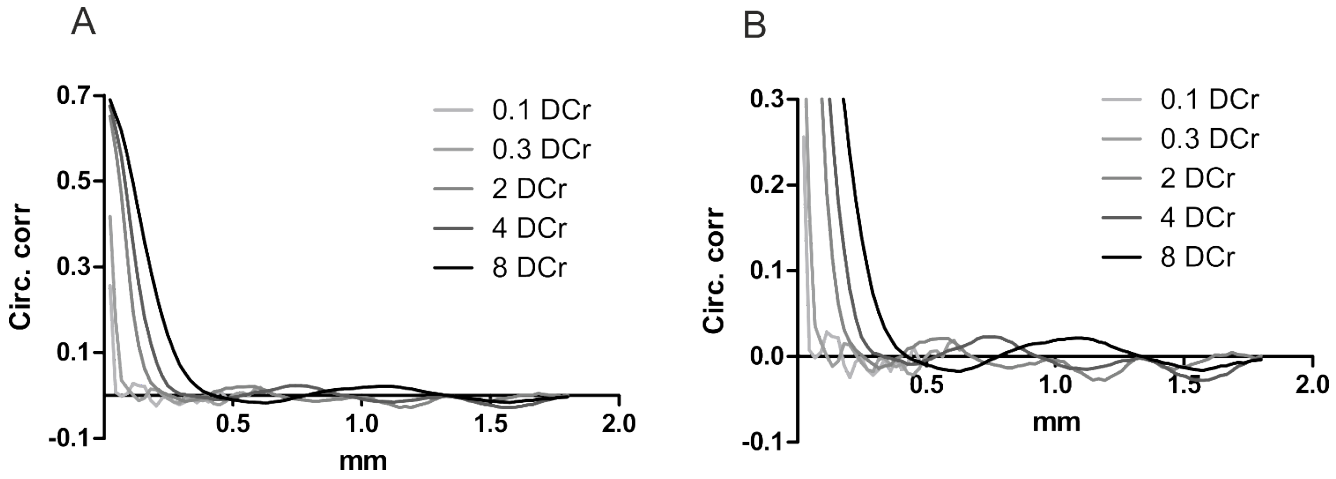

Figure 3.14**. Circular correlation function for different values of DCr as indicated in the labels**. **A**. The circular correlation function obtained for the RAW thalamocortical input. **B**. Same graph but zoomed in to see more clear the long range correlation peaks.

Anatomical data shows that species with a salt and pepper configuration have a lower V1 area/retinal area compared to others that develop OPMs (Figure 3.15). On the one hand, even though the area of the retina and V1 scales with brain weight, there is a clear overexpansion of V1 respect to the retina. This can be seen by the bigger logarithmic slope of V1 area respect to the retinal area as brain weight increases, (Figure 3.15. A, B). On the other hand, it is clear that most of the rodents tend to have a smaller brain weight in comparison to carnivores and primates (Figure 3.15. A, B). Finally, there is also a tendency for rodents to have a bigger retina in comparison to their V1 area (Figure 3.15 C). The ferret and the rabbit have a similar brain weight and V1 size, however the retina of the rabbit is much bigger promoting a salt and pepper topology. The tree shrew has also a bigger V1 and smaller retina than other rodents of similar brain weight, promoting an OPM.

The data in Figure 3.15. D shows a threshold at a V1 area/ Retina area under which all animals should have a salt and pepper configuration and over an OPM. For species that are just in the threshold point such as larger rodents, the capybara (the largest rodent), the agouti and the marsupial Quokka, the model predicts that they

should develop at least stronger local correlations in comparison with animals at the left of threshold that clearly have a salt a pepper configuration.

These results show that a coverage optimization principle shared across mammals and the biological constraints determined by the different size of V1 across species can explain the different functional topologies found across the mammalian orders.

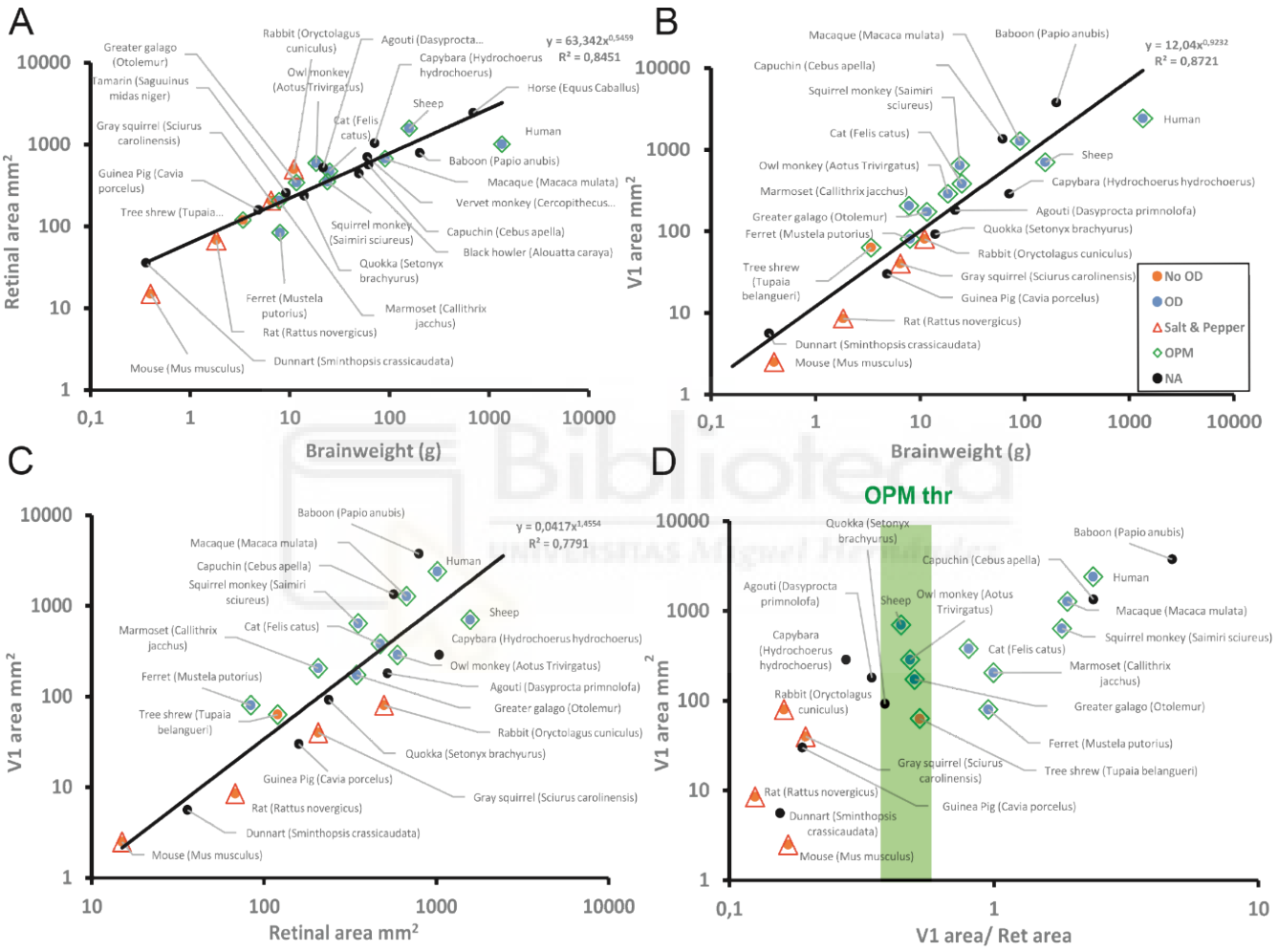

Figure 3.15**. Anatomical data confirms that the different functional topologies found across mammals are due to different Divergence- Convergence ratios. A**. Retina area scales with brain weight (R^2=0.845) (OD, ocular dominance; NA; No data available; OPM; orientation preference map). **B.** V1 area scales with brain weight (R^2=0.872). **C**. V1 area scales with retina area (R^2=0.779). **D**. V1 area against V1/Retina area. The data clearly separates mammals with a salt and pepper configuration with those with an OPM by taking into account the V1 area/Ret area ratio (OPMthr; threshold for the appearance of an OPM). Animals with a small ratio develop a salt and pepper configuration, while those with a high ratio develop an OPM.

Local and long range correlations appear at different DCr thresholds

OPMs are quasiperiodic structures that have a typical circular correlation signature (Figure 3.17 A, B). Strong local correlations, followed by anticorrelations and long range correlations. The long range correlation peak determines the size of the hypercolumn, and the robustness, that is, the area beneath peak indicates the strength of the periodicity (see methods). The strength and distance of each of these characteristic points was quantified for an optimized coverture of On and Off inputs (convergence=60) and different DCr following anatomical data for the raw input or output of local V1 connections maps (Figure 3.17 A, B). Thus, we can study the topological disposition of neurons at different DCr values, that is, against different V1 areas, to see at what point an OPM appears.

As the size of V1 increases the structure of an OPM starts to emerge, just by looking at the raw input that reaches layer 4, local clusters of similar oriented neurons (OSI>0.25) emerge (Figure 3.16; Figure 3.17). Each of the circular correlation parameters for the raw input, in black, was compared against a control, in gray, in which the position of the orientation selective neuron was conserved but the orientation and the OSI was randomized (Wilcoxon test $p<0.05$). For each DCr or Area ratio bin there are 20 independent models with their standard deviation. For each parameter, the green band shows the threshold in which each of the variables is statistically significant respect to the initial DCrs (Friedman Test $p<0.05$) (Figure 3.17 D-H; Appendix 1, S3).

Local correlations increase abruptly and stabilize when DCr>0.1 (Figure 3.16; Figure 3.17. D) and the size of the local correlations columns increases steadily as the DCr increases (Figure 3.16; Figure 3.17. E). For both parameters when the DCr>0.1 they become statistically different from low DCr conditions. The hypercolumn and anticorrelation values, also increase as the DCr increases with a threshold value reached when DCr>2 (Figure 3.16; Figure 3.17. F, G).

The periodicity robustness suggests that for a DCr<1 the long range correlations are indistinguishable from a completely random map. However, when

the DCr > 2, the map starts to become periodic (Figure 3.17. H; Figure 3.16). However, it is important to mention that these long range correlations are weak when compared to real data. It is necessary to apply some kind of band bass filtering to enhance these long range correlations to match experimental values (Schottdorf et al 2015) .

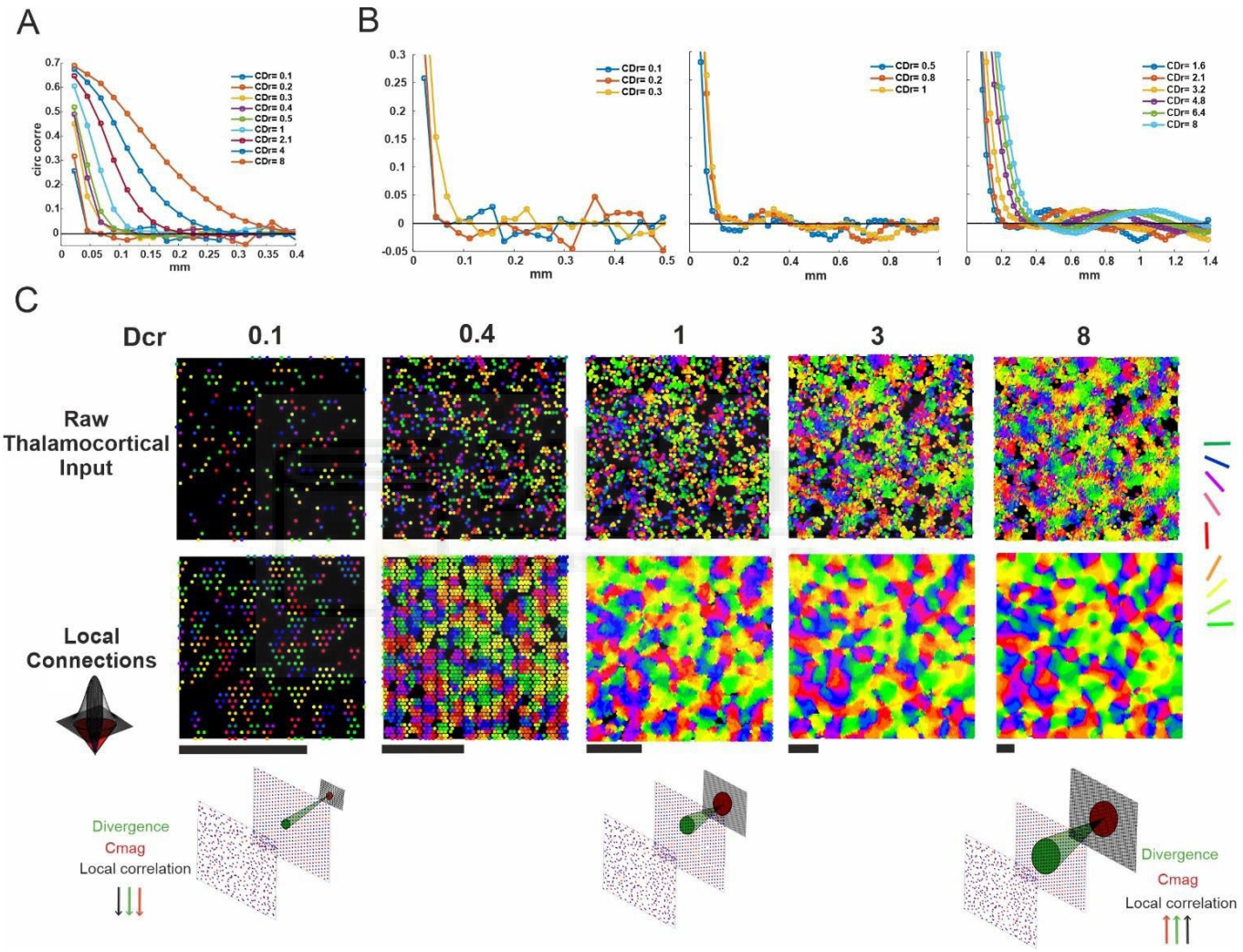

Figure 3.16. **Local and long range correlations as a result of different DCr values. A**. For high convergence values optimizing coverture of visual space (40-60 connections per layer 4 neuron) local correlations and column size increase with DCr. **B**. Long range correlations emerge for a DCr > 2. **C**. Examples of low and high DCr functional topologies in V1. In the first row for the raw thalamocortical input that layer 4 neurons receive. Second row shows the structure after applying local connections from orientation selective neurons to the rest of neurons in V1(Scale bar 0.5 mm).

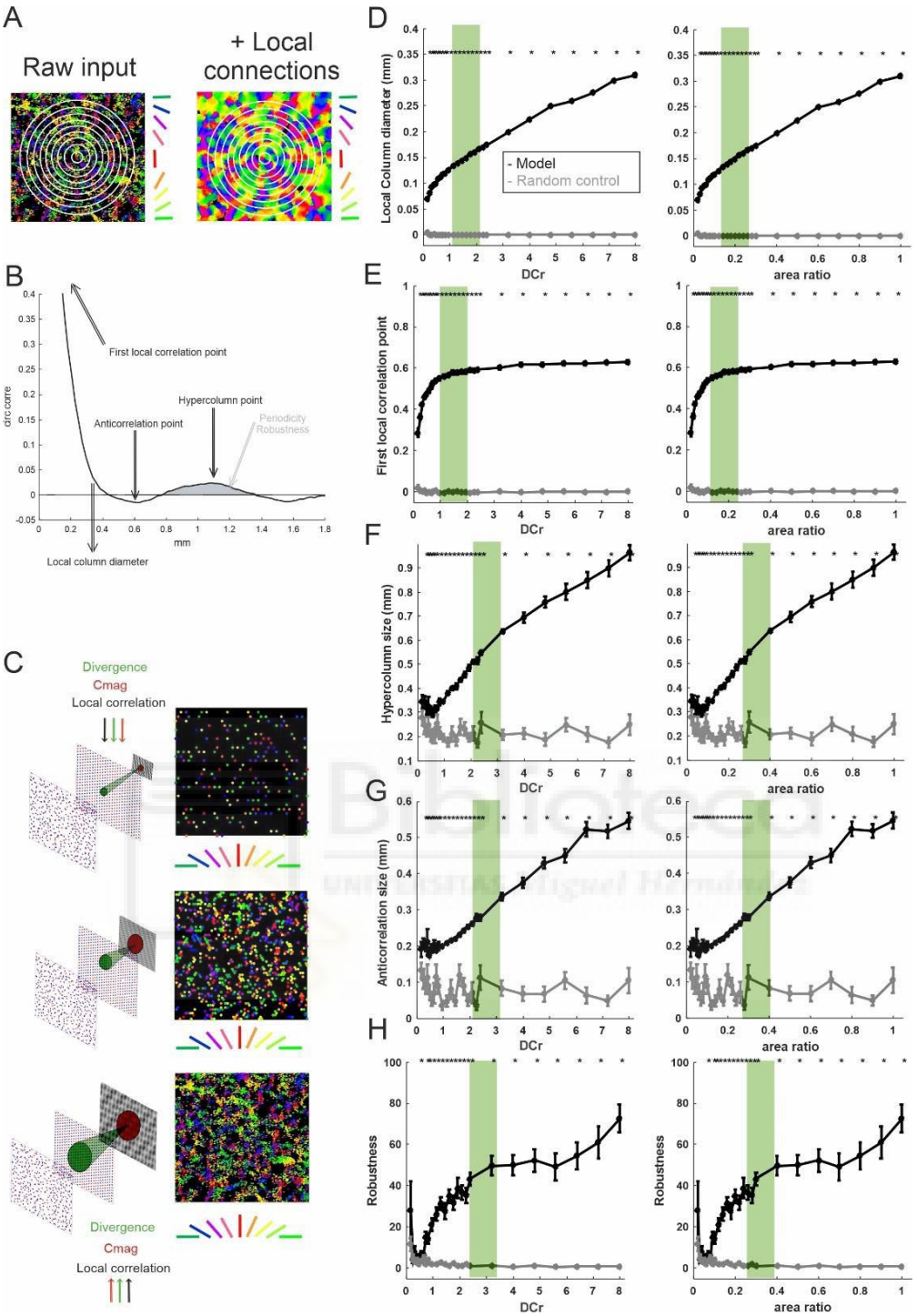

Figure 3.17. **Development of local and long range correlations as a function of DCr and optimum coverage. A**. Circular correlation can be calculated for the raw input from the LGN or after taking into account short range interactions in the cortex (see methods). **B**. Parameters extracted from the circular correlation signature for each model. **C**. Topological structure of orientation selective neurons for: Top: low DCr, middle: intermediate DCr and bottom: high DCr **D-H.** Threshold value in green for each circular correlation signature parameter extracted for the model (in black), hypercolumn size, anticorrelation point, local column diameter, first local correlation point and periodicity robustness respectively, and for a randomized orientation control (grey), Asterisks mark significance differences Wilcoxon test ($p<0.05$). Thresholds determined using the Friedman Test ($p<0.05$) n=20 models per each DCr or area ratio bin.

In fact, as noted Figure 3.18 when applying the same band pass filter, that is, the fermi filter used by (Kaschube et al 2010) for processing experimental data; the local, anti and long range correlations suffer an enhancement. The ferret data showed is from a very good experiment in which the circular correlation signature is present already without filtering. In the model however, the raw input plus the local correlations do generate clearly the local correlations, that is, the mean column size of the OPM, however the anticorrelations and long range correlations are very subtle, and to see them properly it is necessary to zoom in as in Figure 3.14.

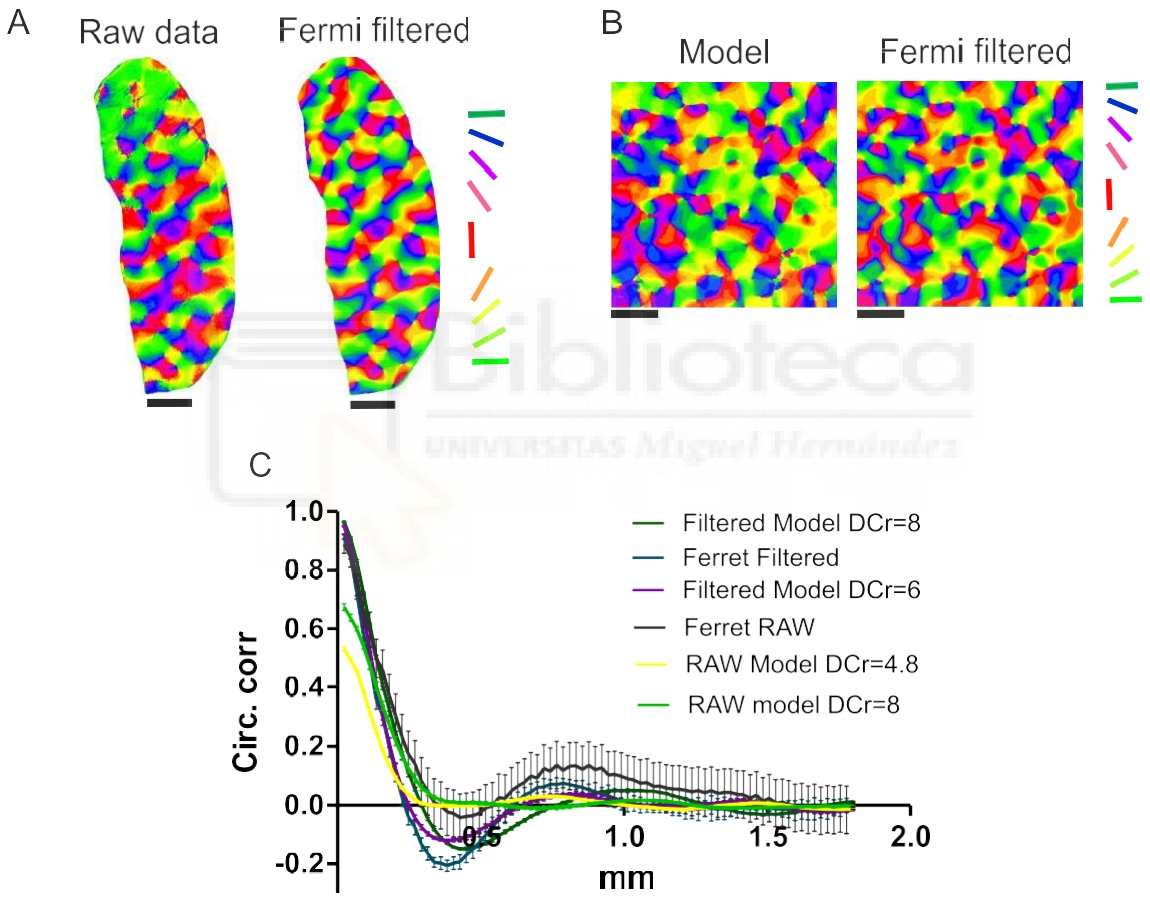

Figure 3.18. **Effect of band pass filtering in real data and computational model maps. A**. Raw OPM and band pass filtered OPM for ferret data obtained with optical imaging. **B**. Raw OPM and band pass filtered OPM for the feedforward statistical wiring model. **C**. Circular correlation as a function of convergence for raw and filtered models and ferret data. The Raw ferret data is from the ferret in A. For the filtered ferret function (n=8). For the raw and filtered models (n=5). Bars represent the standard deviation. Scale bars 1 mm.

In summary, the basic functional topology of V1 is determined by the raw thalamocortical input levels of divergence, since it clearly determines the width of the orientation columns, and therefore subdivides the salt and pepper topology from the OPM characteristic of carnivores and primates. The mean column size will also determine the long range correlation peak and therefore the size of the hypercolumn (λ) of each specie. Species with larger columns such as the cat will have a bigger λ than the tree shrew whose columns are smaller (Schottdorf et al 2015). Therefore, the raw input constrained by the different DCrs gives the basic blueprint for the functional topology of each specie. However, there are limits up to what a purely feedforward model can explain, indeed, the fact that the anticorrelation and long range correlations are subtle when compared to real data suggests some kind of intracortical processing to generate qualitatively similar OPMs in the model.

The SOM model demonstrates that the different DCrs determine de different activity dependent mechanisms required to develop correct and congruent retinotopic maps

Since topographic retinal maps are a common feature of all mammals the mechanisms by which retinotopy is formed and maintained throughout development are extremely important. Furthermore, retinotopic maps need to be congruent across both hemispheres in V1, that is, to generate a continuous representation of the visual field in V1 in both hemispheres.

Taking into account that the retinotopic map and the different DCrs along different species govern the posterior cortical functional structure. On the one hand, we wanted to investigate how these DCrs influence or not the activity-dependent and molecular mechanisms necessary to develop a correct and congruent retinotopic map. Specifically, we wanted to answer if the coordinated activity dependent mechanisms between both retinas transmitted to the postsynaptic layers, are necessary for the correct development of retinotopy. On the other hand, R-R projections have been seen in many species at the beginning of development,

these fibres seem a good candidate for the synchronization of the activity of both retinas since their connections between hemispheres at the level of LGN or superior colicle are non-existent. With this model, what we are trying to understand is the role played by the synchronous activity of both retinas in the formation of retinotopic maps and so to try and dilucidate the role of R-R connections during development. To do this, the problem has been addressed using a Kohonen self-organization model. Where we explore how the synchronization of the activity and the specificity of the molecular mechanisms modulate the formation of these maps (see methods).

The SOM model shows that, when the sizes of the pre- (retina) and postsynaptic (SC, tectum, dLGN or V1) layers are similar (low σ-molecular values), congruent retinotopic maps, that is, correctly oriented on both hemispheres, can emerge by just molecular guidance cues. However, when the postsynaptic layer is larger than the retina (high σ-molecular values), activity dependent mechanisms need to complement molecular guidance cues, in order to avoid topological errors and develop correct topographic maps with bilateral symmetry. The simulation of different types of retinal activity, clearly indicates that the coordination of activity patterns between both retinas is the best way to avoid topological defects. Therefore, it would not be surprising that this synchronization of the stimulus in form of waves is provided by the R-R connections of certain species.

Figure 3.19. A. Shows the effect of random and independent stimulation in both retinas and it can be seen how the percentage of correct orientations decreases rapidly with the σ-molecular. It also shows that when there is an initial period of initial synchrony (local coupling) the formation of correct map improves clearly. Finally, the percentage of topographically correct oriented maps is better when the stimuli takes the form of a synchronized retinal wave (local coupling + waves), with values greater than 80% even in the worse conditions (high σ-molecular and high initial connection noise, σ-noise).

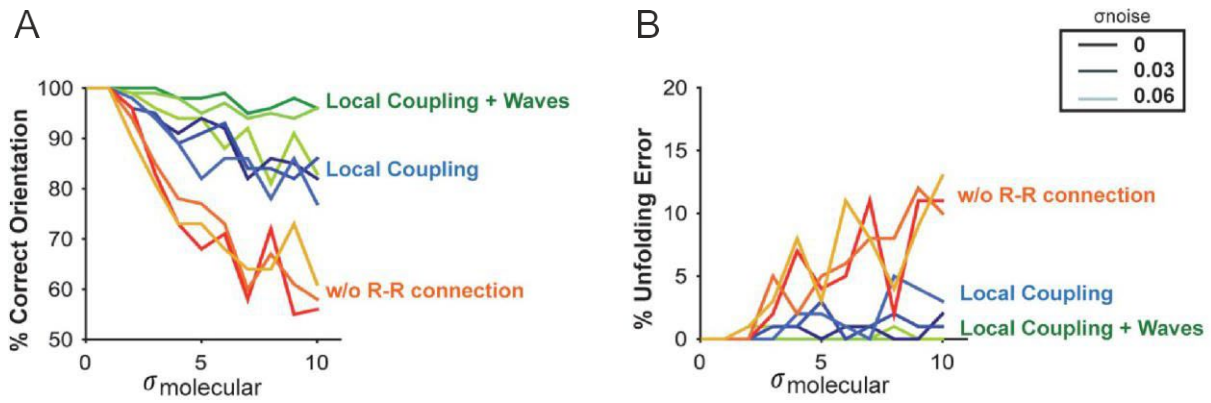

Figure 3.19. **Results of the SOM model as function of different activity dependent mechanisms and molecular guidance. A.** Percentage of maps with the correct orientation in both eyes (as a function of molecular gradients, σ-molecular), for the three types of stimuli (random stimulus that corresponds to no R-R connection (red), local coupling stimulus (blue) and local coupling plus retinal wave stimulus (green)). Noise levels are represented with different shades of the same color and correspond to σ noise: 0, 0.03 and 0.06. **B**. Percentage of maps with topological defects or unfolding errors as a function of the molecular gradient for the three types of stimuli and the three different noise levels.

A particularly striking topological defect is observed when the map is twisted around any of the axis, thus given rise to an unfolded map (see methods). This particular defect is less common but more dramatic. Its occurrence again depends on σ-molecular, the initial noise level and the pattern of stimulation. Figure 3.19.B. shows the results of the percentage of unfolding errors as a function of the variables mentioned above. For a completely random stimulation (no R-R connections), the number of errors increases with σ-molecular but is not much dependent on the initial noise level, σ-noise. Finally, the percentage of unfolding errors is markedly reduced by local coupling of the stimuli and is almost completely eliminated by the retinal wave pattern of stimulation.

Our model indicates that the role of the R-R connections is to synchronize the spontaneous activity across both hemispheres to generate retinotopic maps correctly oriented on both hemispheres in species with high DCrs. However, species with low DCrs, that is, with a small postsynaptic target compared to the presynaptic

area, can develop congruent maps without synchronous activity dependent mechanisms. So the appearance of R-R connections across phylogeny is related to an increase in the DCr through phylogeny. Thus, species with a similar size for their presynaptic and postsynaptic target (low DCr) can rely only on molecular guidance cues and do not have R-R connections. However, as the postsynaptic targets increase (high DCr) across phylogeny, species develop R-R connections to synchronize their spontaneous activity as a complement to the molecular guidance mechanisms, enabling the development of correctly oriented retinotopic maps in both hemispheres.

Predictions of the DCr model for binocular vison: Experimental test

A strain of mutant mice (Brn3b-Zic2) with a larger amount of ipsilateral fibers due to an artificial overexpression of Zic2 was functionally characterized measuring V1 cortical activity through optical imaging of intrinsic signals. Results show that the change in the incoming input, that is, the large amount of retinothalamic ipsilateral projections, generates a larger patch of ipsilateral activity that takes over the activity regions that would normally be colonized by a binocular region, where contralateral and ipsilateral activity regions should normally overlap.

The percentage of ipsilateral projecting RGCs is directly proportional to the frontalization of the eyes across vertebrates (Seabrook et al 2017). In mammals with a larger binocular visual field, such as humans, the ratio of contra and ipsi fibers is 60:40 respectively. However, in mice, due to the lateralization eyes and a greater panoramic field of view, this ratio is 97:3 (Figure. 1.9). The information from each eye is transmitted segregated until it reaches V1 where it integrates to form binocular and monocular neurons. The topological disposition of these neurons varies across mammalian species; carnivores and primates have Ocular Dominance Maps (ODMs), which means that ipsilateral and contralateral neurons are disposed in quasi regular patterns of Ocular Dominance (OD) columns (Van Hooser 2007, Weigand et al 2017a). Mice on the other hand, lack this kind of organization, their V1 in organized in a large contralateral region that contains a smaller binocular

region where a small proportion of ipsilateral fibers arrive (Cang et al 2005a, Sato & Stryker 2008).

The characterization of the visual cortex (V1) with optical imaging (OI) (Grinvald et al 1999) of a strain of Brn3b-Zic2 mutant mice that has a larger proportion of ipsilateral RGCs in the ventro-temporal part of the retina due to overexpression of Zic2 transcription factor (Herrera 2018, Herrera et al 2003, Herrera et al 2019), which is also maintained at the level of the dLGN (unpublished anatomical data), is a good opportunity to test the predictive power and explanatory role of the divergence-convergence ratio (DCr) principle in the emergence of the different functional architectures found across mammalian phylogeny. In fact, Br3nb-Zic2 mice develop ODMs similar to those present in carnivores and primates.

Zic2 mice develop a strong ipsilateral area that takes over the contralateral response region of normal binocular overlap

For each animal ocular dominance (OD) response regions where segmented (Figure 3.20, see methods) so that, from the total response area of each mouse (grey), the binocular, contralateral and ipsilateral areas of response where extracted as colour coded in Figure 3.20. A-C. So, from the total contralateral response (blue) and the total ipsilateral response (yellow), the other 3 OD areas of interest could be extracted. That is, the binocular region (green) where the total ipsilateral and contralateral response overlap, and the isolated contralateral and ipsilateral areas (with no overlap) in red and purple respectively. Once these regions are delimited, from a qualitative perspective, it can be observed that WT have OD regions dominated by a large contralateral zone that overlap the ipsilateral region conforming a binocular area (Figure 3.20.D, left), as experimentally reported by other authors (Cang et al 2005a). Mutants, however, tend to have the contralateral and ipsilateral regions segregated, therefore developing a purely ipsilateral area of response that WT mice lack completely. This segregation varies from animals, some have a partial and others a more complete segregation, which recalls the OD map

structure of carnivores and primates with clearly distinct eye preference sub regions (Weigand et al 2017a, White et al 1999) (Figure 3.20.D).

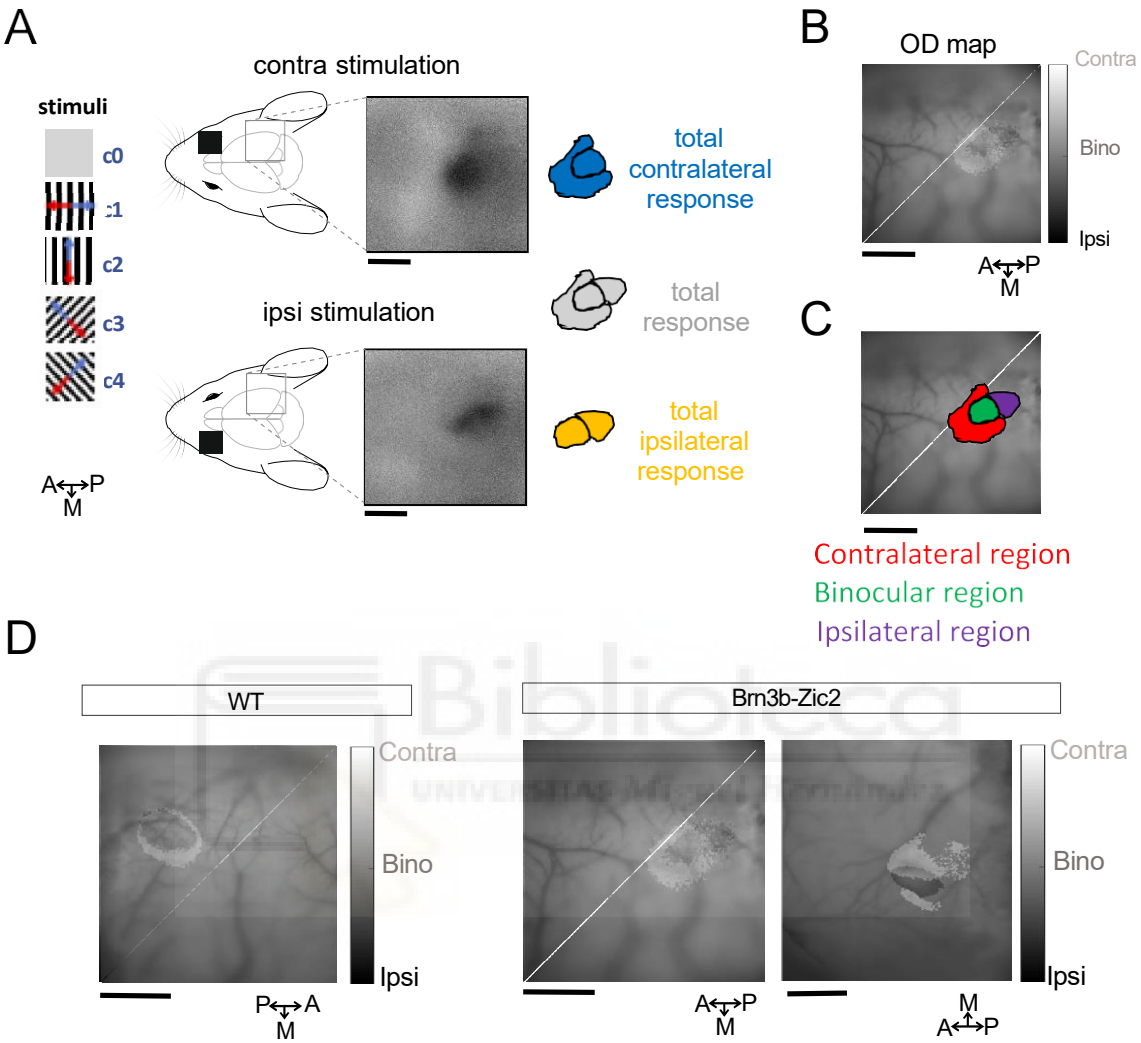

Figure 3.20. **Ocular dominance response regions obtained for mutant and WT mice**. **A.** From the raw contralateral and ipsilateral response obtained experimentally, the total contralateral (blue), ipsilateral (yellow) and total response (grey) can be delimited**. B.** OD map obtained from the ipsi and contra response regions from A**. C.** Colour coded OD response regions obtained for each optical imaging experiment; contralateral region (red), binocular region (green) and ipsilateral region (purple). **D.** Examples of optical imaging phenotypes obtained for WT and mutant Brn3b-Zic2 mice. Scale bar 1mm.

Indeed, a closer quantification clearly remarks that the overall binocular area in mutant mice decreases (Figure 3.21. A; p=0.0049, Mann Whitney test) respect to WT at expense of an increasing isolated ipsilateral region (Figure 3.21.C; p=0.003, Mann Whitney test), without changes in the proportion of the separated and isolated contralateral area (Figure 3.21.B). Furthermore, the fact that the total ipsilateral response does not increase significantly respect to WT (Figure 3.21.D), indicates that the ipsilateral region grows at expense of taking over the area that would normally be occupied by binocular neurons and, therefore, displacing contralateral neurons (Figure 3.21.E; p=0.003, Mann Whitney test), which reduces the total contralateral response of mutants. This can also be viewed by normalizing the

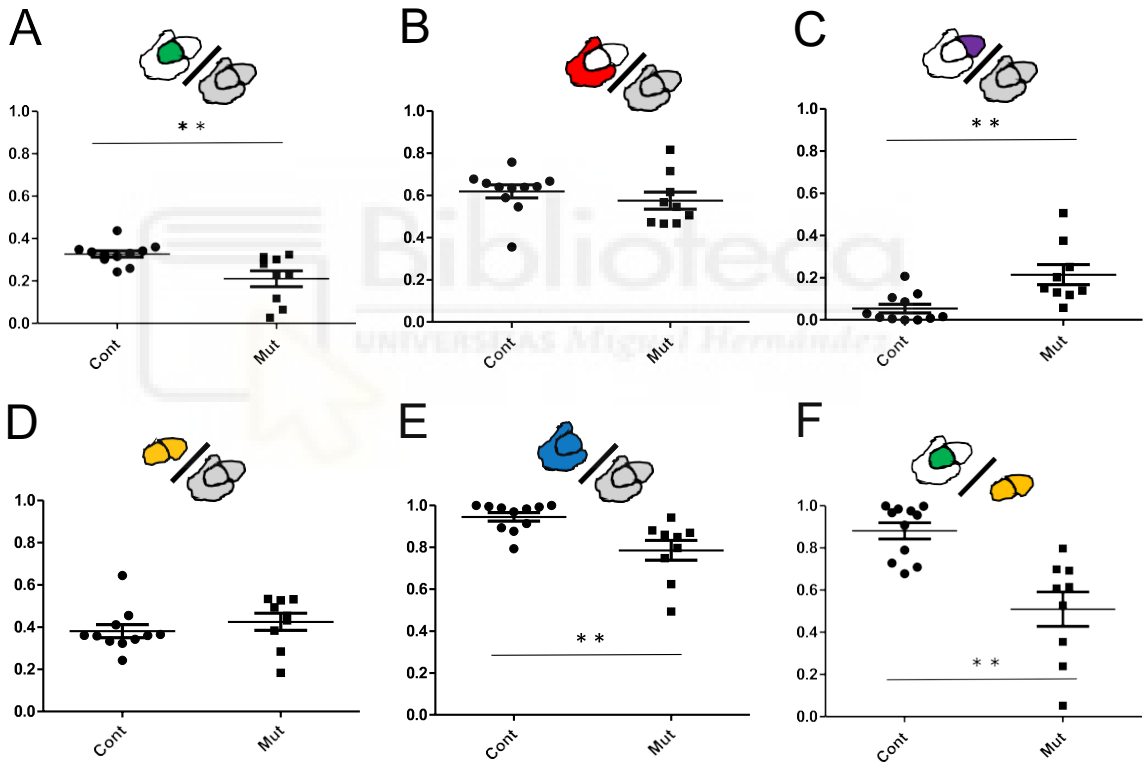

Figure 3.21. **Quantification of ocular dominance response regions for mutant and WT mice. A.** Binocular area normalized by the total response area (p=0.0049). **B.** Contralateral area normalized by the total response area. **C.** Ipsilateral area normalized by the total response area (p=0.003). **D.** Total ipsilateral area normalized by the total response area. **E.** Total contralateral area normalized by the total response area (p=0.003) **F.** Binocular area normalized by the total ipsilateral area (p=0.0011). Two tailed Man Whitney test for all statistically significant plots. Data from the right hemisphere of 11 WT and 9 mutants. (* p<0.05; ** p<0.01; *** p<0.001).

binocular area by the total ipsilateral area where the proportion of binocular neurons is reduced clearly in mutants (Figure 3.21. F; p=0011, Mann Whitney test).

In other words, the proportion of each OD response region normalized by the total response area, shows a 12% reduction of the binocular region in mutant's respect to WT, and this reduction is, in turn, compensated by the appearance a purely ipsilateral region in mutants.

Finally, it is important to mention that mutants have a significant smaller contralateral response area compared to WT. When looking at the data without any kind of normalization the overall take home message remains the same; the binocular region in mutants decreases and is replaced by a segregated ipsilateral region, therefore it not surprising to find a significant reduction in the contralateral response area (Figure S1; Appendix 1). However, there is a significant decrease in the total contralateral response area in mutant mice that does not correspond only to the overlapping binocular field of view but also to the purely isolated contralateral response region (Figure S1, C, F; Appendix 1). What is causing this difference? Weight difference between both groups, even though not significant, could be a possible explanation since mutants tend to be smaller (Figure S2; Appendix 1), but further statistical analysis does not reveal any covariate dependency of the weight and the total response, contralateral and isolated contralateral area (ANOVA tests; p=0.906, p=0,949, p= 0,667 respectively) or any other response region.

Another good explanation comes from the fact that the there are fewer contralateral fibers for the mapped region, because they have become ipsilateral in the other eye, and that the gain of ventro-temporal ipsilateral RGCs is not completely symmetric in both retinas. This irregularity can certainly cause disruptions in the independent contralateral area if the gain of ipsi RGCs is not completely symmetric in both retinas.

Brn3b-Zic2 mutant mice develop clear Ocular Dominance Columns similar to those present in animals with Ocular Dominance maps

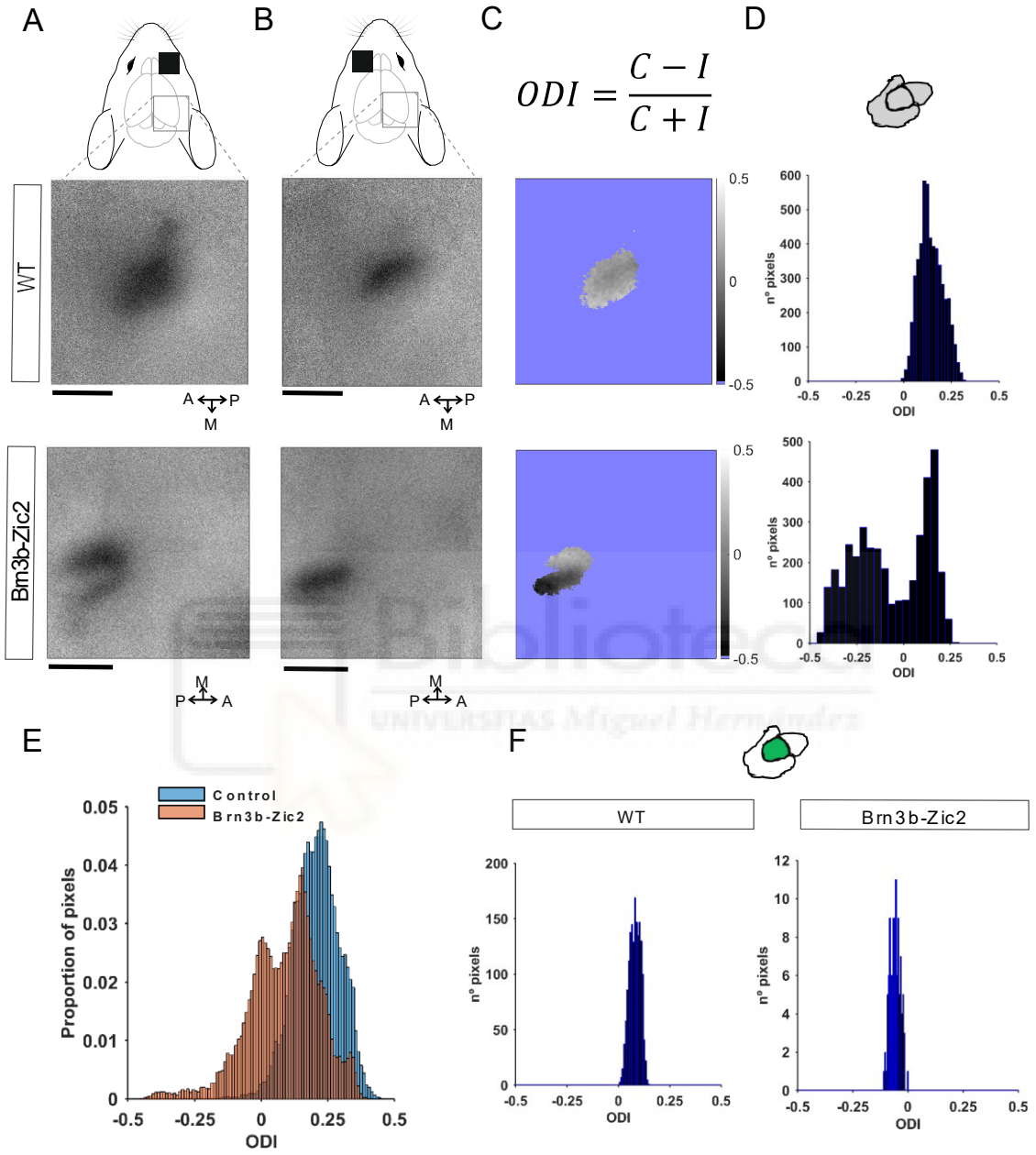

Figure 3.22. **ODI for a WT and Brn3b-Zic2 mice. A.** Raw contralateral response, top WT, bottom mutant. **B.** Raw ipsilateral response, top WT, bottom mutant. **C.** ODI obtained from the contralateral and ipsilateral response, top WT, bottom mutant, computed as ODI= C-I/C+I (see methods). **D.** ODI histogram of the whole response region for the WT and mutant mice from C. **E.** Joint normalized ODI distribution histogram for all experiments. **F.** ODI histogram from just the binocular region for the WT (left) and mutant mouse (right). Scale bar (1mm).

A closer pixel by pixel quantification using the Ocular Dominance Index (ODI, see methods) reveals that Brn3b-Zic2 mutants develop clear contralateral and ipsilateral segmented regions. First, the ODI of the whole response region shows a bimodal histogram with two clear different peaks of response, below and above 0 in mutants with qualitatively clear isolated OD columns (Figure 3.22. A-D), while WT have a unimodal ODI histograms centered at a positive peak value, indicating a clear preponderance of the contralateral response overlapping the ipsilateral (Figure 3.22. A-D) and, therefore, the presence of a clear binocular region as experimentally reported (Cang et al 2005a, Sato & Stryker 2008). In addition to the disposed examples, a normalized joint distribution histogram of all of the experiments performed shows how the WT and mutant profile is maintained over different animals (Figure 3.22, E) and that the mean ODI of the whole response region is significantly lower in mutants (0.08) respect to WT (0.19), (Figure 3.23. A; p=0.0402, Mann Whitney test), indicating a clear increase in strength of the ipsilateral signal in Brn3b-Zic2 mice.

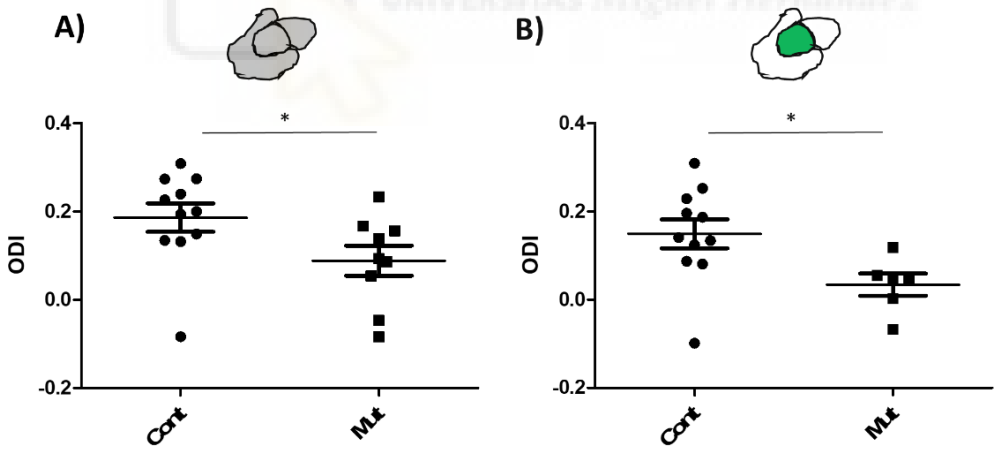

Figure 3.23. **Quantification of ODI for WT and mutant mice. A.** ODI for the whole response region (p=0.0402). **B.** ODI for binocular region (p=0.0138). Points represent median values of the ODI distribution of each mouse. Two tailed Man Whitney test for all statistically significant plots. (* p<0.05)

Furthermore, the ODI of the binocular region in these animals also indicates an increase in ipsilateral strength respect to WT. WT animals have a binocular

region with an ODI~0.15, which implies a clear dominance of the contralateral response in the binocular area as experimentally reported (Sato & Stryker 2008), while mutants have a significantly lower ODI (0.02), (Figure 3.23, B; p=0.0138; 3 mutants with very segregated areas and therefore with a binocular area <0.1 mm^2 where excluded from the analysis). It is important to mention that the ODI value reported for WT is lower than the ODI~0.22 reported by these authors (Cang et al 2005a, Sato & Stryker 2008). This difference is surely due to the OI technique used in our study. While they use fast OI (Kalatsky & Stryker 2003) we use the classical OI setup (Bonhoeffer & Grinvald 1991, Grinvald et al 1999) which implies a greater acquisition time and therefore more vascular changes through the experiment that may affect the contra and ipsi signal stability when comparing pixel intensities. However, our ODI distributions for the whole area and the binocular region are stable, except for a few outliers, validating the stability and reliability of our experimental procedures.

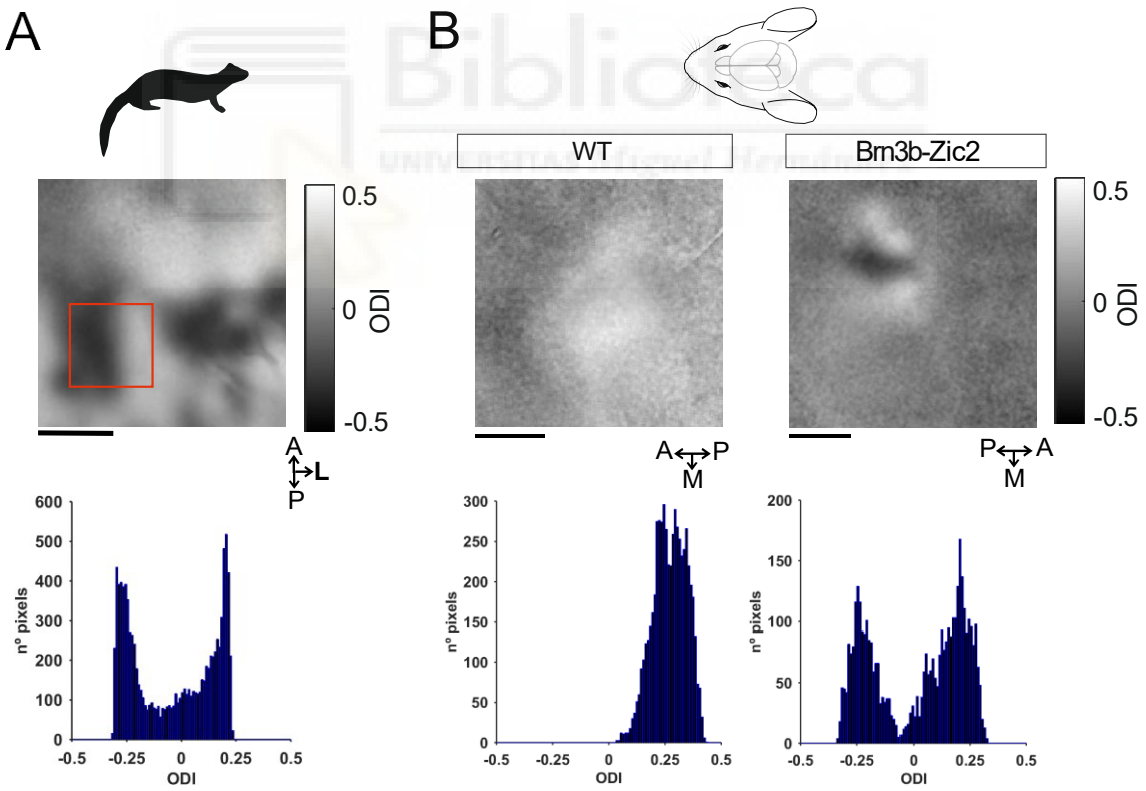

Figure 3.24. **Brn3b-Zic2 mice develop a proper Ocular Dominance Map. A.** Top, ferret ODM viewed as the ODI pixel by pixel. Bottom ODI histogram of the region in red. **B.** Top, WT and Brn3b mouse ODM viewed as the ODI pixel by pixel. Bottom ODI histograms of the whole response regions. Scale bar (1mm).

Finally, OD columns of Brn3b-Zic2 mice resemble those found in animals with ODMs such as ferrets, therefore developing a proper ODM. Ferrets have ODMs, where the V1/ V2 border is delimited by two large and patchy contralateral (V1) and ipsilateral (V2) regions (White et al 1999). Since the binocular region is difficult to see experimentally (and if seen its signal is masked by the strong V1/V2 border bands), an area of around $1mm^2$, similar in size to the response area of mice, that contained a similar proportion of these two strong opposite monocular regions was delimited for comparison (Figure 3.24.A). It is clear, that Brn3b-Zic2 develop proper OD columns with bimodal ODI histograms similar to those found in ferrets (Figure 3.24).

Discussion

The functional constraint of developing retinotopic maps that optimally cover the visual field imposes a series of connectivity rules between layers that have to accommodate to the different DCrs found across mammalian species. This in turn, causes the different OPM or salt and pepper functional topologies found across mammalian phylogeny and determines the molecular and activity depend mechanisms required for the correct development of congruent retinopic maps.

Our feedforward statistical wiring model predicts that the main computation the early visual pathway performs, is to interpolate as much information as possible through convergence of inputs from the dLGN based on a simple developmental wiring rule that minimizes wiring metabolic cost. This optimization principle, common for all mammals, realized by high convergence of thalamocortical inputs, increases the percentage of OSI neurons in V1 and determines the contrasting levels of divergence across mammals, which explains that the different topological architectures found across phylogeny are a consequence of the biological constraints determined by the relative size of V1 respect to the area of the retina.

Furthermore, the SOM model indicates that the appearance of R-R connections its associated with an increase in the DCr across mammalian phylogeny, as a mechanism to generate coordinated retinal waves to assure the wiring and development of congruent retinotopic maps in both hemispheres.

The role of the Early visual pathway

There are many models that try to explain the main computation the early visual pathway performs. In most of the cases these models are related to different optimization principles related with coding efficiency and sparseness (Babadi & Sompolinsky 2014, Beyeler et al 2019, Ganguli & Sompolinsky 2012, Martinez-Garcia et al 2017, Olshausen & Field 1996, Olshausen & Field 1997, Rehn & Sommer 2007), cortical-self organization (Kaschube et al 2010, Kohonen 2013b, Willshaw & von der Malsburg 1976) or feedforward architectures that can generate complexity at higher stages (Martinez & Alonso 2003, Martinez et al 2014, Paik & Ringach 2011, Ringach 2004, Ringach 2007, Schottdorf et al 2015).

The fact that V1 interpolates information from previous layers was proposed by Barlow (Barlow 1981) 40 years ago. This interpolation enables neurons to generate a higher diversity of response and adaptability to different stimuli (Martinez et al 2014). Following this line of though, the model assumes that the main operation the EVP is performing is the interpolation of thalamocortical inputs to maximize the coverage of visual space. In other words, the main operation the EVP is performing is to recover the maximum amount of information as possible after the initial compression of information from fotorreceptors to RGCs in the retina (Babadi & Sompolinsky 2014, Ganguli & Sompolinsky 2012, Martinez et al 2014, Schottdorf et al 2015), through thalamocortical convergence.

Thus, we propose that layer 4 V1 neurons follow a coverage optimization principle mediated by an optimal value of convergence of thalamocortical inputs and intermediate levels of redundancy -that may help to enhance the retinal message and reduce noise (Faisal et al 2008, Martinez et al 2014, Molano-Mazón et

al 2017)-, and that orientation selectivity may be nothing more than an emergent property of these cortical neurons trying to recover the maximum degree of On and Off information as possible (Figures 3.5-11). In other words, orientation selective neurons are not the cause but the side consequence of the main operation that V1 is performing. This does not necessarily mean that the response to a preferred orientation does not have any advantageous computational power in visual processing, but that it is clearly a byproduct of an initial and clearly more important operation V1 is performing.

All mammals share the same common developmental feedforward wiring rules

The fact that the degree of convergence reported experimentally oscillates between 30 to 80 connections per neuron in cats and rodents respectively (Alonso et al 2001, Lien & Scanziani 2018), that the model requires high values of convergence (40-60 connections per V1 neuron) to increase the proportion of OSI neurons (Figure 3.2), that this high convergence values are necessary to predict the orientation of retinotopically aligned V1 neurons from the thalamic population receptive field of the dLGN (Figure 3.3) as experimentally reported by (Jin et al 2011), and that this high convergence seeds the generation of long range correlations (Figure 3.4) characteristics of OPMs (Schottdorf et al 2014), supports the hypothesis that there is an optimal thalamocortical convergence of around 40-80 connections per V1 neuron, conserved across species with different DCrs (Figure 3.15; Table 1) that optimizes coverage by interpolation of inputs.

Thus, the independent interpolation of On and Off inputs that together sum high thalamocortical convergence values is conserved across species with different DCrs. This might imply that it is important to optimally cover the visual field with two separated On and Off antagonistic channels integrating the information in V1, to increase as high as possible the dynamic range of the system (Gjorgjieva et al 2017, Gjorgjieva et al 2019, Gjorgjieva et al 2014, Schiller 1992, Westheimer 2007).

An OPM or a salt and pepper functional topology in V1 is consequence of a coverage optimization principle and the anatomical constraints imposed by the different DCr across phylogeny

The parameters that modify the functional topology of V1 are the area of pre and postsynaptic layers and the degree of connectivity between layers. The DCr formula summarizes these two parameters perfectly (see methods) and, together with the functional constriction that we can extract from the experimental data, it can be concluded that the uneven overexpansion of V1 respect to the retina across phylogeny associated with different degrees of divergence, determine the presence of a salt and pepper or OPM topology.

The model indicates that the different functional architectures found across mammals follow the DCr formula (Figure 3.1, see methods). When the DCr > 1 strong isoorientation domains appear and when DCr > 2 an OPM starts to emerge (Figure. 3.16-17). Since the level of convergence is fixed to optimally cover visual space, the main appearance of an OPM or a salt and pepper depends on the different levels of divergence required to achieve this optimal convergence values. Therefore, the DCr formula clearly indicates that when the size of V1 is small respect to the retina the levels of divergence must be low and as the V1 size increases the divergence value must raise to connect all neurons as required. Therefore, the degree of divergence determines the Cmag, that is, the proportion of neurons that share similar RFs. Consequently, divergence and Cmag values establish the size of the local correlation domains, very small and decorrelated for a salt and pepper and clearly present for an OPM.

Supporting these results, we have the fact that neurons in layer 2/3 of mice have a maximum of seven overlapping RFs (Smith & Hausser 2010). This implies that the divergence in mice must be low, as indicated by the model. Taking also into account the high thalamocortical convergence values in mice and cats (Alonso et al 2001, Lien & Scanziani 2018) and the ratio of pos and presynaptic neurons derived from the Table 1 and the DCr formula, the only way to achieve the optimal level of

convergence for the correct coverage of space is with low divergence values for rodents and high values for carnivores and primates.

The optimal thalamocortical convergence principle for coverage of visual space that we propose enables to fix the convergence value in the formula and explore different functional architectures due to the different size of the retina and V1 across mammalian orders (Table 1). Thus, the presence or absence of OPMs in mammals near the threshold for which we lack functional information will depend in the number of postsynaptic and presynaptic neurons.

Some studies suggest that the density of neurons under 1 mm^2 of cortex is stable across mammals, while it is the glial cells who increase their number (Carlo & Stevens 2013), except in primate's V1 where the density of neurons in V1 is 2.5 times higher (Collins et al 2010, Srinivasan et al 2015). Others, however, suggest that the number of neurons does vary across mammalian species (Herculano-Houzel et al 2008).

Let us assume that the density of neurons in V1 remains constant in rodents, marsupials and carnivores (2200 cells/ mm^2) (Carlo & Stevens 2013). The functional topology will now depend on the number of presynaptic neurons projecting to V1, in other words, the distinct number of functionally different RGCs mosaics in the dLGN that project to V1. A parameter named as w_{mos} from now on. Let us also assume a fixed density of RGCs of about 100 neurons per mm^2 for 7º of eccentricity (Wassle et al 1981a). Even if the density of RGCs varies as a function of the RGC type and across species (Baden et al 2020), for DCr values < 0.2 their V1 area should have to be a lot smaller than what anatomical data suggests (Fig. 3.15). However, in rodents about 75% of RGCs project to the dLGN and the whole functional diversity of RGCs is present in the dLGN (Roman Roson et al 2019). If there are around 32 independent RGCs mosaics in the rodent retina (Baden et al 2016), that leaves us with approximately 24 mosaics in the dLGN. Curiously if w_{mos} =24 the density of pos and pre synaptic cells becomes similar, what makes the DCr to depend, in this case, on the quotient between V1 and retina area which is equal to 0.15, indicating the importance of the % of different RGCs projecting to the dLGN in

different species to predict the functional topology of V1. It is relevant to mention that the same DCr=0.15 for mouse is obtained by dividing Pos_n, understood as the mouse V1 area times V1 density (2200 cells/ mm^2), by de total number of RGCs suggested by the literature; Pre_n= 50000 RGCs from (Baden et al 2020), multiplied by 0,75, that is, the % of RGCs projecting to the LGN in mouse (Roman Roson et al 2019). This indicates precision and robustness of our estimates and the model.

That said, this contrasts with the fact that the diversity of RGCs in the dLGN of carnivores and primates is much lower and that the information encoded by the RGCs is transmitted more segregated and less intermingled to V1 (Chen et al 2016). Supporting this we have the fact the number of RGCs mosaics in primates is estimated in 20, that most part of cat RGCs (86%) are implicated in the response of X and Y neurons in the dLGN (Rathbun et al 2016), and that most part of dLGN RFs of cats and primates are concentric with a classic center-surround response. Thereby, a low w_{mos} in the DCr formula in carnivores and primates enables the emergence of strong isoorientation domains and the formation of OPMS.

Taking all this into account, what functional topology should we expect for large rodents and marsupials of Figure 3.15? The ratio of V1/retina area for the capybara, the agouti and the quokka are 0.28, 0.35, 0.39 respectively, although we might be underestimating the V1 area of the capybara (see Table 1). Assuming that the % of different projecting RGCs is similar in rodents and marsupials ($w_{\text{mos}} \sim$=24), the DCr would more or less equal the area ratios. This in turn, implies that we should at least expect an increase in size and strength of local correlations (Figure 3.16-3.17) with respect to their companions of smaller size. However, if w_{mos} turns to be smaller, the effect would be more enhanced.

It is important mention that recently, some authors have published similar results where they also consider that the salt and pepper and OPM topology in mammals is also due to the different overexpansion of V1 across mammals and convergence of feedforward inputs through statistical wiring (Jang et al 2020). However, they predict an abrupt change due to nyquist sample theorem from a salt and pepper to an OPM instead of a continuum different species, and fail to give a

practical meaning for the need of high and different convergence and divergence values across mammalian species.

Finally, other authors have suggested that the transition from the more unstructured to a structured V1 is due to increasing intracortical connectivity profiles due to the increase of the global number of V1 neurons without changing connection selectivity in V1(Weigand et al 2017a). For these authors, since the total number V1 neurons in the agouti is higher than in the ferret it should develop a clear OPM. We propose that this is unlikely if the nº of RGCs projecting to V1 is similar across rodents. Also, if the density of V1 neurons is constant in carnivores and rodents (Carlo & Stevens 2013) it is difficult to explain why rabbits and ferrets with a similar V1 area and the tree shrew with an even smaller V1 have different V1 architectures. However, the DCr in our model clearly separates the development of OPMs in shrews and ferrets from the salt and pepper topology of rabbits. Thus the DCr predicts intermediate functional topologies for animals lying close to the threshold.

Finally, this model can explain why the threshold of a fully developed OD map is more shifted to the right than the threshold of a fully developed OPM (Figure 4.1), following the criteria from (Weigand et al 2017a). If we take into account the input from both eyes Pre_n will be doubled which decreases local correlations. This obviously also depends on the different degrees of binocularity, higher in carnivores and primates than in rodents and lagomorphs (Kremkow & Alonso 2018). However, overall the model fits perfectly with the fact that primates with a fully developed OD have a bigger Pos_A and that the density of neurons in V1 is 2.5 times bigger in primates than in the rest of species (Srinivasan et al 2015), which overall increases Pos_n, favoring stronger local correlations and a more developed OD map (Weigand et al 2017b).

In conclusion, ODMs, OPMs or salt and pepper configurations are not the cause but the consequence of the V1 trying to recover the maximum amount of information as possible and the uneven overexpansion V1 respect to the retina across mammalian species. This, determines a continuum of different topologies

across species instead of a completely different and binary set of topological architectures.

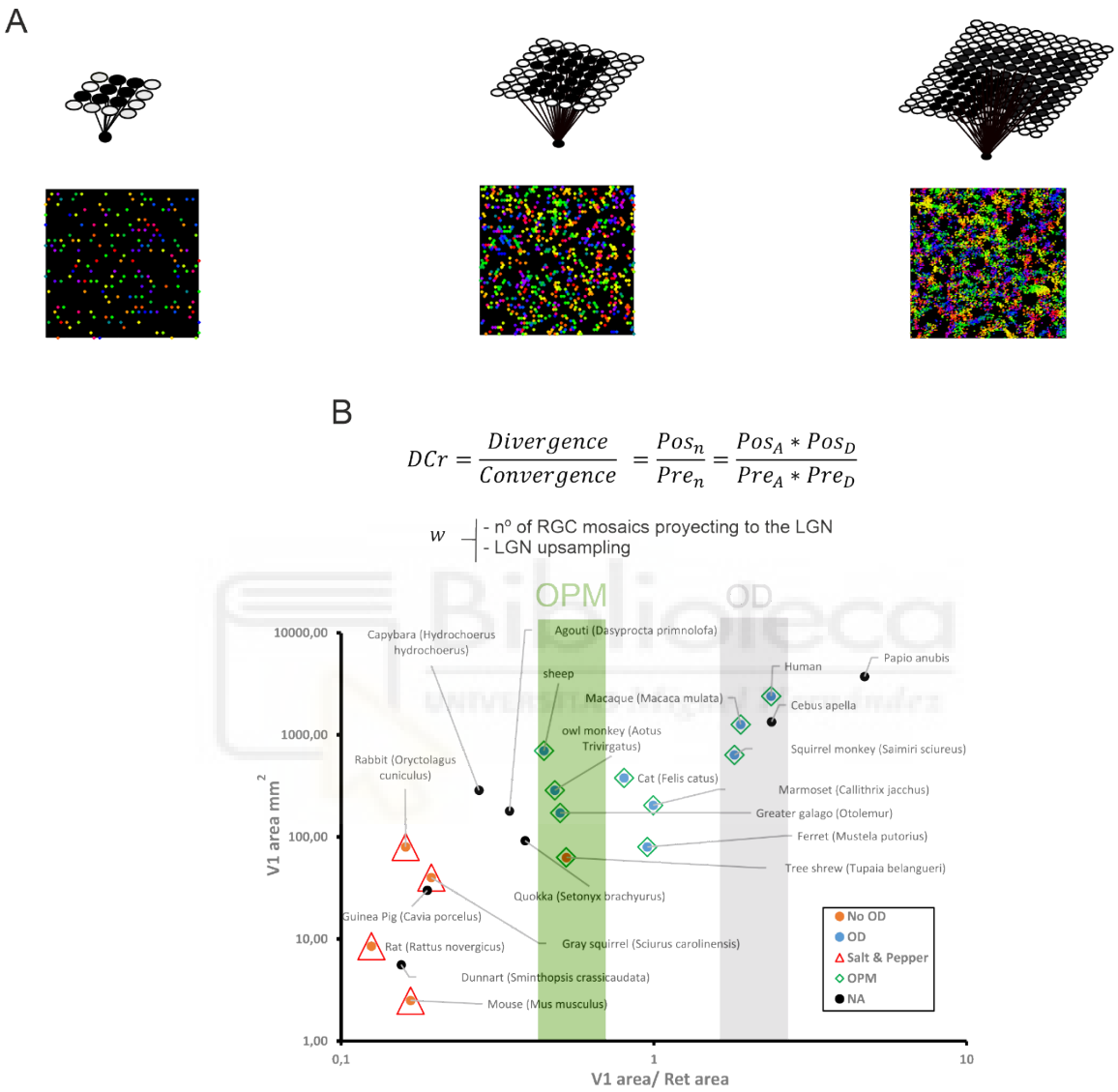

Figure 4.1**. A general developmental rule. A**. As divergence values increase local correlations increase giving birth to well stablished cortical columns of OPMs. **B**. The presence or absence of OPM depends of the DCr ratio of each specie. This same principle might be applied to the emergence of OD maps. In green and gray the threshold for fully developed OPM and OD maps respectively following the criteria from (Weigand et al 2017a).

DCr levels determine the functional topology of early visual targets

The model proposes that in a canonical way the size of the functional blocks in the early visual system is given by the level of divergence between the pre and postsynaptic layers. However, when looking at other visual pathways it is easy to see how a more rigid structure of the input may clearly affect the function of the circuit.

This can be seen when comparing the low divergence levels of the SC compared to V1 found in mice and the size of the local activity domains reported. The axon spread of the thalamic cells in cortex is about 500 μm while in the SC it is of 100 μm. However, the spread of activity patches in V1 area is of 43 μm compared to the 80 μm in the SC. Indeed, it has been reported that the SC is organized in orientation columns (Feinberg & Meister 2015). Yet, if the divergence is lower in the SC, how can there be orientation columns? Unlike V1, the SC does not cover the field of view uniformly with all orientations, instead orientation selective neurons are arranged concentrically around the center of the field of view in mouse (Ahmadlou & Heimel 2015). RFs that respond to different orientations have very little overlap (Feinberg & Meister 2015) and this preference for orientation seems to come from the retina (Dhande et al 2015). This indicates that the input received by the retinal SC is very different from that received by V1. Thus, while V1 is related to fine vision the SC is related to escape, visuomotor coordination and other complex behaviors unrelated to fine vision (Dhande et al 2015, Seabrook et al 2017).

Taking all this into account, the heterogeneous topographic disposition of different RGCs related to the ecological niche of each species (Baden et al 2020, Zhang et al 2012), the radial symmetry in the retina of oriented RGCs found in other mammals like the cat (Levick & Thibos 1982), together with the fact that most DS RGCs project to the SC and not the dLGN in mice (Baden et al 2016, Roman Roson et al 2019), can perfectly explain the great difference between the input received by the SC and the dLGN, which generates completely different functional topologies on both postsynaptic layers. This constitutes a clear example of how the fine structure

of the input can govern the functional topology of the postsynaptic layers in addition to the DCr.

Emergence of orientation selectivity in the early visual pathway

Because there are described routes in the mouse where direction-selective (DS) RGCs project to the shell and from there directly to the surface layers of V1 (Seabrook et al 2017), one might argue that the presence of a salt and pepper is due to the arrival of these inputs to V1.

However, recent studies suggest direction selectivity arises de novo in V1 by convergence of thalamic inputs with concentric RFs and, thereby, with low direction selectivity but with a combination of different spatial-temporal responses. In addition, the same study indicates that the slight selectivity in the direction of thalamic neurons does not match with that developed by layer 4 cells, suggesting that the retina has a minor role in the generation of orientation selectivity in V1 (Lien & Scanziani 2018). Also, another recent study in rabbits shows that the DS input of dLGN neurons to layer 4 and 6 is a powerful driver of layer 4 cells, the DS inputs that arrive directly to layer 1 act as modulators, in other words, they are not strong enough to generate a response in superficial layers (Bereshpolova et al 2019).

In conclusion, although it is possible that direction and orientation selective neurons project directly to the cortex generating a more random disposition, everything seems to indicate that the main mechanism to generate orientation selective neurons is more or less conserved in mammals, being other feedforward connections modulators of the functional circuit.

Comparisons with other models of V1 organization

We have explored the limitations of a purely feedforward model to understand up to what point a stable retinotopy and different Cmag affect the final functional topology of V1. Yet, there are several differences of concept of our model respect to others.

In the first place, if the circular correlation function is calculated directly from the retinal dipoles, no local or long range correlations can emerge from the dipoles of the retina (Schottdorf et al 2014). However, the high thalamocortical convergence values of our model pool the RFs of many RGCs which makes it possible to seed the circular correlation signature of OPMs and to predict the orientation of a V1 neuron by visual inspection of the thalamic population RF (Molano-Mazon 2013) (Figure 3.3). This in turn, implies that it is possible to predict the orientation of a V1 neuron by looking at the retino-topically aligned thalamic neurons as experimentally reported (Jin et al 2011). It is important to take this difference into account, since the take home message is clearly different. The circular correlation analysis of the dipoles implies a local point of view of the circuit that fails to account for the main characteristic of OPMs. Instead, a broader population code that can be viewed as the sum of all the On and OF RFs of the thalamic RFs, mediated by a high thalamocortical convergence, indicates that the cortical circuit is favoring this broader coding.

Taking all this into account, we are measuring the circular correlation of the thalamic population of RFs that are highly selective to orientation (OSI>0.25), that emerge at high thalamocortical convergences, which are necessary for an optimum coverage of On and Off RFs of visual space. As a consequence, the structure of the raw input generates strong isoorientation domains and long range correlations for high DCr values when taking into account the global population code (thalamic population RF map), in contrast to the more local information from the dipoles of the retina. So, even though, long range correlations are absent in RGCs mosaics (Eglen et al 2005, Wassle et al 1981a, Zhan & Troy 2000), long range correlations may emerge when considering the population code of all the RFs covering visual

space. This is also a main difference against authors that consider the RGC mosaic as an moiré interference pattern of On and Off neurons that generate clear and very strong local and long range correlations (Paik & Ringach 2011).

It is also important to mention that the model fails to generate long range correlations as strong as those compared to real data (Schottdorf et al 2014), indicating that the initial structure is guided by the raw input, but some degree of intracortical interactions are also occurring. As noted by (Schottdorf et al 2015), to obtain OPMs from feedforward inputs that give stronger long range correlations some kind of band pass filtering is needed (Figure 3.18). This implies that some degree of more complex intracortical connectivity (other than just local interpolation) is necessary to achieve the universality structure of OPMs as reported by (Kaschube et al 2010).

Overall, the model gives a simple explanation of how the basic functional topologies are seeded across different mammalian orders and accounts for the limitation of a purely feedforward drive in the development of OPMs.

Drivers and modulators of V1 functional topology

The mechanisms that prevail in the emergence of V1's characteristic functional structure are under intense debate. On the one hand, feedforward models propose that the functional topology emerges due to the convergence and integration of inputs coming from the thalamus. On the other hand, intracortical models propose connectivity between V1 neurons as a self-organizing mechanism in the formation of functional maps. There is experimental work that supports one model or another, for review see (Martinez 2006).

Recent work suggests that thalamic or retinal input is not necessary to generate the characteristic activity patterns of OPMs (Smith et al 2018). These authors silence the activity of the thalamic input at p21 (in ferret) and see that the patterns of spontaneous activity characteristic of OPMs are still present, proposing

local anisotropic intracortical interactions as a model of cortical organization. However, this does not exclude at all that the structure of these activity patterns is influenced by the input at early stages of development, since, in spite of having the regions of localized activity preserved, the levels of spontaneous activity decrease drastically when the thalamic input is silenced, and at p1-p10 the thalamocortical connections, that may shape cortical activity, already reach layer 4 and the subplate (Huberman et al 2008). So, to demonstrate that the cortex organizes itself without the influence of the input these experiments should be performed at earlier stages of development.

Furthermore, spontaneous activity of the retina is important for the correct development of retinotopic and OD maps (Cang et al 2005b, Huberman et al 2006). Retinal waves occur approximately up to the EO (eye opening) (p30) in ferrets and even a few days after the EO in mice (p10-p20) (Huberman et al 2008). Recent studies show that retinal waves are transmitted to dLGN, SC (superior colliculus) and V1 (Ackman et al 2012, Weliky & Katz 1999). However, the activity of V1 becomes independent from the retinal waves near EO (Chiu & Weliky 2001, Gribizis et al 2019). The results of these studies seem to clearly indicate that the input has a clear influence at the beginning of the development and acts as a modulator at later stages. This is consistent with the fact that OPMs are present at the moment of the EO (Chapman et al 1996), and visual experience is not a determining factor in the qualitative structure of the OPM, although the maturation of orientation selectivity depends on the presence of lateral connections (White et al 2001).

Finally, it is important to remember that molecular guidance cues are as important, or more important than, activity-dependent mechanisms in the organization of inputs from pre-synaptic to postsynaptic layers (Huberman et al 2008, Swindale 1996). In a recent study we described the appearance of retinal waves as a complement to molecular cues in species with retino-retinal connections, to generate coordinated activity patterns necessary for the formation of congruent retinal maps between both hemispheres (Murcia-Belmonte et al 2019). Another example of the great importance of molecular guidance cues is the fact that there are clusters of OD in enucleated ferrets (Crowley & Katz 1999). This calls into question

the role of the retina as a driver in the formation of cortical circuitry and the importance of molecular cues in the arrangement of ordered afferences between pre and post-synaptic layers across the early visual pathway.

DCr influence the degree of visual acuity across mammalian species

The DCr can also explain differences in visual acuity across mammalian species and may suggest why the levels of convergence reported for cat are lower than those reported for mouse. As noted in the introduction, visual acuity cannot be solely determined by the retina, there are other factors such as the degree of binocular visual field or the number of neurons in V1 that also influence acuity.

On the one hand, the model shows how as the processing capacity in higher stages is increased, that is, the number of neurons in N_{pos} , visual acuity increases - understood as the maximum coverage of On and Off RFs cut at 90% of their peak response (Figure 3.5) - , until it reaches it a plateau where increasing the number of neurons in V1 does not increase coverage of visual space (Figure 3.7). This agrees with experimental data reported by other authors (Collins et al 2010, Srinivasan et al 2015), where there is a clear relationship between V1 size and neuron density with visual acuity in mammalian species (Figure. 1.4; table 1).

On the other hand, the model predicts that the thalamocortical convergence required for optimal coverage of visual decreases as the DCr increases and that divergence increases with the DCr (Figure 3.5-3.6). In other words, species with a higher DCr should require lower thalamocortical convergence than species with a smaller DCr. Looking at figure 3.5 it is easy to see a tendency for the peak of maximum coverage moving to the left as the DCr increases. Especially when comparing species with a low DCr (DCr< 0.2), such as mouse where the convergence required is of about 70-80 connections per cortical neuron, with species with high values DCr (DCr>2), where the convergence can range from 25-50 connections. Furthermore, this fits perfectly with the only available data for thalamocortical

convergence values in mammals. Cats that have a reported thalamacortical convergence of around 30 connections per cortical neuron (Alonso et al 2001), whether mice have around 80 connections per cortical neuron (Lien & Scanziani 2018).

Finally, the mean RF size is another parameter that expands the definition for visual acuity and that depends on the DCr, in fact, as the DCr values increase the mean size of the RFs optimally covering visual space decreases. Indeed, it is possible to argue that coverage of visual space is not perfect for describing acuity, since the capacity of the system to resolve fine spatial detail also depends on the individual size of each RF. Taking this into account, the acuity is clearly enhanced if the mean size of the RFs covering visual space is small. In Figure 3.9 there is a tendency for the peak of maximum coverage moving to the left as the DCr increases. Especially when comparing species with a low DCr (DCr< 0.2), such as mouse where the mean RFs is of about 0.02 mm^2, with species with high values DCr (DCr>2), where the size is around 0.015 mm^2. This is not surprising, since the mean RF size scales with convergence independently of the DCr value (Figure 3.8), and therefore the lower the degree of convergence necessary to optimally cover visual space, the smaller the RFs will be. Therefore, similar values of RF size can be extrapolated from Figure 3.8, if the convergence is high as in mouse, 0.02 mm^2, and for lower convergence values as in cat, 0.015 mm^2.

In summary, RF size decrease adds up the to the better coverage of visual space as the DCr ratio increases, to explain why visual acuity increases with V1 size (Figure. 1.4; table 1). Although there are other factors such as the degree of binocular vision, the size of the dLGN and retinal specializations that may enhance acuity (Caves et al 2018, Mazade & Alonso 2017, Srinivasan et al 2015, Veilleux & Kirk 2014). It is remarkable how species with a similar V1 size, but different DCr have similar acuities (rabbit, ferret, tree shrew). Even more remarkable is the case of the squirrel, which has an even smaller V1 area than those mentioned above and a DCr similar to the rabbit. However, it is a highly visual rodent with an acuity slighly higher than the rest. This certainly implies the importance of other parameters that may compensate and help to process acuity other than the EVP. In fact, the EVP is

not the only route for visual information processing and there are parameters other than V1 size than may contribute to enhance acuity.

Evolution of V1 and SC, functional consequences

The EVP is not the only rout of transmission of visual information. Apart from many other visual nuclei, the SC-pulvinar pathway is responsible for object recognition and correct spatial navigation (Petry & Bickford 2019, Seabrook et al 2017), that is clearly favored in rodents and prosimians in comparison to carnivores and primates (Table 2). To reach this conclusion, data of the relative size of the SC was extracted by measuring coronal sections of the SGS, that is, the most external part of the sensory SC that together with the stratum opticum receives all retinal afferents (May 2006). Since the SGS receives a good majority of the retinal input, I have considered its relative size respect to V1 a good measure of the weight of the SC-pulvinar in visual processing compared to the dLGN-V1 across mammalian species.

However, the SGS does not scale homogenously across mammals. It is clear that the increase in brain size has not been associated with a substantial increase in the size of the SGS in carnivores and primates when compared to rodents and the tree shrew (Figure 4.2. A). Furthermore, the scaling of V1 size respect to the SGS follows two different paths; carnivores and primates tend to have a smaller SGS compared to their V1 size whether rodents and shrews have a clearly bigger SGS (Figure 4.2 B). This becomes clear when comparing the relative size of the SGS/V1 and the SGS/ret respect to the size of V1 (Figure 4.2 C-D). Overall, as V1 increases the SGS decreases abruptly, and rodents tend to have the retina-SGS pathway enhanced at expense of the retina-V1 pathway promoted by carnivores and primates (Figure 4.2 E). The shrew, as a prosimian, lies in an interesting point in the threshold for the emergence of OPMs due to its V1/ret divergence ratio but with a clearly bigger SGS, similar to rodents. Finally, as visual acuity increases with V1 size (Figure 1.4) and V1 increments at expense of the SGS, in other words, as the SC-pulvinar pathways reduces its weight across mammals, visual acuity increases (Figure 4.2 F). It is

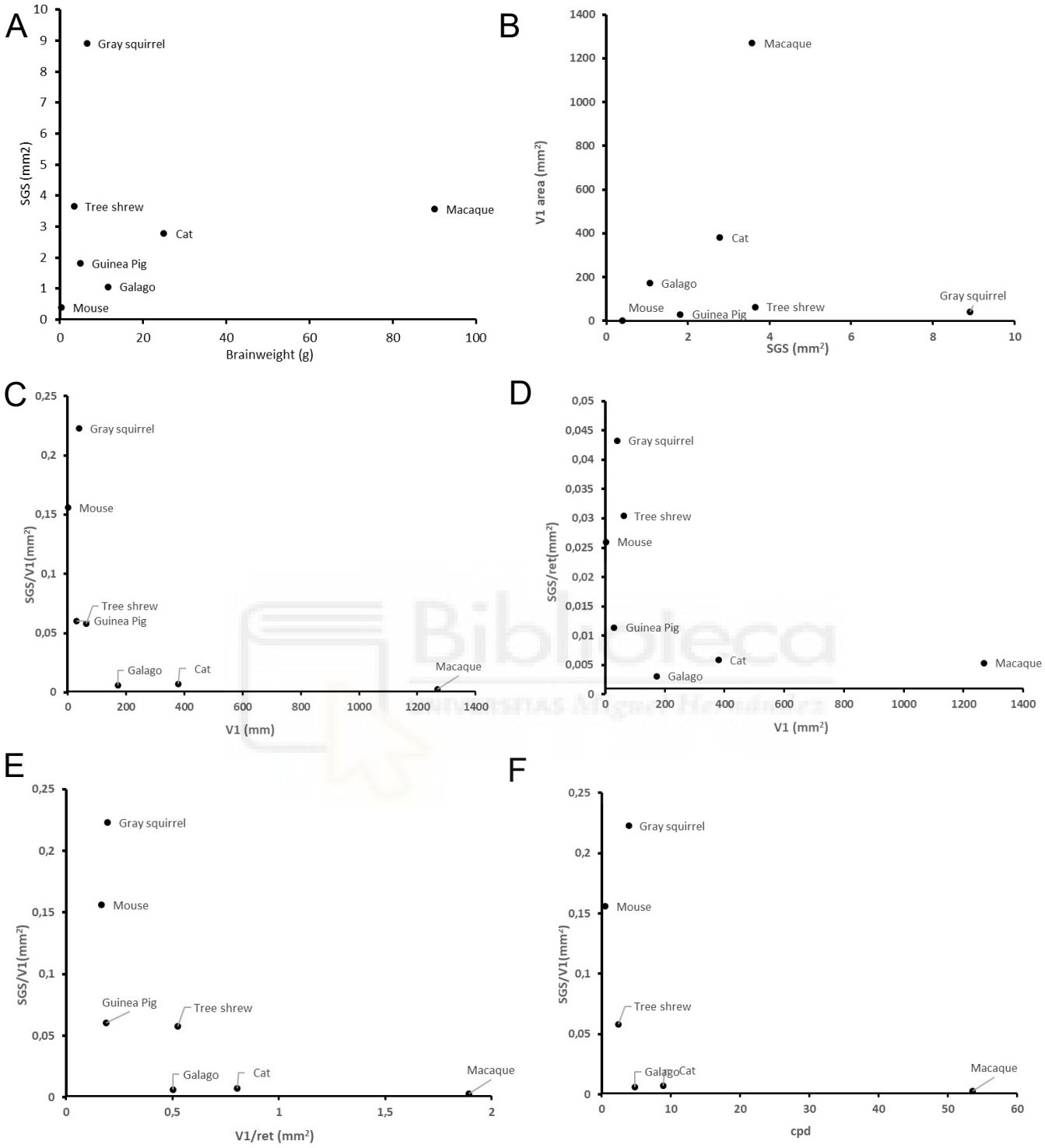

Figure 4.2**. Evolution of the primary and secondary visual pathways. A**. SGS area as a function of brainweight. **B**. V1 area as a function SGS area. **C**. SGS/V1 as function of V1. **D**. SGS/ret as a function of V1. **E**. SGS/V1 as a function of V1. **F**. SGS/V1 as a function of acuity (cpd).

important to mention, the unusual size of the squirrel SGS compared to its V1, and its outstanding acuity when compared to other mammals with a bigger V1 like the shrew and the galago.

Across mammalian evolution the size of each neocortical area and subcortical structure and their relationships determine the behavior and specialization of each specie to its ecological niche (Herculano-Houzel et al 2008, Kaas 2005, Kaas 2012a, Kaas 2013, Krubitzer 1995, Krubitzer et al 2011). Mammals from the superorder of the Euarchontoglires (primates and rodents) and Laurasitheria (carnivores, ungulates), have overall evolved a large neocortex with clearly differentiated sensory areas compared to the small neocortex characteristic of more primitive ancestors (Kaas 2013). However, there are clear differences in size of sensory regions even across similar species raised in different environmental conditions (Campi et al 2011, Campi & Krubitzer 2010, Krubitzer 1995, Krubitzer et al 2011).

Across these superorders, different biological constraints associated with the ecological needs of each species may have determined the weight of the SC-pulvinar against the dLGN-V1 pathway.

On the one hand, rodents have in general promoted bigger retinas and the SC-pulvinar pathway because their behavior is mostly associated with looming and rapid reflex responses (Dhande et al 2015, Mazade & Alonso 2017, Seabrook et al 2017), whether other species such as carnivores, and primates have promoted their visual acuity through the dLGN-V1 pathway.

On the other hand, the size of each specie is also a parameter to take into account (Keil et al 2012), since the expansion of the neocortex comes at a high energy cost (Kaas 2013). Smaller animals have smaller brains and an increase in neocortex size might come at a higher cost that an increase in size of a more primitive subcortical structure such as the SC.

This said, rodents, due to their biological constraints, have a much more developed SGS with respect to the size of V1. Having and overall smaller size may be associated with the fact that they cannot rely all the bulk of their operations on V1 and therefore

they do so on the SC. This may be the reason why the squirrel has a much larger SGS than normal, due to the need to develop a greater visual acuity which allows to have a higher acuity with relative smaller V1.

Following this line of thought, the larger size of carnivores and primates, together with the advantages of projecting to the cortex, have clearly promoted the delegation of many of their functions to V1. Interestingly, the complete segmentation of operations from the first and second visual pathways has probably been gradual throughout the evolution. Therefore, a small mammal like tree shrew who like the squirrel had the pressure to develop a good acuity due to its arboreal way of life, lies in an intermediate point where its V1 is larger than rodents but its SGS is bigger compared to carnivores and primates. Furthermore, loss of function experiments demonstrate that shrews without a functional V1 can relearn to recognize objects throughout the SC-pulvinar pathway, while primates are completely unable to recover their normal function (Petry & Bickford 2019, Stoerig & Cowey 1997).

So, as V1 expands at expense of the more primitive SC-pulvinar pathway, each pathway gradually specializes and visual acuity increases, therefore, the emergence of a salt and pepper or OPM is consequence of increasingly devoting the processing capacity to V1 due to cortical expansion through phylogeny.

Divergence-convergence ratios may modify the structure of the cortex required for information processing

So far we have seen how the early visual system adapts its levels of divergence and convergence to optimize a certain function, that is, the optimum coverage of the visual field. If that is the case, does the structure of the primary sensory areas relate to the different DCr found across primary sensory areas? In other words, does the type of thalamacortical input predict the cortical structure required to integrate the information? As we will see, the structure of the main thalamorecipient layer (layer 4) can be related to the different DCr across sensory areas and species.

The proportion of spiny or pyramidal layer 4 neurons may be related to the different DCr found across sensory layers. Spiny stellate neurons develop from pyramidal neurons that lose their apical dendrites during development (Callaway & Borrell 2011) and the proportion of these neurons varies across species and sensory layers. Layer 4 of V1 and S1 non rodent mammals is predominantly populated by stellate neurons, however rodents have stellates in S1 and pyramids in V1 (Smith & Populin 2001).

Following this line of though, one can hypothesize the different proportion of neurons might be due to how the input reaches layer 4 (the levels of divergence) and on the levels of integration required to perform a certain computation (convergence). Indeed, some authors hypothesize that the morphology of stellates to the need of a greater integration of inputs. As an example, for convergence, cats' auditory cortex (A1), unlike V1, is populated by pyramidal neurons because the convergence of input from the two ears occurs in the brainstem, therefore the levels of integration required in A1 cortex might me lower in comparison to V1.

On the other hand, the levels of divergence may also instruct the type of neurons required to handle the fibers reaching the cortex. The fact that the degree of convergence in primates, carnivores and rodents in V1 are high, but that divergence is much lower in rodents, might explain why the latter do not require stellate neurons. This could be because stellate neurons, apart from favoring integration, could also be related to the need for a better differentiation of the input if the there is a high amount of fibers reaching layer 4. Therefore, the low divergence values in rodents' V1 should not require stellate neurons. However, the more developed S1 of rodents might establish a high DCr which in turn demands a higher proportion of stellate neurons. Supporting this view is the fact that binocular enucleated ferrets do not develop a normal proportion of stellate neurons. This neurons instead remain pyramidal during development (Callaway & Borrell 2011), which shows how altering the input, and therefore the DCr, that reaches the cortex, shapes the structure of the neurons in layer 4.

The dLGN stabilizes the retinal message

So far I have not stressed the computations the dLGN might be exerting in the EVP, and certainly more anatomical data and further modelling is required to reach a proper conclusion. The comparative biology approach is useful to identify the main parameters that might be constraining the function of the system across different species. However, for the dLGN this approach was not as fruitful since there are clear anatomical, connectivity and functional differences in the dLGN of carnivores, rodents and primates that added too many parameters to the model and, furthermore, comparative data is not as clear and extensive as for V1. Species like the cat and the ferret have an upsampling of around x2.5 and x1.5 respectively, whether for mice and primates this numbers seem to be lower (Kremkow & Alonso 2018, Martinez et al 2014, Mazade & Alonso 2017). Furthermore, the anatomical structure of a the dLGN of a carnivore and a primate is completely different (Kaas 2013). Therefore, more clear anatomical studies are required to identify and quantify exactly, the main parameters that might describe the proper differences in the dLGN found across mammals.

Taking this into account, for the model the area of the dLGN was considered to be the same as the retina, with an upsampling of 1.5 respect to the retina across all DCr values explored for different species. This value was used because there is clear work in cat that highlights the importance of upsampling and some degree of convergence (1:3), from the retina to the dLGN, for a better coverage of visual space and noise reduction in the dLGN (Martinez et al 2014, Molano-Mazon 2013).

Furthermore, the degree of convergence and crosstalk between different RGCs is different across species. Rodents seem to have a higher degree of convergence from the retina with more crosstalk between different RGCs (1:5), whether carnivores and primates have a lower diversity of RGCs and a lower crosstalk and convergence between layers (Liang et al 2018, Nassi & Callaway 2009, O'Brien et al 2002, Rathbun et al 2016, Roman Roson et al 2019). Therefore, 3 different levels of retinothlamic convergence where explored 1:1, 1:3 1:9 in the model that really did

not exert many major changes in the functional topology of orientation selective neurons present in V1.

However, the presence of the dLGN is crucial to stabilize the retinal message as it can be seen in Figure 4.3 when calculating the orientation bias (see methods) on models with and without dLGN. This results we reproduced as in (Molano-Mazon 2013), and basically indicate how the irregular upsampling, due to statistical wiring, generates local clusters that enhance contrast borders in the dLGN stabilizing the appearance of orientation selective neurons in the On-Off contrast borders. On the contrary, models without dLGN are more decorrelated and it is more difficult to predict the orientation of a V1 cortical neuron from the thalamic population RF. This means that the dLGN is necessary in order to predict the orientation of a V1 neuron from retinotopically aligned V1 neurons as experimentally reported by (Jin et al 2011). Also, this becomes more patent at increasing thalamocortical convergences, necessary to optimally cover visual space, where the Obias of models without dLGN approximate the values of a completely random control (0.2), whether models with dLGN maintain a high Obias at increasing thalamocortical convergence values (Molano-Mazon 2013).

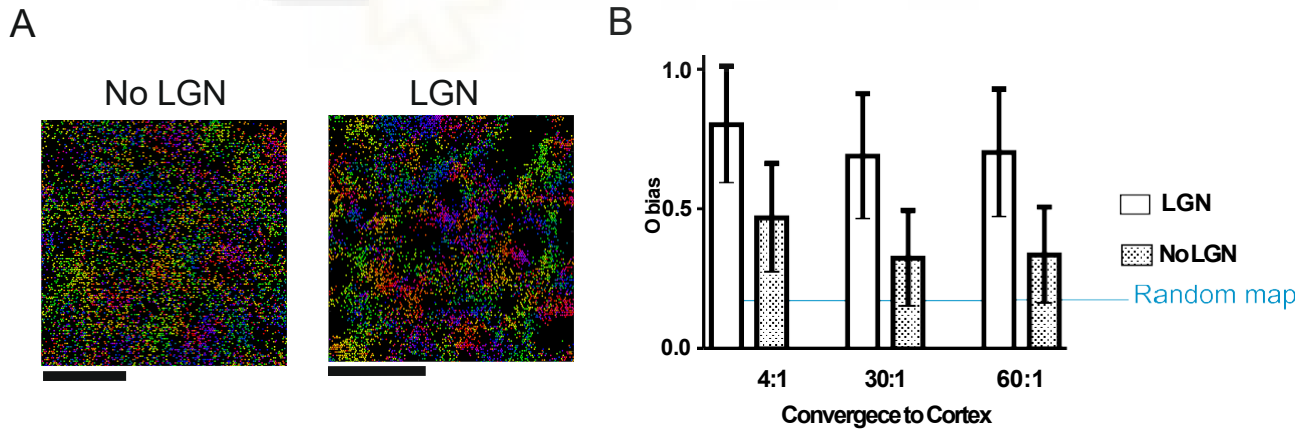

Figure 4.3. **Thalamus stabilizes retinal message. A**. OPM of a model without dLGN (Left) and with dLGN (right). **B**. Orientation Bias as a function of 3 different levels of thalamocortical convergence for models with and without dLGN (error bars std).

DCr determine the developmental mechanisms for correct topographic ordering

The different DCrs across mammalian species are the cause of the activity dependent mechanisms required for the development of correct and congruent retinotopic maps in both hemispheres. The SOM model when stimulated random and uniformly produces postsynaptic maps that reproduce the geometry of the presynaptic layer but are not correctly orientated (Hjorth et al 2015). In fact, there are 4! ways in which two square grids can be orientated relative to each other and only one of these orientations is the topologically correct one, thus the probability of getting a correct mapping is $1/24 \approx 4\%$. If we consider furthermore that two retinas have to be mapped correctly at the same time, then the probability drops to $1/24^2 \approx 0.02\%$.

The SOM model shows that as the DCr increases across mammals, due to an increase in postsynaptic target, the concurrent contribution of the gradients of molecular guidance cues and the bilateral coordination of retinal activity afforded by a R-R projection, helps avoid such an orientation error which enables the correct development of bilateral symmetry.

The retina and the postsynaptic layers (tectum, dLGN, V1) of lower vertebrates like the zebrafish, have similar sizes and is established with strong molecular guidance cues, without much further axonal refinement (McLaughlin & O'Leary 2005) (Figure 4.4). In contrast, the postsynaptic layer is larger than the retina higher order vertebrates (chicken, mouse, carnivores, primates), in other words, the DCr is higher, and a higher level of axonal refinement is necessary to establish the final retinotopic map (McLaughlin & O'Leary 2005) (Figure 4.4). This, refinement is realised by retinal waves (Huberman et al 2008), and the SOM model indicates that, the synchronization of this activity, presumably done by the presence of R-R connections, is crucial to develop correct and congruent retinotopic maps.

Thus, the SOM model seeds a clear evolutionary explanation for the emergence of R-R connections as the size of the postsynaptic layers increased across

phylogeny as a need to improve the complexity and computational power of the visual system.

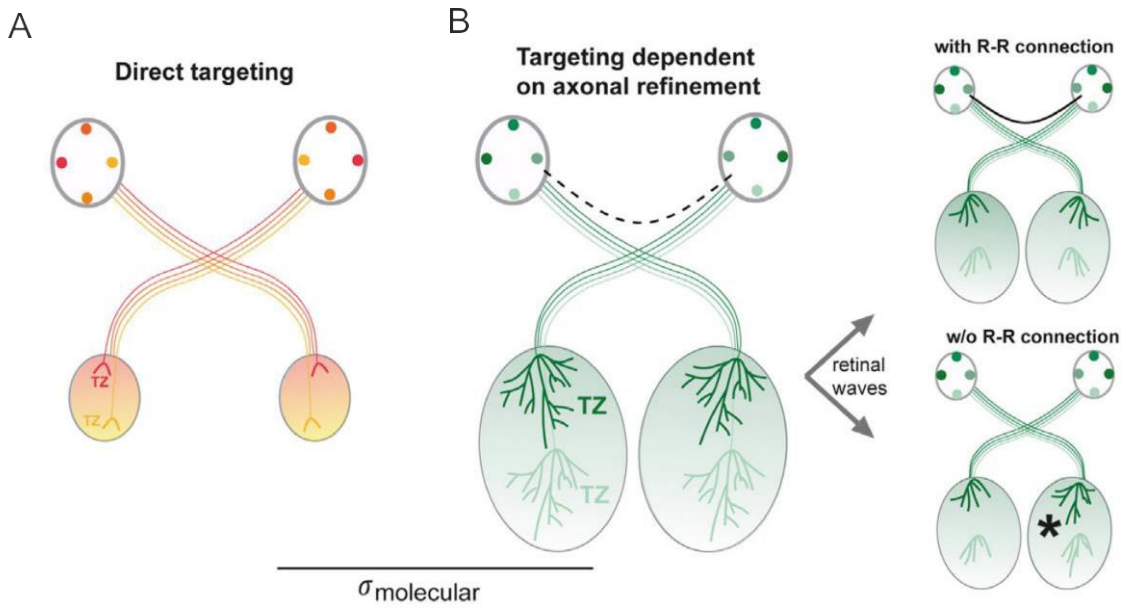

Figure 4.4**. The presence of R-R connections as a function of DCr through evolution. A**. In species where the size of the postsynaptic layer (tectum, dLGN) respect to the retina is small (low DCr), correct retinal topography in both hemispheres relies on molecular guidance cues. **B.** In species where the size of the visual target is bigger than the retina (high DCr), correct retinotopy relies on a molecular guidance cues and activity dependent mechanisms. The emergence of R-R connections could allow to synchronize the activity from both retinas to develop congruent retinotopic maps in both hemispheres. Adapted from (Murcia-Belmonte et al 2019).

A change in the DCr through phylogeny determined the appearance of ODMs

As noted in equation [1] from materials and methods (main text), the DCr is equal to,

$$DCr = \frac{N_{pos}}{N_{pre}} = \frac{div}{conv}$$

Where N_{pos} and N_{pren} are the number of postsynaptic and presynaptic neurons respectively, and div and conv represent the divergence and convergence connectivity between layers.

The Brn3b manipulation does not modify the total number of RGCs or dLGN neurons, but the proportion of ipsilateral and contralateral RGCs in the retina. Therefore, if retinotopy and divergence is maintained for the contralateral and ipsilateral inputs, but the diversity of convergent inputs from the ventrotemporal part of the retina is reduced, the DCr rises increasing local correlations for the ipsilateral inputs and generating segregated OD columns as those found in carnivores and primates.

In other words, the total proportion of neurons remains constant, so a diminution of contralateral neurons in both retinas translates in an increase of ipsilateral neurons in both retinas (Figure 4.5). In such a way that, the increase in the proportion of ipsi fibers on one side that reach the dLGN is combined with the fact that the contralateral fibers of the binocular region also decrease, which favors the appearance of a monocular retinotopic region of the frontal visual field in V1 of mutant mice.

Finally, the fact that the total ipsilateral response area is not increased in mutant mice, and therefore, that an increase in the binocular region is not seen, indicates, on the one hand, that the molecular mechanisms that determine that RGCs differentiate to ipsi RGCs are specific to the ventro-temporal part of the retina (Herrera 2018, Herrera et al 2003) and, therefore, to the binocular visual field of view. On the other hand, it also indicates the Brn3b-Zic2 mice, are at least roughly or completely replicating the retinotopic map of the retina in V1. Since retinotopy develops before OD this is not surprising (Herrera et al 2019, Huberman et al 2008, Kremkow & Alonso 2018, Swindale 1996).

All these results determine the importance of the input and the preservation of retinotopy as keys for understanding the cortical functional topology present in V1 across phylogeny. These experiments support the idea that ODMs are nothing but a consequence of the different DCr found across phylogeny. The idea that the

single overexpression of Zic2 in RGCs is able to generate proper ODMs in Brn3b-Zic2 mice, together with the fact that a the different levels of expression of Zic2 across phylogeny determine the degree of binocular visual field across different species (Herrera 2018, Herrera et al 2003), implies that the levels of expression of a single gene can regulate different visual specializations, cortical wiring and functional topology across phylogeny by modifying the DCr in primary sensory areas.

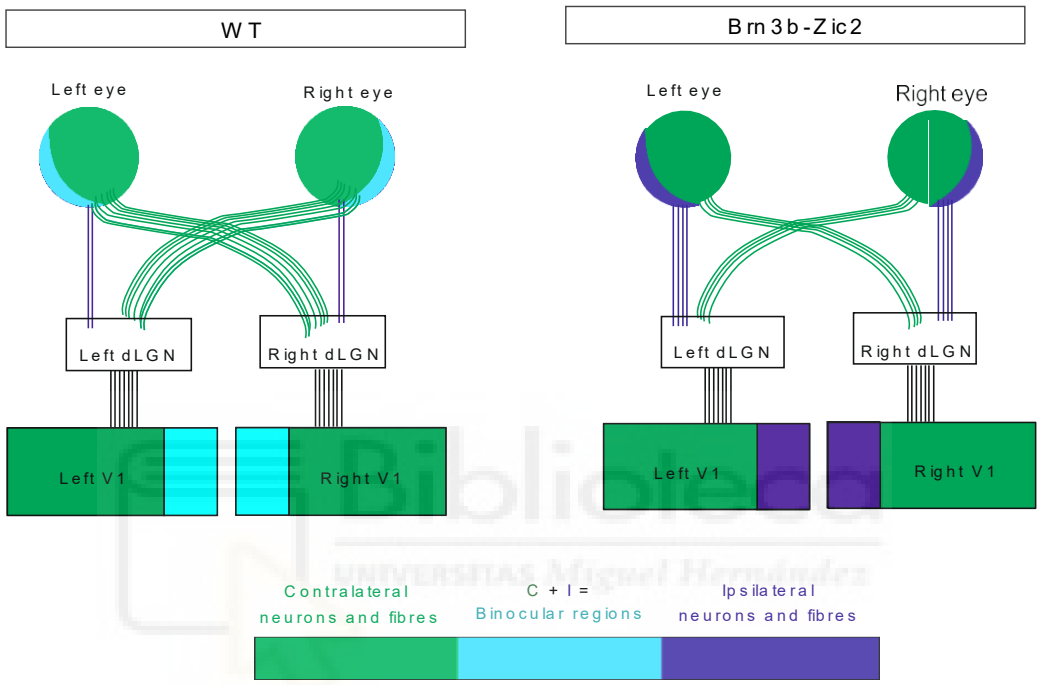

Figure 4.5. **Model proposed for the phenotype of Brn3b-Zic2 mice.**

Conclusions/Conclusiones

This work highlights the power of a comparative biology approach combined with mathematical modelling as a useful tool to relate structure with function and to generate hypothesis of the main operations a certain region of the brain is performing. This approximation enabled to summarize in a mathematical expression, the DCr, the main anatomical parameters that we hypothesized to be responsible for the cortical functional topology observed across the mammalian phylogenetic tree.

Thus, the DCr expression helped as a framework to explore how the size of each layer of the EVP and different connectivity rules may alter the function of V1 and to generate and confirm hypothesis of the main computations the EVP is performing, applying different computational models of cortical connectivity and development.

On the one hand, a feedforward statistical connectivity model highlights that the fundamental operation the EVP performs is to develop a retinotopic map that optimally covers visual space, through a series of common thalamocortical connectivity rules, that determine the different levels of divergence across mammalian species as a result of the contrasting Divergence-Convergence ratios found through phylogeny due to the different degree of overexpansion of V1. This gives a clear answer to why functional columns in V1 have astonishing different sizes in rodents and lagomorphs compared to carnivores and primates.

On the other hand, the SOM model shows how the different divergence-convergence ratios across mammalian phylogeny determine the type of molecular and activity dependent mechanisms required for the correct development of congruent retinotopic maps in both hemispheres, which sheds light on role for the emergence of R-R connections in species with high divergence-convergence ratios, as a way of synchronizing activity in both hemispheres to avoid topological defects.

Finally, the experimental manipulation that increases the DCr of the ipsilateral fibres through the EVP shows that the presence or absence of Ocular Dominance maps (ODM) across mammals is nothing but a consequence of the different DCr found across phylogeny guided by a similar coverage optimization principle to optimally sample visual space.

In summary, Divergence-Convergence ratios govern functional circuitry and developmental mechanisms across mammalian species as they accommodate to the imposed biological constraint of developing congruent and correct retinotopic maps that optimally cover the visual field.

Este trabajo destaca la ventaja de combinar un enfoque de biología comparada con modelos matemáticos como una herramienta útil para relacionar la estructura con la función y generar hipótesis acerca de las principales operaciones que realiza una determinada región del cerebro. De tal manera que, esta aproximación, permitió resumir en una expresión matemática, la ratio divergencia-convergencia, los principales parámetros anatómicos responsables de la topología funcional observada en el árbol filogenético de los mamíferos.

Así, la expresión de la ratio divergencia-convergencia sirvió como marco para explorar cómo el tamaño de cada capa del sistema visual temprano y diferentes reglas de conectividad, pueden alterar la función de V1, lo que permitió desarrollar y confirmar hipótesis de las principales operaciones que está realizando V1, aplicando diferentes modelos computacionales de conectividad y desarrollo cortical.

Por un lado, el modelo feedforward de conectividad estadística demuestra que la principal operación que realiza el sistema visual temprano es desarrollar un mapa retinotópico que cubra de forma óptima el espacio visual. Todos los mamíferos siguen una serie de reglas de conectividad tálamocorticales comunes y, como resultado de las diferentes ratios de divergencia-convergencia debido al diferente grado de sobre expansión de V1 a lo largo de la filogenia, los mamíferos presentan distintos niveles de divergencia que determinan la topología funcional presente en V1. Damos así, una respuesta clara a por qué las columnas funcionales en V1 tienen tamaños tan diferentes en roedores y lagomorfos en comparación con los carnívoros y primates.

Por otro lado, el modelo SOM muestra cómo las diferentes relaciones de divergencia-convergencia en la filogenia de mamíferos determinan el tipo de mecanismos dependientes de actividad y moleculares necesarios para el correcto desarrollo de mapas retinotópicos congruentes en ambos hemisferios. Dando una posible función a la aparición de conexiones R-R, en especies con altas relaciones divergencia-convergencia, como mecanismo para sincronizar la actividad en ambos hemisferios y evitar defectos topológicos.

Finalmente, la manipulación experimental que aumenta la DCr de las fibras ipsilaterales a través del EVP muestra que, la presencia o ausencia de mapas de dominancia ocular en mamíferos no es más que una consecuencia de las diferentes ratios de divergencia-convergencia encontradas en la filogenia, constreñidas por un principio similar de optimización de cobertura para muestrear de manera óptima el espacio visual.

En resumen, las relaciones de divergencia-convergencia gobiernan la topología funcional y los mecanismos de desarrollo cortical en mamíferos, al acomodarse y generar cambios por la imposición biológica de desarrollar mapas retinotópicos congruentes y correctos que cubren de forma óptima el campo visual.

References

Ackman JB, Burbridge TJ, Crair MC. 2012. Retinal waves coordinate patterned activity throughout the developing visual system. *Nature* 490: 219-25

Ahmadlou M, Heimel JA. 2015. Preference for concentric orientations in the mouse superior colliculus. *Nat Commun* 6: 6773

Alonso J-M, Martinez L. 1998. Functional connectivity between simple cells and complex cells in cat striate cortex. *Molecular Cell* 1: 395-403

Alonso JM, Usrey WM, Reid RC. 2001. Rules of connectivity between geniculate cells and simple cells in cat primary visual cortex. *J Neurosci* 21: 4002-15

Babadi B, Sompolinsky H. 2014. Sparseness and expansion in sensory representations. *Neuron* 83: 1213-26

Baden T, Berens P, Franke K, Roman Roson M, Bethge M, Euler T. 2016. The functional diversity of retinal ganglion cells in the mouse. *Nature* 529: 345-50

Baden T, Euler T, Berens P. 2020. Understanding the retinal basis of vision across species. *Nat Rev Neurosci* 21: 5-20

Banihani SM. 2010. Crossing of neuronal pathways: Is it a response to the occurrence of separated parts for the body (limbs, eyes, etc.) during evolution? *Medical Hypotheses* 74: 741-45

Barlow H. 1961. Possible Principles Underlying the Transformations of Sensory Messages. *Sensory Communication* 1

Barlow H. 2001. Redundancy reduction revisited. *Network (Bristol, England)* 12: 241-53

Barlow HB. 1953a. Action potentials from the frog's retina. *J Physiol* 119: 58-68

Barlow HB. 1953b. Summation and inhibition in the frog's retina. *J Physiol* 119: 69-88

Barlow HB. 1981. The Ferrier Lecture, 1980. Critical limiting factors in the design of the eye and visual cortex. *Proc R Soc Lond B Biol Sci* 212: 1-34

Bereshpolova Y, Stoelzel CR, Su C, Alonso JM, Swadlow HA. 2019. Activation of a Visual Cortical Column by a Directionally Selective Thalamocortical Neuron. *Cell Rep* 27: 3733-40 e3

Beyeler M, Rounds EL, Carlson KD, Dutt N, Krichmar JL. 2019. Neural correlates of sparse coding and dimensionality reduction. *PLoS Comput Biol* 15: e1006908

Binzegger T, Douglas RJ, Martin KA. 2004. A quantitative map of the circuit of cat primary visual cortex. *J Neurosci* 24: 8441-53

Blasdel G. 1992a. Differential imaging of ocular dominance and orientation selectivity in monkey striate cortex. *The Journal of neuroscience : the official journal of the Society for Neuroscience* 12: 3115-38

Blasdel G. 1992b. Orientation selectivity, preference, and continuity in monkey striate cortex. *The Journal of neuroscience : the official journal of the Society for Neuroscience* 12: 3139-61

Bonhoeffer T, Grinvald A. 1991. Iso-orientation domains in cat visual cortex are arranged in pinwheel-like patterns. *Nature* 353: 429-31

Callaway EM, Borrell V. 2011. Developmental sculpting of dendritic morphology of layer 4 neurons in visual cortex: influence of retinal input. *J Neurosci* 31: 7456-70

Campi KL, Collins CE, Todd WD, Kaas J, Krubitzer L. 2011. Comparison of area 17 cellular composition in laboratory and wild-caught rats including diurnal and nocturnal species. *Brain Behav Evol* 77: 116-30

Campi KL, Krubitzer L. 2010. Comparative studies of diurnal and nocturnal rodents: differences in lifestyle result in alterations in cortical field size and number. *J Comp Neurol* 518: 4491-512

Cang J, Kalatsky VA, Lowel S, Stryker MP. 2005a. Optical imaging of the intrinsic signal as a measure of cortical plasticity in the mouse. *Vis Neurosci* 22: 685-91
Cang J, Niell CM, Liu X, Pfeiffenberger C, Feldheim DA, Stryker MP. 2008. Selective Disruption of One Cartesian Axis of Cortical Maps and Receptive Fields by Deficiency in Ephrin-As and Structured Activity. *Neuron* 57: 511-23
Cang J, Renteria RC, Kaneko M, Liu X, Copenhagen DR, Stryker MP. 2005b. Development of precise maps in visual cortex requires patterned spontaneous activity in the retina. *Neuron* 48: 797-809
Capozzoli NJ. 1995. Why are vertebrate nervous systems crossed? *Med Hypotheses* 45: 471-5
Carandini M, Heeger DJ. 2011. Normalization as a canonical neural computation. *Nat Rev Neurosci* 13: 51-62
Carlo CN, Stevens CF. 2013. Structural uniformity of neocortex, revisited. *Proc Natl Acad Sci U S A* 110: 1488-93
Catania KC. 2013. Stereo and serial sniffing guide navigation to an odour source in a mammal. *Nat Commun* 4: 1441
Caves EM, Brandley NC, Johnsen S. 2018. Visual Acuity and the Evolution of Signals. *Trends Ecol Evol* 33: 358-72
Chapman B, Stryker MP, Bonhoeffer T. 1996. Development of orientation preference maps in ferret primary visual cortex. *J Neurosci* 16: 6443-53
Chen C, Bickford ME, Hirsch JA. 2016. Untangling the Web between Eye and Brain. *Cell* 165: 20-21
Chiu C, Weliky M. 2001. Spontaneous activity in developing ferret visual cortex in vivo. *J Neurosci* 21: 8906-14
Chklovskii DB, Koulakov AA. 2004. MAPS IN THE BRAIN: What Can We Learn from Them? *Annual Review of Neuroscience* 27: 369-92
Chklovskii DB, Schikorski T, Stevens CF. 2002. Wiring optimization in cortical circuits. *Neuron* 34: 341-7
Clarke PG, Whitteridge D. 1976. The cortical visual areas of the sheep. *J Physiol* 256: 497-508
Collin SP. 2008. A web-based archive for topographic maps of retinal cell distribution in vertebrates. *Clinical and Experimental Optometry* 91: 85-95
Collins CE, Airey DC, Young NA, Leitch DB, Kaas JH. 2010. Neuron densities vary across and within cortical areas in primates. *Proc Natl Acad Sci U S A* 107: 15927-32
Crair MC, Ruthazer ES, Gillespie DC, Stryker MP. 1997. Ocular dominance peaks at pinwheel center singularities of the orientation map in cat visual cortex. *J Neurophysiol* 77: 3381-5
Crowley JC, Katz LC. 1999. Development of ocular dominance columns in the absence of retinal input. *Nature neuroscience* 2: 1125-30
DeFelipe J, Alonso-Nanclares L, Arellano JI. 2002. Microstructure of the neocortex: comparative aspects. *J Neurocytol* 31: 299-316
DeFelipe J, Lopez-Cruz PL, Benavides-Piccione R, Bielza C, Larranaga P, et al. 2013. New insights into the classification and nomenclature of cortical GABAergic interneurons. *Nat Rev Neurosci* 14: 202-16
Demb JB, Singer JH. 2015. Functional Circuitry of the Retina. *Annu Rev Vis Sci* 1: 263-89
Dhande OS, Stafford BK, Lim JA, Huberman AD. 2015. Contributions of Retinal Ganglion Cells to Subcortical Visual Processing and Behaviors. *Annu Rev Vis Sci* 1: 291-328
Diggle PJ. 2013. *Statistical analysis of spatial and spatio-temporal point patterns, third edition*. 1-264 pp.
Douglas RJ, Martin KA. 2004. Neuronal circuits of the neocortex. *Annu Rev Neurosci* 27: 419-51

Dyer MA, Martins R, da Silva Filho M, Muniz JA, Silveira LC, et al. 2009. Developmental sources of conservation and variation in the evolution of the primate eye. *Proc Natl Acad Sci U S A* 106: 8963-8

Eglen SJ, Diggle PJ, Troy JB. 2005. Homotypic constraints dominate positioning of on- and off-center beta retinal ganglion cells. *Vis Neurosci* 22: 859-71

Eglen SJ, Gjorgjieva J. 2009. Self-organization in the developing nervous system: Theoretical models. *HFSP Journal* 3: 176-85

Faisal AA, Selen LP, Wolpert DM. 2008. Noise in the nervous system. *Nat Rev Neurosci* 9: 292-303

Feinberg EH, Meister M. 2015. Orientation columns in the mouse superior colliculus. *Nature* 519: 229-32

Ganguli S, Sompolinsky H. 2012. Compressed sensing, sparsity, and dimensionality in neuronal information processing and data analysis. *Annu Rev Neurosci* 35: 485-508

Gerhard D. 2013. Neuroscience. 5th Edition. *Yale J Biol Med* 86: 113-14

Gjorgjieva J, Meister M, Sompolinsky H. 2017. Optimal Sensory Coding By Populations Of ON And OFF Neurons.

Gjorgjieva J, Meister M, Sompolinsky H. 2019. Functional diversity among sensory neurons from efficient coding principles. *PLOS Computational Biology* 15: e1007476

Gjorgjieva J, Sompolinsky H, Meister M. 2014. Benefits of pathway splitting in sensory coding. *J Neurosci* 34: 12127-44

Godement P, Salaün J, Imbert M. 1984. Prenatal and postnatal development of retinogeniculate and retinocollicular projections in the mouse. *Journal of Comparative Neurology* 230: 552-75

Gonzalez R, Faisal Z. 2019. *Digital Image Processing Second Edition*.

Gribizis A, Ge X, Daigle TL, Ackman JB, Zeng H, et al. 2019. Visual Cortex Gains Independence from Peripheral Drive before Eye Opening. *Neuron* 104: 711-23 e3

Grinvald A, Shoham D, Shmuel A, Glaser D, Vanzetta I, et al. 1999. In-vivo Optical Imaging of Cortical Architecture and Dynamics, pp. 893-969

Harris KD, Mrsic-Flogel TD. 2013. Cortical connectivity and sensory coding. *Nature* 503: 51-8

Hartline HK. 1938. THE RESPONSE OF SINGLE OPTIC NERVE FIBERS OF THE VERTEBRATE EYE TO ILLUMINATION OF THE RETINA. *American Journal of Physiology-Legacy Content* 121: 400-15

Hebb DO. 1949. The Organization of Behavior: A Neuropsychological Theory

Heimel JA, Hooser SDV, Nelson SB. 2005. Laminar Organization of Response Properties in Primary Visual Cortex of the Gray Squirrel (Sciurus carolinensis). *Journal of Neurophysiology* 94: 3538-54

Helga Kolb EF, Ralph N. 2007. *Webvision : the organization of the retina and visual system*. [Bethesda, Md.] : National Library of Medicine : [National Center for Biotechnology Information], 2007.

Herculano-Houzel S, Collins CE, Wong P, Kaas JH, Lent R. 2008. The basic nonuniformity of the cerebral cortex. *Proc Natl Acad Sci U S A* 105: 12593-8

Herrera E. 2018. Rodent Zic Genes in Neural Network Wiring In *Zic family: Evolution, Development and Disease*, ed. J Aruga, pp. 209-30. Singapore: Springer Singapore

Herrera E, Brown L, Aruga J, Rachel RA, Dolen G, et al. 2003. Zic2 patterns binocular vision by specifying the uncrossed retinal projection. *Cell* 114: 545-57

Herrera E, Erskine L, Morenilla-Palao C. 2019. Guidance of retinal axons in mammals. *Semin Cell Dev Biol* 85: 48-59

Hirsch JA, Martinez LM. 2006a. Circuits that build visual cortical receptive fields. *Trends Neurosci* 29: 30-9

Hirsch JA, Martinez LM. 2006b. Laminar processing in the visual cortical column. *Curr Opin Neurobiol* 16: 377-84
Hirsch JA, Wang X, Sommer FT, Martinez LM. 2015. How Inhibitory Circuits in the Thalamus Serve Vision. *Annual Review of Neuroscience* 38: 309-29
Hjorth JJJ, Sterratt DC, Cutts CS, Willshaw DJ, Eglen SJ. 2015. Quantitative assessment of computational models for retinotopic map formation. *Developmental Neurobiology* 75: 641-66
Howland HC, Merola S, Basarab JR. 2004. The allometry and scaling of the size of vertebrate eyes. *Vision Res* 44: 2043-65
Hubel DH, Wiesel TN. 1962. Receptive fields, binocular interaction and functional architecture in the cat's visual cortex. *J Physiol* 160: 106-54
Huberman AD, Feller MB, Chapman B. 2008. Mechanisms underlying development of visual maps and receptive fields. *Annu Rev Neurosci* 31: 479-509
Huberman AD, Speer CM, Chapman B. 2006. Spontaneous retinal activity mediates development of ocular dominance columns and binocular receptive fields in v1. *Neuron* 52: 247-54
Hughes A. 1977. The Topography of Vision in Mammals of Contrasting Life Style: Comparative Optics and Retinal Organisation In *The Visual System in Vertebrates*, ed. F Crescitelli, CA Dvorak, DJ Eder, AM Granda, D Hamasaki, et al, pp. 613-756. Berlin, Heidelberg: Springer Berlin Heidelberg
Jang J, Song M, Paik S-B. 2020. Retino-Cortical Mapping Ratio Predicts Columnar and Salt-and-Pepper Organization in Mammalian Visual Cortex. *Cell Reports* 30: 3270-79.e3
Jimenez LO, Tring E, Trachtenberg JT, Ringach DL. 2018. Local tuning biases in mouse primary visual cortex. *J Neurophysiol* 120: 274-80
Jin J, Wang Y, Swadlow HA, Alonso JM. 2011. Population receptive fields of ON and OFF thalamic inputs to an orientation column in visual cortex. *Nature neuroscience* 14: 232-8
Kaas JH. 2005. From mice to men: the evolution of the large, complex human brain. *J Biosci* 30: 155-65
Kaas JH. 2012a. Evolution of columns, modules, and domains in the neocortex of primates. *Proc Natl Acad Sci U S A* 109 Suppl 1: 10655-60
Kaas JH. 2012b. The evolution of neocortex in primates. *Prog Brain Res* 195: 91-102
Kaas JH. 2013. The evolution of brains from early mammals to humans. *Wiley Interdiscip Rev Cogn Sci* 4: 33-45
Kalatsky VA, Stryker MP. 2003. New paradigm for optical imaging: temporally encoded maps of intrinsic signal. *Neuron* 38: 529-45
Kaschube M. 2014. Neural maps versus salt-and-pepper organization in visual cortex. *Curr Opin Neurobiol* 24: 95-102
Kaschube M, Schnabel M, Lowel S, Coppola DM, White LE, Wolf F. 2010. Universality in the evolution of orientation columns in the visual cortex. *Science (New York, N.Y.)* 330: 1113-6
Keil W, Kaschube M, Schnabel M, Kisvarday ZF, Löwel S, et al. 2012. Response to Comment on "Universality in the Evolution of Orientation Columns in the Visual Cortex". *Science (New York, N.Y.)* 336: 413
Kelly EA, Opanashuk LA, Majewska AK. 2014. The effects of postnatal exposure to low-dose bisphenol-A on activity-dependent plasticity in the mouse sensory cortex. *Front Neuroanat* 8: 117
Kohonen T. 1982. Self-organised formation of topologically correct feature map. *Biological Cybernetics* 43: 59-69
Kohonen T. 1998. The self-organizing map. *Neurocomputing* 21: 1-6

Kohonen T. 2013a. Essentials of the self-organizing map. *Neural Networks* 37: 52-65
Kohonen T. 2013b. Essentials of the self-organizing map. *Neural Netw* 37: 52-65
Kremkow J, Alonso JM. 2018. Thalamocortical Circuits and Functional Architecture. *Annu Rev Vis Sci* 4: 263-85
Kremkow J, Jin J, Wang Y, Alonso JM. 2016. Principles underlying sensory map topography in primary visual cortex. *Nature* 533: 52-7
Krubitzer L. 1995. The organization of neocortex in mammals: are species differences really so different? *Trends in Neurosciences* 18: 408-17
Krubitzer L, Campi KL, Cooke DF. 2011. All rodents are not the same: a modern synthesis of cortical organization. *Brain Behav Evol* 78: 51-93
Kuffler SW. 1953. Discharge patterns and functional organization of mammalian retina. *J Neurophysiol* 16: 37-68
Lemke G, Reber M. 2005. RETINOTECTAL MAPPING: New Insights from Molecular Genetics. *Annual Review of Cell and Developmental Biology* 21: 551-80
Levick WR, Thibos LN. 1982. Analysis of orientation bias in cat retina. *J Physiol* 329: 243-61
Liang L, Fratzl A, Goldey G, Ramesh RN, Sugden AU, et al. 2018. A Fine-Scale Functional Logic to Convergence from Retina to Thalamus. *Cell* 173: 1343-55 e24
Lien AD, Scanziani M. 2018. Cortical direction selectivity emerges at convergence of thalamic synapses. *Nature* 558: 80-86
Markram H, Lubke J, Frotscher M, Sakmann B. 1997. Regulation of synaptic efficacy by coincidence of postsynaptic APs and EPSPs. *Science (New York, N.Y.)* 275: 213-5
Marr DC, Poggio T. 1976. From Understanding Computation to Understanding Neural Circuitry. *Conference Proceedings*
Martinez-Garcia M, Martinez LM, Malo J. 2017. Topographic Independent Component Analysis reveals random scrambling of orientation in visual space. *PLoS One* 12: e0178345
Martinez LM. 2006. The generation of receptive-field structure in cat primary visual cortex. *Prog Brain Res* 154: 73-92
Martinez LM. 2011. A new angle on the role of feedfoward inputs in the generation of orientation selectivity in primary visual cortex. *J Physiol* 589: 2921-2
Martinez LM, Alonso JM. 2001. Construction of complex receptive fields in cat primary visual cortex. *Neuron* 32: 515-25
Martinez LM, Alonso JM. 2003. Complex receptive fields in primary visual cortex. *Neuroscientist* 9: 317-31
Martinez LM, Molano-Mazon M, Wang X, Sommer FT, Hirsch JA. 2014. Statistical wiring of thalamic receptive fields optimizes spatial sampling of the retinal image. *Neuron* 81: 943-56
Masland RH. 2012. The neuronal organization of the retina. *Neuron* 76: 266-80
Masters B. 2014. The New Visual Neurosciences. Eds: John S. Werner and Leo M. Chalupa ISBN-13: 978-0-262-01916-3 The MIT Press. *Graefe's Archive for Clinical and Experimental Ophthalmology* 252: 1341-43
May PJ. 2006. The mammalian superior colliculus: laminar structure and connections. *Prog Brain Res* 151: 321-78
Mazade R, Alonso JM. 2017. Thalamocortical processing in vision. *Vis Neurosci* 34: E007
McLaughlin T, O'Leary DDM. 2005. MOLECULAR GRADIENTS AND DEVELOPMENT OF RETINOTOPIC MAPS. *Annual Review of Neuroscience* 28: 327-55
Molano-Mazon M. 2013. (HOW THE THALAMUS CHANGES) WHAT THE CAT'S EYE TELLS THE CAT'S BRAIN. *PhD Thesis UMH- CSIC*
Molano-Mazón M, Valiño-Perez AJ, Sala S, Martínez-García M, Malo J, et al. *Converging Clinical and Engineering Research on Neurorehabilitation II, Cham, 2017*: 81-83. Springer International Publishing.

Muller T, Stetter M, Hubener M, Sengpiel F, Bonhoeffer T, et al. 2000. An analysis of orientation and ocular dominance patterns in the visual cortex of cats and ferrets. *Neural Comput* 12: 2573-95
Murcia-Belmonte V, Coca Y, Vegar C, Negueruela S, de Juan Romero C, et al. 2019. A Retino-retinal Projection Guided by Unc5c Emerged in Species with Retinal Waves. *Curr Biol* 29: 1149-60 e4
Nassi JJ, Callaway EM. 2009. Parallel processing strategies of the primate visual system. *Nature Reviews Neuroscience* 10: 360-72
O'Brien BJ, Isayama T, Richardson R, Berson DM. 2002. Intrinsic physiological properties of cat retinal ganglion cells. *The Journal of physiology* 538: 787-802
Ohki K, Chung S, Ch'ng YH, Kara P, Reid RC. 2005. Functional imaging with cellular resolution reveals precise micro-architecture in visual cortex. *Nature* 433: 597-603
Ohki K, Chung S, Kara P, Hubener M, Bonhoeffer T, Reid RC. 2006. Highly ordered arrangement of single neurons in orientation pinwheels. *Nature* 442: 925-8
Ohki K, Reid RC. 2007. Specificity and randomness in the visual cortex. *Curr Opin Neurobiol* 17: 401-7
Olavarria JF. 2001. Callosal connections correlate preferentially with ipsilateral cortical domains in cat areas 17 and 18, and with contralateral domains in the 17/18 transition zone. *J Comp Neurol* 433: 441-57
Olshausen BA, Field DJ. 1996. Emergence of simple-cell receptive field properties by learning a sparse code for natural images. *Nature* 381: 607-9
Olshausen BA, Field DJ. 1997. Sparse coding with an overcomplete basis set: a strategy employed by V1? *Vision Res* 37: 3311-25
Paik SB, Ringach DL. 2011. Retinal origin of orientation maps in visual cortex. *Nature neuroscience* 14: 919-25
Paley W. 2009. *Natural Theology: Or, Evidences of the Existence and Attributes of the Deity, Collected from the Appearances of Nature*. Cambridge: Cambridge University Press.
Parker AJ. 2007. Binocular depth perception and the cerebral cortex. *Nat Rev Neurosci* 8: 379-91
Peichl L. 2005. Diversity of mammalian photoreceptor properties: adaptations to habitat and lifestyle? *Anat Rec A Discov Mol Cell Evol Biol* 287: 1001-12
Petry HM, Bickford ME. 2019. The Second Visual System of The Tree Shrew. *J Comp Neurol* 527: 679-93
Pettigrew JD. 2004. Bi-sensory, striped representations: comparative insights from owl and platypus. *J Physiol Paris* 98: 113-24
Rathbun DL, Alitto HJ, Warland DK, Usrey WM. 2016. Stimulus Contrast and Retinogeniculate Signal Processing. *Front Neural Circuits* 10: 8
Rehn M, Sommer FT. 2007. A network that uses few active neurones to code visual input predicts the diverse shapes of cortical receptive fields. *J Comput Neurosci* 22: 135-46
Rieke F, Warland D, Steveninck R, Bialek W. 1996. *Spikes, Exploring the Neural Code*. 416 pp.
Ringach DL. 2002. Spatial Structure and Symmetry of Simple-Cell Receptive Fields in Macaque Primary Visual Cortex. *Journal of Neurophysiology* 88: 455-63
Ringach DL. 2004. Haphazard wiring of simple receptive fields and orientation columns in visual cortex. *J Neurophysiol* 92: 468-76
Ringach DL. 2007. On the origin of the functional architecture of the cortex. *PLoS One* 2: e251
Ringach DL, Mineault PJ, Tring E, Olivas ND, Garcia-Junco-Clemente P, Trachtenberg JT. 2016. Spatial clustering of tuning in mouse primary visual cortex. *Nat Commun* 7: 12270
Roman Roson M, Bauer Y, Kotkat AH, Berens P, Euler T, Busse L. 2019. Mouse dLGN Receives Functional Input from a Diverse Population of Retinal Ganglion Cells with Limited Convergence. *Neuron* 102: 462-76 e8

Rompani SB, Mullner FE, Wanner A, Zhang C, Roth CN, et al. 2017. Different Modes of Visual Integration in the Lateral Geniculate Nucleus Revealed by Single-Cell-Initiated Transsynaptic Tracing. *Neuron* 93: 1519

Ross CF, Kirk EC. 2007. Evolution of eye size and shape in primates. *J Hum Evol* 52: 294-313

Sakmann B, Creutzfeldt OD. 1969. Scotopic and mesopic light adaptation in the cat's retina. *Pflugers Arch* 313: 168-85

Sato M, Stryker MP. 2008. Distinctive features of adult ocular dominance plasticity. *J Neurosci* 28: 10278-86

Schiller PH. 1992. The ON and OFF channels of the visual system. *Trends in Neurosciences* 15: 86-92

Schottdorf M, Eglen SJ, Wolf F, Keil W. 2014. Can retinal ganglion cell dipoles seed iso-orientation domains in the visual cortex? *PLoS One* 9: e86139

Schottdorf M, Keil W, Coppola D, White LE, Wolf F. 2015. Random Wiring, Ganglion Cell Mosaics, and the Functional Architecture of the Visual Cortex. *PLoS Comput Biol* 11: e1004602

Seabrook TA, Burbridge TJ, Crair MC, Huberman AD. 2017. Architecture, Function, and Assembly of the Mouse Visual System. *Annu Rev Neurosci* 40: 499-538

Shannon CE. 1948. A Mathematical Theory of Communication. *Bell System Technical Journal* 27: 379-423

Sherman M. 2016. Thalamus plays a central role in ongoing cortical functioning. *Nature neuroscience* 16: 533-41

Sherman SM, Guillery RW. 1998. On the actions that one nerve cell can have on another: Distinguishing "drivers" from "modulators". *Proceedings of the National Academy of Sciences* 95: 7121-26

Simoncelli EP, Olshausen BA. 2001. Natural image statistics and neural representation. *Annu Rev Neurosci* 24: 1193-216

Smith GB, Hein B, Whitney DE, Fitzpatrick D, Kaschube M. 2018. Distributed network interactions and their emergence in developing neocortex. *Nature neuroscience* 21: 1600-08

Smith PH, Populin LC. 2001. Fundamental differences between the thalamocortical recipient layers of the cat auditory and visual cortices. *Journal of Comparative Neurology* 436: 508-19

Smith SL, Hausser M. 2010. Parallel processing of visual space by neighboring neurons in mouse visual cortex. *Nature neuroscience* 13: 1144-9

Soodak RE. 1987. The retinal ganglion cell mosaic defines orientation columns in striate cortex. *Proc Natl Acad Sci U S A* 84: 3936-40

Sperry RW. 1943. Effect of 180 degree rotation of the retinal field on visuomotor coordination. *Journal of Experimental Zoology* 92: 263-79

Springer MS, Stanhope MJ, Madsen O, de Jong WW. 2004. Molecules consolidate the placental mammal tree. *Trends Ecol Evol* 19: 430-8

Srinivasan S, Carlo CN, Stevens CF. 2015. Predicting visual acuity from the structure of visual cortex. *Proc Natl Acad Sci U S A* 112: 7815-20

Stoerig P, Cowey A. 1997. Blindsight in man and monkey. *Brain* 120 (Pt 3): 535-59

Swindale NV. 1996. The development of topography in the visual cortex: a review of models. *Network* 7: 161-247

Swindale NV, Shoham D, Grinvald A, Bonhoeffer T, Hubener M. 2000. Visual cortex maps are optimized for uniform coverage. *Nature neuroscience* 3: 822-6

Van Hooser SD. 2007. Similarity and diversity in visual cortex: is there a unifying theory of cortical computation? *Neuroscientist* 13: 639-56

Van Hooser SD, Heimel JAF, Chung S, Nelson SB, Toth LJ. 2005. Orientation Selectivity without Orientation Maps in Visual Cortex of a Highly Visual Mammal. *The Journal of Neuroscience* 25: 19-28

Van Hooser SD, Nelson SB. 2006. The squirrel as a rodent model of the human visual system. *Vis Neurosci* 23: 765-78

van Meer N, Houtman AC, Van Schuerbeek P, Vanderhasselt T, Milleret C, ten Tusscher MP. 2016. Interhemispheric Connections between the Primary Visual Cortical Areas via the Anterior Commissure in Human Callosal Agenesis. *Frontiers in Systems Neuroscience* 10

Veilleux CC, Kirk EC. 2014. Visual acuity in mammals: effects of eye size and ecology. *Brain Behav Evol* 83: 43-53

Wassle H. 2004. Parallel processing in the mammalian retina. *Nat Rev Neurosci* 5: 747-57

Wassle H, Boycott BB, Illing RB. 1981a. Morphology and mosaic of on- and off-beta cells in the cat retina and some functional considerations. *Proc R Soc Lond B Biol Sci* 212: 177-95

Wassle H, Peichl L, Boycott BB. 1981b. Morphology and topography of on- and off-alpha cells in the cat retina. *Proc R Soc Lond B Biol Sci* 212: 157-75

Weigand M, Sartori F, Cuntz H. 2017a. Universal transition from unstructured to structured neural maps. *Proc Natl Acad Sci U S A* 114: E4057-E64

Weigand M, Sartori F, Cuntz H. 2017b. Universal transition from unstructured to structured neural maps. 114: E4057-E64

Weliky M, Katz LC. 1999. Correlational structure of spontaneous neuronal activity in the developing lateral geniculate nucleus in vivo. *Science (New York, N.Y.)* 285: 599-604

Westheimer G. 2007. The ON-OFF dichotomy in visual processing: from receptors to perception. *Prog Retin Eye Res* 26: 636-48

White LE, Bosking WH, Williams SM, Fitzpatrick D. 1999. Maps of Central Visual Space in Ferret V1 and V2 Lack Matching Inputs from the Two Eyes. *The Journal of Neuroscience* 19: 7089-99

White LE, Coppola DM, Fitzpatrick D. 2001. The contribution of sensory experience to the maturation of orientation selectivity in ferret visual cortex. *Nature* 411: 1049-52

White LE, Fitzpatrick D. 2007. Vision and cortical map development. *Neuron* 56: 327-38

Willshaw DJ, Malsburg CVD, Longuet-Higgins HC. 1976. How patterned neural connections can be set up by self-organization. *Proceedings of the Royal Society of London. Series B. Biological Sciences* 194: 431-45

Willshaw DJ, von der Malsburg C. 1976. How patterned neural connections can be set up by self-organization. *Proc R Soc Lond B Biol Sci* 194: 431-45

Zhan XJ, Troy JB. 2000. Modeling cat retinal beta-cell arrays. *Vis Neurosci* 17: 23-39

Zhang X, An X, Liu H, Peng J, Cai S, et al. 2015. The topographical arrangement of cutoff spatial frequencies across lower and upper visual fields in mouse V1. *Sci Rep* 5: 7734

Zhang Y, Kim IJ, Sanes JR, Meister M. 2012. The most numerous ganglion cell type of the mouse retina is a selective feature detector. *Proc Natl Acad Sci U S A* 109: E2391-8

Appendix 1:
Supplementary Figures

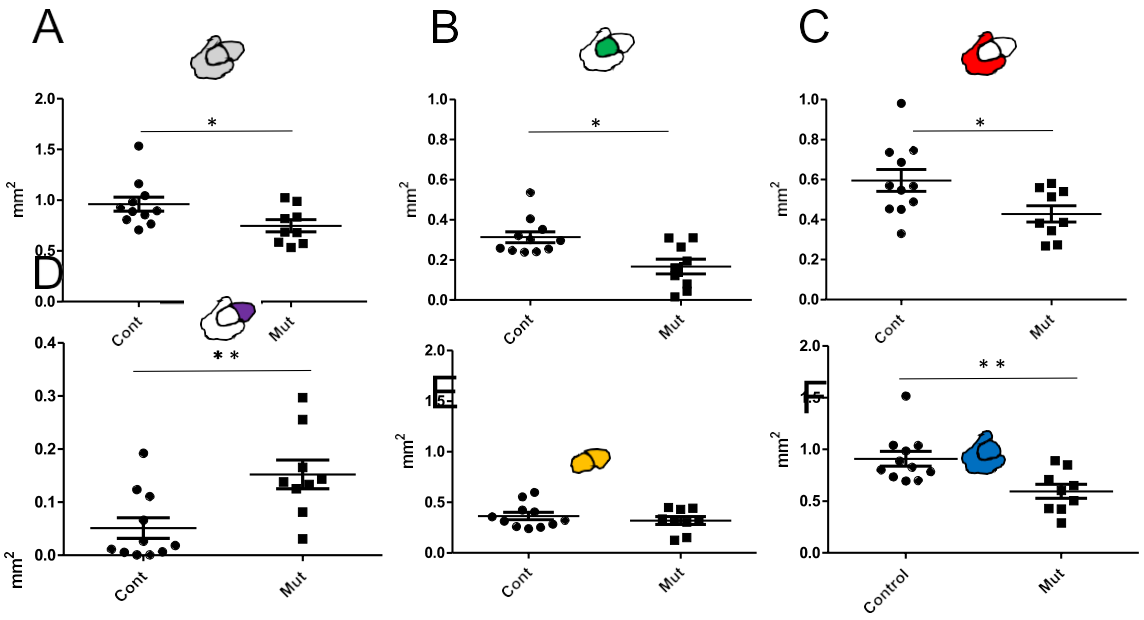

S1. **Quantification of ocular dominance response regions for mutant and WT mice. A.** Total response area (p=0.0402). **B.** Binocular area (p=0.0227). **C.** Contralateral area (p=0.0482). **D.** Ipsilateral area (p=0.0049). **E.** Total ipsilateral response area. **F)** Total contralateral response area (p=0.0098). Two tailed Man Whitney test for all statistically significant plots. Data from the right hemisphere of 11 WT and 9 mutants.

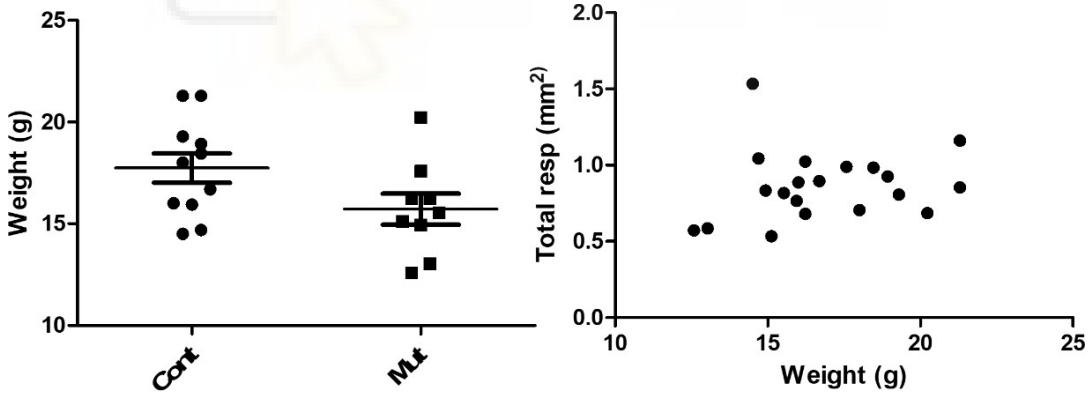

S2. **Effect of the weight in the final response area of experimental mice. A.** Weight (g) for WT and mutant mice. **B.** Total response area (mm^2) as a function of weight. Data from the right hemisphere of 11 WT and 9 mutants.

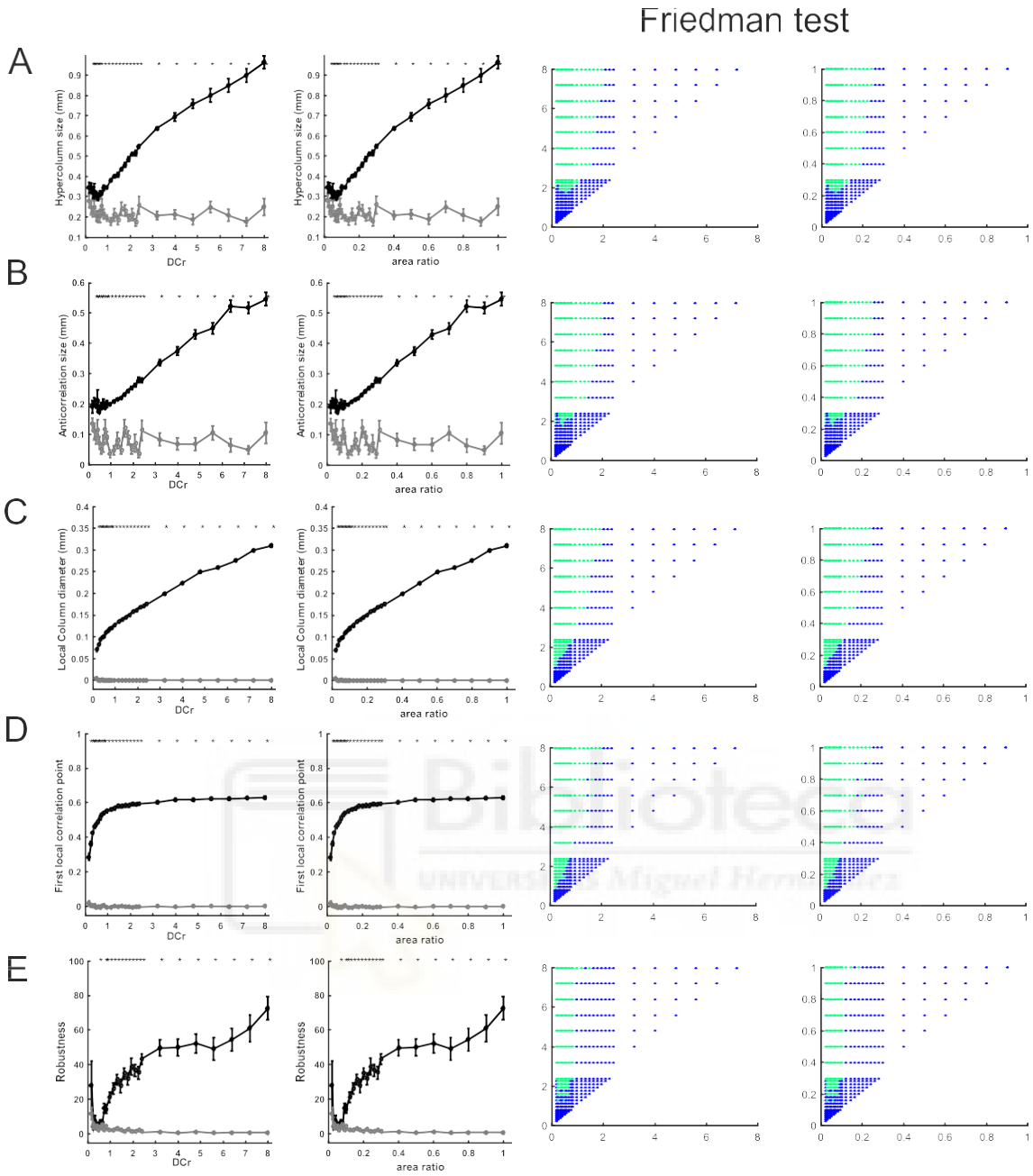

S3. **Friedman test for each of the circular correlation function parameters for the Raw input reaching layer 4. A-E.** Each row shows one of the parameters extracted from the circular correlation function; that is, hypercolumn size, anticorrelation size, local column diameter, first local correlation point and periodicity robustness respectively. The first and second columns represent each of these parameters as a function of DCr and the V1/Retina area ratio respectively. The Friedman test for each variable is represented in the third and for fourth columns against the DCr and the V1/Retina area respectively. (Green points $p<0.05$, blue points $p>0.05$). The place where the green points start to appear is where the threshold is placed for each of the variable.

Table 1

Animal	Body weight (g)	Brain weight (g)	Retina area (mm^2)	AD (mm)	V1 area (mm2)	Cpd	MT	Body weight ref	Brain weight ref	Retina area ref	AD ref	V1 area ref	Cpd ref
Human (Homo sapiens)	72340	1350	1012	24,52	2399,00	64	B	[1]	[2]	[1]	35,36,37,38	[1]	35
Macaque (Macaca mulata)	4613	90	670	17,6	1269,00	53,6	B	[8]	[34]	[14]	35,36,37,38	[34]	35
Cat (Felis catus)[a]	3050	25	473,5	21,94	380,00	8,85	B	[1]	[2]	[1,3][b]	35,36,37,38	[1]	35
Tree shrew (Tupaia belangueri)	120	3,4	120	8,07	63,00	2,4	B	[1]	[5]	[1]	35,36,37,38	[1,4][b]	35
Ferret (Mustela putorius)[c]	990	8	84	7,5	80,00	3,57	B	[1,6]	[7,8]	[1]	35,36,37,38	[1]	35
sheep (Ovis aries)[a]	35000	157,5	1572,5	26,113	700,00	5,61	B	[9,8]	[2,8][b]	[9,10][d]	35,36,37,38	[9]	35
owl monkey (Aotus trivirgatus)[e]	966	18,37	595	19,9	287,00	10	B	[8]	[8][f]	[14,13]	35,36,37,38	[4]	35
Squirrel monkey (Saimiri sciureus)[g]	817,97	23,86	352	15,5	637,00	40,5	B	[17][h]	[11,13][i]	[14][j]	35,36,37,38	[4][k]	35
Greater galago (Otolemur)[l]	957	11,64	344	16,3	172,50	4,8	B	[8][o]	[8][p]	[18][m]	35,36,37,38	[19,4][n]	35
Rabbit (Oryctolagus cuniculus)	2720	11	498	18,07	80,00	3	B	[1]	[8]	[1]	35,36,37,38	[1]	35
Mouse (Mus musculus)	30	0,4	15	5,28	2,50	0,5	B	[1]	[8]	[1]	35,36,37,38	[1]	35
Rat (Rattus novergicus)	508,3	1,83	68	5,58	8,50	1,6	B	[8]	[22][x]	[21][q]	35,36,37,38	[22][r]	35
Gray squirrel (Sciurus carolinensis)	635	6,46	206	11,8	40,00	3,9	B	[23]	[23][x]	[24][s]	35,36,37,38	[23][t]	35
Capybara (Hydrochoerus hydrochoerus)	40000	71	1039	21,04	286,92	5,8	A	[17]	[28][v]	[3]	35,36,37,38	[28][u]	35
Guinea Pig (Cavia porcelus)	476	4,83	159	10	30,00	NA	NA	[8]	[8]	[28,29]	35,36,37,38	[28]u	NA
Agouti (Dasyprocta primnolofa)[w]	2900	21,62	521	13,3	180,00	6,21	A	[8]	[8]	[3]	35,36,37,38	[30,31][y]	35
Golden Hamster (Mesocricetus auratus)	98,6	NA	NA	6,32	NA	0,5	B	17	8	NA	35,36,37,38	NA	35
Anubis baboon (Papio anubis)[z]	17728,56	201	793	21	3742,00	NA	NA	17	14	14	35,36,37,38	19	NA
Horse (Equus caballus)	40359,5	693	2444	42	NA	23,3	B	17	8	3	35,36,37,38	NA	35
Brown capuchin (Cebus apella)	2589	61,6	565	14,1	1344,00	54,75	A	8	14	14	35,36,37,38	32	35
Marmoset (Callithrix jacchus)	347,45	7,8	206	11,3	205,00	30	A	8	14	14	35,36,37,38	34	35
Midas Tamarin (Saguinus midas niger)	563	9,2	258	12,2	NA	24,87	A	8	14	14	35,36,37,38	NA	35
Black howler monkey (Alouatta caraya)	5012,5	49,5	444	16,2	NA	59,61	A	8	14	14	35,36,37,38	NA	35
Green monkey (Cercopithecus aethiops)	4099	59,8	707	17,3	NA	55,23	A	36	14	14	35,36,37,38	NA	35
Quokka (Setonyx brachyurus)	3250	13,9	237,5	10,4	92,00	4	A	8	8	41	35,36,37,38	39	35
Dunnart (Sminthopsis crassicaudata)	15	0,36	36	5,08	5,60	2,36	B	8	8	40	35,36,37,38	39	35

a. Unidentified breed.
b. Mean from both references.
c. Data from specie and subspecies intermingled (Mustela putorius furo). And from special breeds (Marshall BioResources, North Rose, NY).
d. Mean from whole mount measurements using Matlab from Figure 6 in (9) and Figure 4. B in (10).
e. Until 1983 all ten species of the genus Aotus where considered subspecies of Aotus trivirgatus (12, 13). To generalize data from different papers we will consider Aotus azarae and Aotus Trivirgatus the same species. Take also into account that the axial diameter of the eye is exactly the same for both species (35).
f. Mean from data of Aotus Trivirgatus and Aotus Azarae from (8).
g. The classification of the species of the genus Saimiri has changed over time (15, 16). We will integrate data from Saimiri Sciureus and Saimiri Ustus. Both species have similar brain weights (11, 13).
h. Mean body weight of Saimiri Sciureus and Saimiri Ustus.
i. Mean brain weight from both species; mean of 4 subjects in Table 1 (13) and data from (11).
j. Retinal area from Saimiri ustus.
k. V1 area from Saimiri sciureus.
l. Values for species of greater galagos Otolemur crassicaudatus and Otolemur garnetti intermingled. Garnetti are smaller (764 g) compared to crassicaudatus (1150 g) and were once considered a subspecie of craussicatus (20). However, their mean brain weight is quite similar, 11.5 g and 11.77 g respectively.
m. The study reports no differences in the retinal area between a lesser galago (Galago senegalensis) and a greater galago (Otolemur crassicaudatus).
n. There is quite a discrepancy in the area reported by (19) 139 mm^2 and data from (4) 206.649 mm^2. The mean from both values was included in the table.
o. Body weight is the mean of Otolemur garnetti and Otolemur crassicaudatus.
p. Brain weight as the mean of Otolemur garnetti and Otolemur crassicaudatus.
q. Data for Long Evans strain, rest of data for Norway rat strain.
r. Data extracted from Figure 6 and Table 3.
s. Measured from whole mount in figure 20 using Matlab. Also indirect measurements of whole mounts in (25, 26) for California ground squirrel (Spermophilus beecheyi) also give a similar value of around 200 mm^2.
t. Data extracted from table 3 (% of dorsolateral cortex devoted to V1) and Figure 7 in (27).
u. Indirect measurement of visual cortex area from figure 6.
v. Electrophysiological data is from young males. With their body weight ranging from 4.5-15.4 kg and the brain weight ranging from 42.5-64.0 g. Because a complete adult capybara can weight about 50 kg we must look carefully at this data, there is a possibility of underestimating V1 area.
w. Also known as Dasyprocta Aguti or Dasyprocta Aguti (30).
x. Brains weighted without he LGN
y. Measurements with Matlab from Figure 3. A-B (136-150 mm^2) (30) and from Figure 3. C (307.57 mm^2) (31) differed substantially. Because there is a discrepancy in the scales between Figure 3. A-B (30) and Figure 2. A (31) of about 6mm. Taking also into account that anteroposterior length of V1 is of about 20mm in Figure 3.C (31) in comparison to 26.5 mm in Figure 3.B (31). For the total area we have multiplied the maximum anteroposterior length

of V1 20.47mm by the mean medio-lateral distance~=8.5mm from Figure 3 A-B (30). We assume that the area is around 180 mm^2. This contradicts the data of 280 mm^2 from (38).

z. Data from different species of the genus Papio.

aa. From references (6, 35-37). Dasyprocta primnolopha mean from references (35, 37).

bb. Cpd: all from reference [35] mixture of behavioural and anatomic visual acuity data.

cc. Saguinus midas and agouti data from species of the same genus

Table 2

Animal	Retina area	SGS area (mm^2)	V1 area (mm^2)	Brainweight (g)	cpd
Guinea Pig	159	1,81	30	4,83	NA
Gray squirrel	206	8,91	40	6,46	3,9
Macaque	670	3,57	1269	90	53,6
Cat	473,5	2,78	380	25	8,85
Galago	344	1,06	172,5	11,64	4,8
Tree shrew	120	3,65	63	3,4	2,4
Mouse	15	0,39	2,5	0,4	0,5

The area of the stratum griseum superficiale (SGS) for the guinea pig, gray squirrel, macaque, cat and galago was extracted measuring coronal sections using Matlab from Figure 1 in [42]. The area of the SGS for the tree shrew was measured from a coronal section from Figure 2. A in [43], and for the mouse the a representative coronal section of the Allen Brain Atlas was used [44]. The rest of the data was obtained from the same references as in table 1.

Table 1 & 2 References

1. R. Mazade, J. M. Alonso, Thalamocortical processing in vision. *Vis Neurosci* **34**, E007 (2017).
2. G. Roth, U. Dicke, Evolution of the brain and intelligence. *Trends Cogn Sci* **9**, 250-257 (2005).
3. S. M. de Lima *et al.*, Horizontal cells in the retina of a diurnal rodent, the agouti (Dasyprocta aguti). *Vis Neurosci* **22**, 707-720 (2005).
4. X. Xu *et al.*, Functional organization of visual cortex in the owl monkey. *J Neurosci* **24**, 6237-6247 (2004).
5. U. Drenhaus, G. Rager, P. Eggli, R. Kretz, On the postnatal development of the striate cortex (V1) in the tree shrew (Tupaia belangeri). *Eur J Neurosci* **24**, 479-490 (2006).
6. H. C. Howland, S. Merola, J. R. Basarab, The allometry and scaling of the size of vertebrate eyes. *Vision Res* **44**, 2043-2065 (2004).
7. A. R. Barnette *et al.*, Characterization of brain development in the ferret via MRI. *Pediatr Res* **66**, 80-84 (2009).
8. J. R. Burger, M. A. George, C. Leadbetter, F. Shaikh, The allometry of brain size in mammals. *Journal of Mammalogy* **100**, 276-283 (2019).
9. P. G. Clarke, D. Whitteridge, The cortical visual areas of the sheep. *J Physiol* **256**, 497-508 (1976).
10. A. Shinozaki, Y. Hosaka, T. Imagawa, M. Uehara, Topography of ganglion cells and photoreceptors in the sheep retina. *J Comp Neurol* **518**, 2305-2315 (2010).
11. M. F. Williams, Primate encephalization and intelligence. *Med Hypotheses* **58**, 284-290 (2002).
12. C. Lang, Primate Factsheets: Owl monkey (Aotus) Taxonomy, Morphology, & Ecology. (2005).
13. B. L. Finlay *et al.*, Number and topography of cones, rods and optic nerve axons in New and Old World primates. *Vis Neurosci* **25**, 289-299 (2008).
14. M. A. Dyer *et al.*, Developmental sources of conservation and variation in the evolution of the primate eye. *Proc Natl Acad Sci U S A* **106**, 8963-8968 (2009).
15. C. L. KA, Primate Factsheets: Squirrel monkey (Saimiri) Taxonomy, Morphology, & Ecology . <http://pin.primate.wisc.edu/factsheets/entry/squirrel_monkey>. Accessed 2019 July. (2006 March 16).
16. M. Ruiz-Garcia, K. Luengas-Villamil, N. Leguizamon, B. de Thoisy, H. Galvez, Molecular phylogenetics and phylogeography of all the Saimiri taxa (Cebidae, Primates) inferred from mt COI and COII gene sequences. *Primates* **56**, 145-161 (2015).
17. K. Jones *et al.*, PanTHERIA: a species-level database of life history, ecology, and geography of extant and recently extinct mammals. *Ecology* **90**, 2648 (2009).
18. E. J. DeBruyn, V. L. Wise, V. A. Casagrande, The size and topographic arrangement of retinal ganglion cells in the galago. *Vision Res* **20**, 315-327 (1980).
19. C. E. Collins, D. C. Airey, N. A. Young, D. B. Leitch, J. H. Kaas, Neuron densities vary across and within cortical areas in primates. *Proc Natl Acad Sci U S A* **107**, 15927-15932 (2010).
20. R. Tao, "Otolemur garnettii" (On-line), Animal Diversity Web. Accessed February 06, 2020 at https://animaldiversity.org/accounts/Otolemur_garnettii/. (2006).
21. F. M. Nadal-Nicolas, M. Vidal-Sanz, M. Agudo-Barriuso, The aging rat retina: from function to anatomy. *Neurobiol Aging* **61**, 146-168 (2018).

22. K. L. Campi, C. E. Collins, W. D. Todd, J. Kaas, L. Krubitzer, Comparison of area 17 cellular composition in laboratory and wild-caught rats including diurnal and nocturnal species. *Brain Behav Evol* **77**, 116-130 (2011).
23. K. L. Campi, L. Krubitzer, Comparative studies of diurnal and nocturnal rodents: differences in lifestyle result in alterations in cortical field size and number. *J Comp Neurol* **518**, 4491-4512 (2010).
24. A. Hughes, "The Topography of Vision in Mammals of Contrasting Life Style: Comparative Optics and Retinal Organisation" in The Visual System in Vertebrates, F. Crescitelli *et al.*, Eds. (Springer Berlin Heidelberg, Berlin, Heidelberg, 1977), 10.1007/978-3-642-66468-7_11, pp. 613-756.
25. K. A. Linberg, S. Suemune, S. K. Fisher, Retinal neurons of the California ground squirrel, Spermophilus beecheyi: a Golgi study. *J Comp Neurol* **365**, 173-216 (1996).
26. B. Sajdak *et al.*, Noninvasive imaging of the thirteen-lined ground squirrel photoreceptor mosaic. *Vis Neurosci* **33**, e003 (2016).
27. L. Krubitzer, K. L. Campi, D. F. Cooke, All rodents are not the same: a modern synthesis of cortical organization. *Brain Behav Evol* **78**, 51-93 (2011).
28. G. B. Campos, W. I. Welker, Comparisons between Brains of a Large and a Small Hystricomorph Rodent: Capybara, Hydrochoerus and Guinea Pig, Cavia;Neocortical Projection Regions and Measurements of Brain Subdivisions. *Brain, Behavior and Evolution* **13**, 243-266 (1976).
29. J. L. Do-Nascimento, R. S. Do-Nascimento, B. A. Damasceno, L. C. Silveira, The neurons of the retinal ganglion cell layer of the guinea pig: quantitative analysis of their distribution and size. *Braz J Med Biol Res* **24**, 199-214 (1991).
30. G. N. Elston *et al.*, Specialization of pyramidal cell structure in the visual areas V1, V2 and V3 of the South American rodent, Dasyprocta primnolopha. *Brain Res* **1106**, 99-110 (2006).
31. I. A. Dias *et al.*, Topography and architecture of visual and somatosensory areas of the agouti. *J Comp Neurol* **522**, 2576-2593 (2014).
32. M. Weigand, F. Sartori, H. Cuntz, Universal transition from unstructured to structured neural maps. **114**, E4057-E4064 (2017).
33. C. SP, A database of retinal topography maps. Clin Exp Optom 2008; 91: 1: 85-95. Database at URL http://www.retinalmaps.com.au.
34. S. Srinivasan, C. N. Carlo, C. F. Stevens, Predicting visual acuity from the structure of visual cortex. *Proc Natl Acad Sci U S A* **112**, 7815-7820 (2015).
35. C. C. Veilleux, E. C. Kirk, Visual acuity in mammals: effects of eye size and ecology. *Brain Behav Evol* **83**, 43-53 (2014).
36. A. D. Kemp, E. Christopher Kirk, Eye size and visual acuity influence vestibular anatomy in mammals. *Anat Rec (Hoboken)* **297**, 781-790 (2014).
37. C. F. Ross, E. C. Kirk, Evolution of eye size and shape in primates. *J Hum Evol* **52**, 294-313 (2007).
38. M. Weigand, F. Sartori, H. Cuntz, Universal transition from unstructured to structured neural maps. *Proc Natl Acad Sci U S A* **114**, E4057-E4064 (2017).
39. C. J. Tyler *et al.*, Anatomical comparison of the macaque and marsupial visual cortex: Common features that may reflect retention of essential cortical elements. *Journal of Comparative Neurology* **400**, 449-468 (1998).
40. C. Arrese *et al.*, Retinal structure and visual acuity in a polyprotodont marsupial, the fat-tailed dunnart (Sminthopsis crassicaudata). *Brain Behav Evol* **53**, 111-126 (1999).
41. L. D. Beazley, S. A. Dunlop, The evolution of an area centralis and visual streak in the marsupial Setonix brachyurus. *J Comp Neurol* **216**, 211-231 (1983).

42. P. J. May, The mammalian superior colliculus: laminar structure and connections. *Prog Brain Res* **151**, 321-378 (2006).
43. H. M. Petry, M. E. Bickford, The Second Visual System of The Tree Shrew. *J Comp Neurol* **527**, 679-693 (2019).
44. A. Jones, C. Overly, S. Sunkin, The Allen Brain Atlas: 5 years and beyond. *Nature reviews. Neuroscience* **10**, 821-828 (2009).

Appendix 2:
Scientific contributions used for the thesis

The Brain's Camera. Optimal Algorithms for Wiring the Eye to the Brain Shape How We See

https://doi.org/10.1007/978-3-319-46669-9_15

The brain's camera. Optimal algorithms for wiring the eye to the brain shape how we see

M. Molano-Mazón, A.J. Valiño-Perez, S. Sala, M. Martínez-García, J. Malo F.T. Sommer, J.A. Hirsch and L.M. Martinez

***Abstract*— The problem of sending information at long distances, without significant attenuation and at a low cost, is common to both artificial and natural environments. In the brain, a widespread strategy to solve the cost-efficiency trade off in long distance communication is the presence of convergent pathways, or bottlenecks. In the visual system, for example, to preserve resolution, information is acquired by a first layer with a large number of neurons (the photoreceptors in the retina) and then compressed into a much smaller number of units in the output layer (the retinal ganglion cells), to send that information to the brain at the lowest possible metabolic cost. Recently, we found experimental evidence for an optimal compression-decompression algorithm in the early visual pathway that reproduces the strategies used in digital image processing. Our results bear strong consequences for our current understanding of the development and function of the visual thalamus and cortex.**

INTRODUCTION

The problem of acquiring, communicating, and processing high-dimensional information at long distances, without significant attenuation and at a low cost, is common to both artificial and natural settings. Thus, sending and processing large amounts of data through wireless networks of finite capacity poses a comparable challenge to that faced by the visual system of our brain when extracting information from images containing millions of pixels. In the brain, a widespread strategy to solve the cost-efficiency trade off in long distance communication is the presence of convergent pathways, or bottlenecks, in which information is acquired by a first layer with a large number of neurons and then compressed into a much smaller number of units in the output layer. A classic example is the retinothalamic connection where the information captured by 10e8 photoreceptors undergoes a 100-fold convergence and is carried onto the thalamus by only 10e6 retinal axons. Visual information is then expanded again in a two-step process starting in the thalamus and continuing in the primary visual cortex, which hosts several orders of magnitude more neurons than the number of retinal ganglion cells.

We have recently provided experimental evidence for a convergent neural circuit that allows efficient communication despite drastic reductions in the dimensionality of neural representations through information bottlenecks.

METHODS AND RESULTS

We explored how the lateral geniculate nucleus (LGN) of the thalamus contributes to visual processing, by combining computational tools with electrophysiological data. We developed a detailed computational model of the early visual pathway based on experimental data obtained from a large population of retinal, lgn and first order cortical neurons in layer 4. We next investigated how the retinal input is transformed into orientation selective receptive fields and periodic maps by thalamocortical circuits.

Sponsor and financial support acknowledgment goes here.

This work was supported by the Spanish Ministry of Economy and Competitiveness grants BFU2010-22220 and BFU2014-58776R (to LMM) and the Instituto de Neurociencias is a "Center of Excellence Severo Ochoa"

L.M. Martinez is with the Instituto de Neurociencias of the Spanish National Research Council, Sant Joan d'Alacant, Spain (corresponding author to provide e-mail: l.martinez@umh.es).

M. Molano-Mazón is with the Center for Neuroscience and Cognitive Systems, IIT, Trento, Italy. (manuelmolanomazon@gmail.com)

A.J. Valiño-Perez is with the Instituto de Neurociencias of the Spanish National Research Council, Sant Joan d'Alacant, Spain (arturo.jvalino@gmail.com)

S. Sala is with the Instituto de Neurociencias of the Spanish National Research Council, Sant Joan d'Alacant, Spain (salvador.sala@umh.es)

M. Martinez-Garcia is with the Instituto de Neurociencias of the Spanish National Research Council, Sant Joan d'Alacant, Spain (marina.martinez.garcia@gmail.com)

J. Malo is with the Department of Optics, University of Valencia, Valencia, Spain. (jesus.malo@uv.es)

F.T. Sommer is with The Redwood Center for Theoretical Neuroscience, UC Berkeley, Berkeley, CA, USA. (fsommer@berkeley.edu)

J.A. Hirsch is with The Department of Biological Sciences/Neurobiology, University of Southern California, Los Angeles, CA, USA. (jhirsch@usc.edu)

First, we have shown that retinothalamic convergence, combined with the increase in cell number in the LGN, provides an interpolated map of visual space that heightens the LGN's capacity to resolve a visual stimulus more readily than the retina is able to do. We demonstrated that neighboring relay cells in the LGN process information independently, even if some of their input derives from a common retinal source. This independence reduces redundancy in the sampling of the retinal mosaics and supports the view that visual processing in the thalamus serves to recode information efficiently (Barlow, 1981). The benefits of interpolation come at a cost, however. Interpolation blurs the image, reducing local contrast to degrade edge perception. Our results also point to a solution to this problem. We have found that relay cells and interneurons in the LGN are spatially correlated producing physiological arrangements of excitation and inhibition in the thalamic receptive field (RF) centers that effectively boost contrast borders and increase the dynamic range of the visual message that the LGN sends to cortex. Thus, the retino-thalamic circuit operates like techniques manmade devices employ to improve the appearance of visual images (Martinez et al., 2015; Hirsch et al., 2015).

Second, we have demonstrated that our two-step model produces cortical receptive fields and orientation maps that perfectly fit those obtained in the experiments. Third, we have also shown that these cortical features are already encoded in the LGN population activity. Finally, we have found that the structure of this LGN population activity is essential to maintain the stability of cortical orientation maps even in the presence of the relatively large levels of thalamocortical convergence that have been reported experimentally.

CONCLUSION

The simple, two-steps developmental rule based on statistical connectivity and wiring optimization we have reported could have the potential to profoundly shape not only information coding strategies but also the emergence of diverse receptive fields, precise local circuits and maps anywhere in the nervous system.

References

[1] H.B. Barlow (1981) "Critical limiting factors in the design of the eye and the visual cortex". *Proc. R. Soc. B* 212:1-34.

[2] L.M. Martinez, M. Molano-Mazon, X. Wang, F.T. Sommer and J.A. Hirsch (2014) "Statistical wiring of thalamic receptive fields optimizes spatial sampling of the retinal image". *Neuron* 81:943-56.

[3] J.A. Hirsch, X. Wang, F.T. Sommer and L.M. Martinez (2015) "How inhibitory circuits in the thalamus serve vision". *Annu. Rev. Neurosci.* 38:309-329.

Summary of the following congress communications:

- A.J. Valiño, M. Molano, J. Brotons, V. Borrell, S. Sala, L. Martínez. A developmental threshold relating retinal and V1 areas predicts the structure of V1 Orientation Preference Maps. SENC (Sociedad Española de Neurociencia), Palacio de Santiago, Santiago de Compostela, 4/9/2019 – 6/9/2019. SENC-2019_Preliminary-Programme.pdf

- A.J. Valiño, J. Brotons, F.T. Sommer, J.A. Hirsch, S. Sala, L. Martínez. Thalamic influence on the statistical wiring of visual cortical receptive fields and maps. SFN (Society for Neuroscience), Walter E. Washington Convention Center (Washington D.C), 11/11/2017 - 15/11/2017. Thalamic influence on the statistical wiring of visual cortical receptive fields and maps (abstractsonline.com)

- A.J. Valiño, J. Brotons, V. Borrell, S. Sala, L. Martínez. Statistical Wiring of visual cortical receptive fields and maps. SENC, Alicante, 27/09/2017 – 30/09/2017. SENC2017_ebook.pdf (mcusercontent.com)

A developmental threshold relating retinal and V1 areas predicts the structure of V1 Orientation Preference Maps.

A.J. Valiño Pérez [1], M. Molano Mazón [2], J.R. Brotons-Mas[1], V. Borrell [1], S. Sala Pla[1], L.M. Martínez[1]
[1]. Instituto de Neurociencias de Alicante. Alicante. España
[2]. IDIBAPS. Institut d'Investigacions Biomèdiques August Pi i Sunyer. Barcelona. España.

Neurons in the primary visual cortex (V1) of most mammals respond only to a restricted set of stimulus orientations. However, the cortical organization of these neurons differs between species. In carnivores and primates, V1 cells with similar orientation preferences tend to cluster together in an orderly fashion giving rise to the renowned cortical orientation preference maps (OPMs). On the other hand, in rodents these clusters of cells are more decorrelated and smaller giving birth to a "salt and pepper" configuration in V1. Since these different types of cortical organization are present and highly preserved in closely related phylogenetic clades, it is important to understand if there are common developmental rules that can account for their differential emergence across mammalian species.

To study the developmental and functional mechanisms involved in the formation of the mammalian early visual pathway we have built a feedforward statistical connectivity model linking the retina to V1 through the lateral geniculate nucleus of the thalamus (LGN). Our model accounts for many features of the different mammalian V1 organizations across evolution, including the presence or absence of a regular map structure, and the diversity of orientation selectivity profiles and receptive field lay-outs. Finally, the model indicates that the retino-thalamo-cortical divergence-convergence mechanisms related to cortical expansion are tuned similarly in the different species in order to recover as much information as possible through the retinothalamic bottleneck (Martinez et al., 2014); as a consequence, OPMs or salt and pepper configurations are established according to a developmental threshold relating retinal and V1 areas.

Thalamic influence on the statistical wiring of visual cortical receptive fields and maps

A.J. Valiño Pérez [1], J.R. Brotons-Mas[1], F.T. Sommer[2], J.A. Hirsch[3], S. Sala Pla[1], L.M. Martínez[1]
[1]. Instituto de Neurociencias de Alicante. Alicante. España
[2]. The Redwood Center for Theoretical Neuroscience, UC Berkeley, Berkeley, CA, USA.
[3]. The Department of Biological Sciences/Neurobiology, University of Southern California, Los Angeles, CA, USA

Neurons in the primary visual cortex (V1) of most mammals respond only to a restricted set of stimulus orientations. Furthermore, in some species but not in others, V1 cells with similar orientation preferences tend to cluster together in an orderly fashion giving rise to the renown cortical orientation preference maps (OPMs). Over the years, contrasting models emphasizing the role of feedforward vs. intracortical connectivity have been proposed to explain the emergence and function of this salient feature of cortical organization. Still highly debated, both types of developmental models have, nonetheless, in common that they largely neglect the potential role that the thalamus (lateral geniculate nucleus, LGN) plays in this process. Recently, we have demonstrated that the retinothalamic circuit is optimized to increase the resolution of the retinal output on its way to V1 through a straight process of information upsampling and interpolation occurring at the level of the LGN (Martinez et al., 2014). Here, we use a similar approach to show that the probabilistic, convergent connectivity from retina to LGN required to increase visual resolution significantly transforms the thalamic representation of the retinal mosaics generating partially segregated thalamic domains of On- and Off-center receptive fields cells arranged in locally correlated clusters of dipoles with different orientations. We further demonstrate that this new thalamic structure has the same properties as those previously shown in cortical orientation maps and suggest that it might be essential for their emergence and stability: First, our results revealed that the structure of the emergent cortical maps perfectly correlates very well with the arranging of the thalamic ON and OFF domains. Second, the periodicity and stability of the cortical orientation map depend critically on the biological constraint imposed by the upsampling and interpolation procedure performed in the LGN. Finally, the retinothalamic rewiring allows to maintain large values of

thalamocortical convergence, and still conserving the stability of the map, without requiring complex developmental rules or very precise patterns of spontaneous or visually driven feedforward activity.

STATISTICAL WIRING OF VISUAL CORTICAL RECEPTIVE FIELDS AND MAPS

A.J. Valiño Pérez [1], J.R. Brotons-Mas[1], S. Sala Pla[1], L.M. Martínez[1]
[1]. Instituto de Neurociencias de Alicante. Alicante. España

.

Neurons in the primary visual cortex (V1) of most mammals respond only to a restricted set of stimulus orientations. Furthermore, in some species but not in others, V1 cells with similar orientation preferences tend to cluster together in an orderly fashion giving rise to the so called cortical orientation preference maps (OPMs). The developmental rules underlying the emergence of cortical receptive fields and maps are highly debated. Over the years, contrasting intracortical and feedforward models have been proposed to explain the emergence and function of this salient feature of cortical organization. Both types of models, however, have in common that they largely neglect the potential role that the thalamus plays in this process. Recently, we have used a powerful combination of experimental and computational techniques to demonstrate that the retinothalamic circuit is optimized to increase the resolution of the retinal output on its way to V1 through a straight process of information upsampling and interpolation (Martinez et al., 2014). Here, we use a similar approach to show that the probabilistic, convergent connectivity from retina to LGN required to increase visual resolution transforms significantly the thalamic representation of the retinal mosaics generating partially segregated thalamic domains of On- and Off-center cells. We demonstrate that this new thalamic structure is essential for the emergence and stability of cortical receptive fields and orientation maps: First, our results revealed that these cortical features perfectly correlate with the arranging of the thalamic ON and OFF domains. Second, they also show that the periodicity and stability of the cortical orientation map depend critically on the biological constraint imposed by the upsampling and interpolation performed in the thalamus. Finally, the retinothalamic rewiring allows to maintain large values of thalamocortical convergence, without requiring complex developmental rules or very precise patterns of spontaneous or visually driven activity.